2-MIX

codet

JANUARY 1971

NASA CR-114816

Parametric Analysis of RF Communication and Tracking System for Manned Space Station

NASA Contract NAS 2-10300

CONTENTS

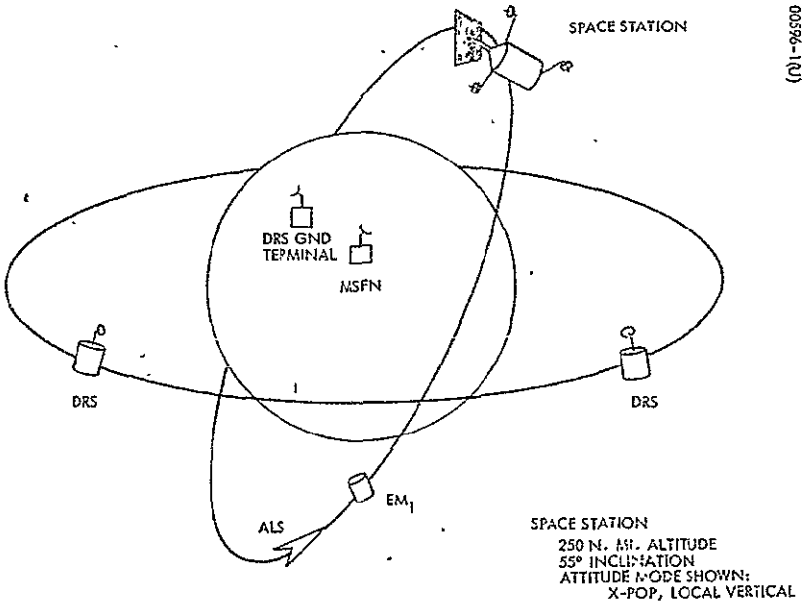

Figure 1-1. Communication Terminals

1. INTRODUCTION

This document is the final report of the Parametric Analysis of RF Communication and Tracking Systems for Manned Space Stations, conducted by the Space Systems Division, Hughes Aircraft Company, for the Manned Spacecraft Center, National Aeronautics and Space Administration, under Contract NAS 9-10409.

The 1-year (5 January 1970 to 5 January 1971) study was divided into two major phases. Phase I provided analyses and assessment of the significant parameters and factors associated with RF communication systems for manned space stations. Phase II used these results in the design of a baseline external communications system for a 12-man Space Station.

Part I of this report describes the baseline system. The basic Space Station mission profile is given in Table 1-1. Wherever definitive requirements or constraints were required during the design phase, the North American Rockwell (NAR) Solar-Powered Space Station was assumed. The basic link geometry of the mission is illustrated in Figure 1-1. The low-altitude orbit Space Station utilizes a data relay satellite (DRS) for all normal communication to the ground. The stations of the Manned Space Flight Network (MSFN) perform tracking of the spacecraft for orbit determination. Communication links are established between the Space Station and the orbital vehicle of the Advanced Logistic System (ALS) whenever the ALS approaches for rendezvous. Links are also provided to the Station's free-flying experiments module. Section 2 provides a system level description of the all-digital system. The design outlined avoids the compatibility problems encountered in the Apollo Unified S-Band System. The system's antenna, RF-IF, and baseband subsystems are detailed in Sections 3, 4, and 5, respectively.

Part II of this report documents the studies and parametric trades performed. Many of the studies can be used in the development of communication system designs for application to missions other than the Space Station mission (for example, the ALS mission) but the detailed design trades consider only the Space Station requirements and constraints. Section 6 considers the geometry of the various links. The pointing problems associated with the use of a high gain antenna for the data relay link are analyzed in detail. Section 7 describes the link analyses performed and the link design [illegible]. Section 8 summarizes the antenna acquisition and tracking studies [illegible] special attention is given to the use of a [illegible] level monopulse

TABLE 1-1. · MISSION PROFILE

- 12-man Space Station
- NAR solar powered configuration
- Launch 1977
- Duration > 5 years
- Primary attitude mode: X-POP LV
- Orbital parameters: 250 n. mi. altitude, 55 degree inclination
- Operational system interfaces:
  - MSFN
  - ALS
  - EM_1
  - DRS

pointing technique. Section 9 includes analyses of a portion of the baseband electronics for a digital communication system. The design of both a PSK modem and a time division multiplex system are considered. Section 10 documents surveys made of the state-of-the-art in several different technologies.

Appendix A contains the final link power budgets for the Space Station communications system design. Appendix B summarizes a special task performed as the request of MSC; namely, the use of electronically steered arrays for communication during artificial gravity operations.

PART I

BASELINE SYSTEM

2. BASELINE SYSTEM SUMMARY

INTRODUCTION

Overview

A brief outline of the baseline system design and the rationale behind development is helpful as an orientation to the description which follows. Coverage of the system extends from digital and analog signals at baseband to the antenna and RF transmission equipment. It provides color television, voice, telemetry, and wideband digital data communications services. The system operates in three frequency bands (nominally 140 MHz, 2.2 GHz, and 14 GHz).

A data relay satellite system is employed as the primary means of space-to-ground communications. The wideband service over this link utilizes three high gain tracking antennas at 14 GHz. Omnidirectional coverage services are provided at the other frequencies for voice and data links to ATS and the detached experiments module (EM_1).

Except for the emergency voice service, which is provided by a simple analog system, digital modulation and associated source and channel coding is the selected transmission mode for all the links and the services they carry.

Some Design Objectives

In developing the baseline system, there were several objectives observed to guide the direction and determine the scope of the design. Foremost one, which influenced several design decisions, was the intention to integrate the maximum communication capabilities that technology would provide in the mission time frame. This was to be done not by extrapolating specific device performance levels to 7 years in the future, but by observing relative growth in different technologies and arranging these in a system which derived maximum system level performance. The device capabilities actually required are generally quite conservative and are within present state of the art. An example is the selection of digital transmission for the data relay link where the design of the digital radio was based on manufacturer's current data sheets.

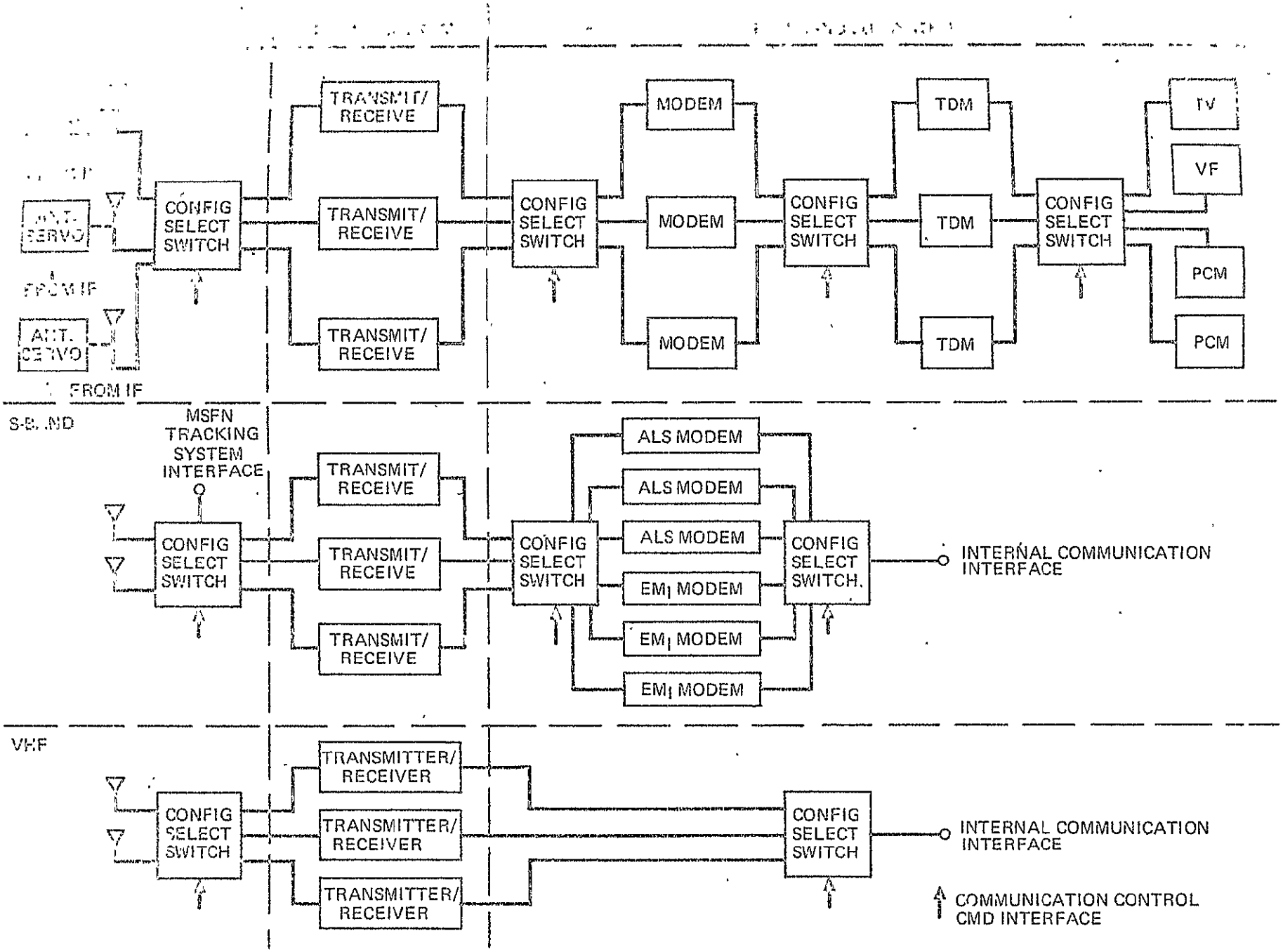

Figure 2-1. System Block Diagram

...econd major objective was to avoid the problems encountered in ... communication system. The design philosophy provides a ...egree of independence between the functions of ranging, antenna ... and data transmission, and preliminary analysis indicates that ...ach should prevent the incompatibilities found within the Apollo ...-Band System.

Another objective of the baseline design was to determine technical ...ity or risk areas. For this reason, certain areas of the design were ...ded in more depth than others. For example, the time division ...xer (TDM) was investigated to the level of digital device block dia- ...d circuit board estimates. Similarly, achievable solid state power ...er performance was carefully considered and the specified capabili- ...re based on devices and circuits currently employed in Hughes' ...ms.

Two additional objectives in the system design were: 1) to assist ...m planning by providing a representative set of performance capa- ...versus Space Station resource demand, and 2) to provide a design ...l for requirements analysis and verification. In connection with the ...f these, special emphasis was given to developing a comprehensive ...tion of the system and operational interfaces.

...GENERAL CONFIGURATION AND SUMMARY CHARACTERISTICS

The basic system concept is shown in Figure 2-1, where the sub- ...ms are organized by equipment location and function, with the antenna ...system on the left, the RF-IF subsystem in the middle, and the baseband ...stem to the right. Each of these, in turn, is divided into sections which ...espond to the operating frequency band and communications circuits ...ded in that band. The top (K-band) section handles all the communica- ...traffic between the Station and the ground with the exception of the ...ency voice link. The S-band section carries the telemetry and wide- ...communications between the Space Station and the shuttle (ALS) and ...tached experiments module (EM_1). The bottom portion of Fig- ...-1 shows the dedicated, emergency voice facility which provides com- ...tion: 1) between the Station and the ALS, and 2) to the ground, either ...tly or through the data relay satellite (DRS).

The use of redundancy is indicated by the parallel equipment in each ... The required level of redundancy is as yet undetermined, but ...nt units are included here to assure that weight and power estimates ...mble. In general, a "hot" spare is provided where feasible which ...tivated via the configuration selection switches shown. This spare ...d in addition to the parallel units required during antenna hand- ...antennas do not have this level of redundancy because of their ...weight requirements, although there are backup provisions in ...n.

Three K-band antennas are provided which are the minimum required to handle uninterrupted relay satellite handover with the spacecraft stabilized in a standard mission attitude. In the event of failure of one (and under some circumstances, two) of these antennas, the third could still provide the full link capacity through the relay satellite. There would be an interruption in service however, as the single antenna was repositioned for acquisition of a second relay satellite.

The S-band and VHF antennas each consist of two independent arrays (one circumferential and one axial) with their patterns oriented for maximum coverage in a given Station attitude mode. As these are not tracking antennas, their reliability is quite high. If a failure should occur in the primary pattern, the alternate array can be used. This generally would not provide full capability (either in range or continuous visibility) but would give minimum, essential service.

In the S-band section of the antenna subsystem, a tracking system interface is shown. This is a pair of isolated transmit and receive ports which give full access to the S-band antenna for ground tracking or command functions. The receive port follows a wideband preamplifier so that the tracking system noise temperature would not be penalized by attenuation in waveguide runs, filters, and couplers associated with the communications channels.

On the transmit side, it will be necessary to coordinate transmit filter bandwidths and power levels so that appropriate isolation can be provided to prevent interference due to reflected signals in the common antenna transmission line.

In the K-band section of the baseband subsystem, parallel PCM and single TV and voice sources are shown. This is because the TV and voice signal processing is included within the communication system, whereas, the PCM is provided from a system external to the communication system. To provide continuous flow of data as may be required by the PCM users during relay satellite handover, a parallel interface is provided. For the TV and voice, the input and output circuits would be switched between satellite circuits at the multiplexer (TDM) interface when the new link is established. This would cause a transient interruption of the analog signal, but probably would not be noticed by the users.

The S-band section of the baseband subsystem contains separate modulator/demodulators for the ALS and EM_1 circuits. This is required because of the decision to employ quadriphase modulation for bandwidth conservation in the EM_1 link. Rather than attempt to define a dual mode modem which could be configured for either quadriphase or biphase, separate modems were specified as these are relatively small, low power units.

The configuration selection switches, as already noted, are used to switch in redundant units in the event of a failure. In addition, they are used to connect the appropriate antenna, RF, and baseband units together as required by Space Station communications link geometries and service requirements. These switches are controlled by a communications control facility,

external to the system. It is assumed that this facility will all internal and external communication functions and preplanned and handover sequences.

Locations

The mounting locations of the baseline communications equipment shown in Figure 2-2. These locations are based on a North American all Solar-Powered Space Station configuration. (The solar cell panels omitted for clarity.) The three K-band, high gain antennas are about the circumference at 120 degree intervals. Two are mounted edge of the conical section and the third at the rear. Each has a cradle and erection mechanism. The two near the conical section radially against the cone surface while the third is folded across the surface.

The S-band and VHF circumferential arrays form bands around the rical section in the middle region. The exact location is not critical, that the VHF array should be 10 feet or more from the ends of the here so that a symmetrical pattern is achieved. There is a single and VHF element at each extremity of the longitudinal axis. One hown in Figure 2-2 on the narrow end where the solar panels are ed; there are two more on the flat surface at the end of the cylindri- ection.

At the base of each K-band antenna, there is an equipment section houses the RF power amplifier, its power supply, and the servo tronics. These are unpressurized spaces with prime power and ther- sink provisions. A compartment at the rear of the antenna reflector ins the preamplifier and the monopulse circuitry. Another equipment ion, the external equipment bay, is located at a convenient point on the rical section. This contains the majority of the RF-IF equipment similar power and thermal sink facilities. The bay is accessible a hatch in the surface for modular replacement of units.

There are two internal equipment bays; one in each of two pressur- ctions of the Space Station. This is an agreement with the Station philosophy which provides for two isolated areas for survival in an ency which threatens the habitable environment.

The antenna locations were selected primarily by coverage require- and blockage problems, and by launch stowage considerations. The of the electronic equipment was governed by the desire to locate as of it as possible in a single external bay to minimize the following: nstruction management difficulties, 2) signal and power cable runs, ower and thermal load demands on the manned environment. It was to locate the K-band power amplifiers near their associated anten- to avoid the excessive waveguide losses at this frequency. The ulse were then included at this location to simplify servo feed- and checkout problems.

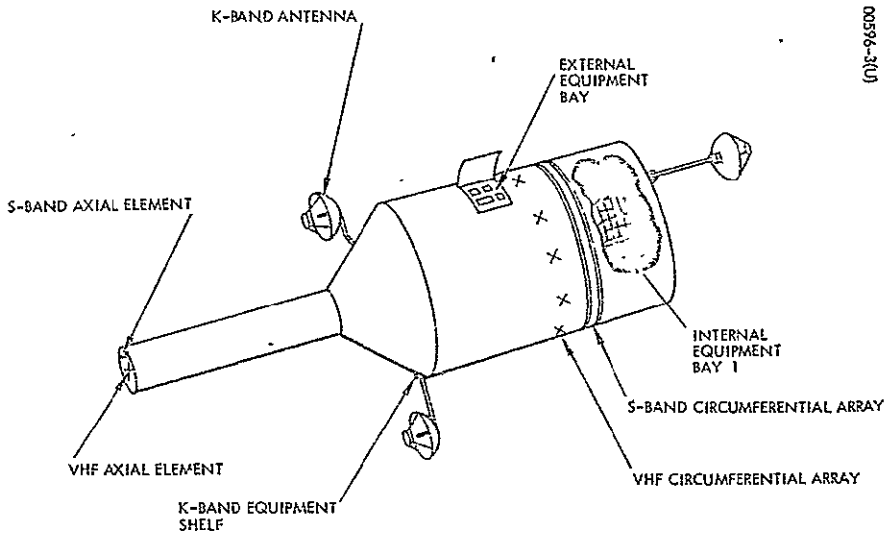

Figure 2-2. Equipment Locations

Subsystem	Section	Weight, pounds	Power, watts	Volume[1], cubic feet	Location[2]
ANTENNA	K-band	299.0	245.0	0.75	A, B, & C
	S-band	423.0	18.0	0.24	A & C
	VHF	94.0	0.3	0.03	A & C
Total		816.0	263.0[3]	1.0	
RF-IF	K-band	30.0	20.0	1.28	C
	S-band	96.0	476.0	1.95	C
	VHF	27.0	166.0	1.40	C
Total		153.0	496.0[3]	4.60	
BASEBAND	K-band	410.0	217.0	6.40	D & E
	S-band	102.0	59.0	2.66	D & E
	VHF	2.0	—	0.23	D & E
Total		514.0	276.0[3]	9.3	
Total external communications system		1,483.0	1,035.3[3]	14.9	

[1] Electronic equipment only

[2] Location code:
A = Antenna
B = K-band equipment shelf
C = External bay
D = Internal bay No. 1
E = Internal bay No. 2

[3] One K-band and two S-band links active

The division between the RF-IF and baseband subsystems (located in the external and internal equipment bays, respectively) was determined principally by the objective of minimizing the cabling requirements. There are a large number of command and monitoring functions associated with the equipment grouped in the baseband subsystem which would lead to a severe penalty in wire harness weight if it was necessary to carry these to the external bay from the internally located communication control facility.

System Physical Characteristics

Table 2-1 summarizes the physical characteristics of the baseline system. The weights indicated include all the equipment shown in the previous system block design, including redundant units. The power demand is the average load with links established to a single DRS, ALS, and EM_1. The volumes shown are for the electronic components only and do not include the antenna apertures or gimbals.

Communications Performance

The communication capabilities of the baseline system are summarized in Table 2-2. The channel capacities are specified in terms of their digital bit rates. The 12.2880 megabits/sec and 19.2 kilobits/sec rates handle the color TV and engineering voice requirements, respectively, using appropriate source encoding.

As stated above, the DRS system is employed as the primary means of space to ground communications, although the emergency voice and S-band links have more than adequate capability to work directly into a modest ground terminal. For the EM_1 and the ALS, the achievable communications range is given as an important communications performance parameter.

2.3 SYSTEM OPERATIONS

The design of the baseline system assumes autonomy of the Space Station in establishing its half of the various communications links. In addition, it is assumed that the Station initiates all acquisition sequences according to a preplanned schedule. Appropriate monitoring and configuration command test points, redundant units, and signal test patterns are provided for circuit and equipment performance monitoring, fault isolation, and restoration.

These activities are under the control of a separate communications control facility. This facility coordinates all frequency and traffic assignments with its counterpart either on the ground or aboard the ALS or EM_1 and establishes appropriate circuit interconnections with the internal communication system. These functions are assumed to be automated with no required operator supervision during normal operations, but with certain manual override provisions.

TABLE 2-2. SUMMARY COMMUNICATIONS PERFORMANCE

Link	Frequency	Service	Channel Capacity* (full duplex)	Number	Range, n. mi.
DRS	K-band	Television	12.2880 Megabits/sec	1	—
		Engineering voice	19.2 Kilobits/sec	12	—
		Telemetry	307.2 Kilobits/sec	7	—
		Priority telemetry	19.2 Kilobits/sec	4	—
TDRS	VHF	Emergency voice	3 kHz	1	—
EM_1	S-band	Wideband data	7.3728 Megabits/sec	1	450
ALS	S-band	Telemetry, voice	57.6 Kilobits/sec	1	303
ALS	VHF	Emergency voice	3 kHz	1	3000
MSFN	VHF	Emergency voice	3 kHz	1	-
MSFN	S-band	Ranging	MSFN standard	1	-

*Digital channel BER = 10^{-5}

Table 2-3 summarizes the various communications system modes and mode changes as a function of several mission operations. For example, during Station attitude changes, the K-band link is interrupted during the handover and reestablished when the Station is stabilized in the new orientation.

In the event of a mission emergency, power can be conserved and minimal communications capabilities sustained by powering down the two wideband links to the DRS and EM_1. The emergency voice remains operational and the narrowband data link normally providing telemetry to the MCS can be used for a 57.6 kilobits/sec link to the ground. The S-band tracking interface also remains operational.

A DRS link handover is accomplished by establishing the new link in parallel with the old during the period of mutual visibility. (This assumes that the number and location of the relay satellites and the Space Station orbit provide such overlap.) There are three functions which must be performed in sequence for each half of the duplex link: antenna acquisition, signal acquisition, and TDM synchronization.

The link is first established in the direction from the DRS to the Space Station. Prior to initiating the sequence, the data listed below must be coordinated with the ground facility controlling the DRS. This information may be transmitted to the Station via the DRS link at regular intervals.

1) DRS look angles in Space Station coordinates (The final data is generated onboard the spacecraft. The fundamental calculation is based on DRS and Space Station ephemerides.)

2) Transmit and receive channel assignments

3) Beacon frequency doppler offset derived from item (1) data

4) Ground station TDM timing offset to compensate for path length variation during the pass

The Station and DRS coordinate the pointing of their high antennas by the use of K-band tracking beacons. The Space Station K-band antenna, which is to carry the new link, is commanded to point at the DRS to within its beamwidth (1.25 degree). The estimated doppler offset is inserted in the K-band beacon local oscillator in the receiver and the beacon code tracking loop locks to the PN-coded, DRS beacon signal. This beacon signal is transmitted over the earth coverage antenna of the DRS so it is not necessary to orient the high gain antenna on the relay satellite at this point. When code tracking synchronization is accomplished, the Space Station antenna commences automatic tracking on the beacon signal.

The Space Station beacon is then transmitted to assist the DRS in tracking its high gain antenna. When this has been accomplished, a confirmation signal is sent over the DRS beacon and detected at the Space Station. This tells the ground and the Space Station that the communications links have been established.

TABLE 2-3. COMMUNICATION SYSTEM MODES

Operations	Response/Configuration
Mode change	Programmed reconfiguration and re-acquisition of antenna, signal, and data
	Emergency voice and MSFN telemetry operational
Mission emergency	Powerdown EM_1 wideband data
	Powerdown DRS wideband data
	Emergency voice and MSFN telemetry operational
Handover	Maintain communication on primary link
	Programmed secondary antenna acquisition on DRS beacon
	Programmed signal and data sync acquisition on communications channel
	Accept data on new channel
Rendezvous/docking	Programmed K-band antenna reconfiguration and power control
	Programmed S-band power control, automatic antenna reconfiguration
Restore/maintain	Select redundant baseband or RF-IF equipment
	Select alternate antennas
	Reduce capacity on all digital links
	Manually assisted antenna pre-positioning
	Replace major equipment modules
Artificial g	DRS coverage limited to two K-band antennas
	Automatic switching of S-band and VHF antennas

At this point in the acquisition sequence, the communications signal is transmitted by the ground station, relayed by the DRS, and received at the Space Station. The design of the receiver is such that when the beacon demodulator is tracking the beacon signal, there is automatic doppler compensation provided in the communications channel. This communications signal is therefore quickly acquired and processed by the communications demodulator/decoder. The Space Station begins transmitting its communications carrier at about the same time as the ground station in order to establish the other half of the full duplex link.

Initially, the signal carries no data, but has only the digital frame structure with the sync word. The TDM equipment scans this sequence and establishes frame and bit synchronization. As each half of the link achieves TDM sync, it confirms this by transmitting an acknowledgement in the reverse direction. This completes the link acquisition procedure and traffic can now be transferred from the previous DRS link to the new.

During rendezvous and docking maneuvers, it is necessary to manage the antenna selection and transmitted power to provide continuous coverage and avoid interference with electronics systems on spacecraft maneuvering in the near vicinity of the Station. S-band antenna selection is provided automatically, while the K-band antenna selection is preplanned by consideration of look angles and relative geometries.

In the event of circuit degradation or equipment failure, new circuits or equipment can be configured by switching to alternative units or, for the K-band link, reducing the capacity. Electronic modules may also be removed for later repair or refurbishment. There are also provisions for tracking on the DRS communications signal in the event of beacon failure and for manually assisting the positioning of the high gain antennas for initial alignment and acquisition.

During the artificial gravity experiment, the antenna look angle considerations become complicated by virtue of the sun-oriented geometry (See Figure 2-3). The two K-band antennas with collinear azimuth axes are 'despun' at the 4 rpm spin rate and used for DRS coverage. Depending on the number and longitude of the relay satellites which comprise the DRS network, and the time of the year that the month-long experiment is conducted, there may be interruptions of this link.

While three high gain antennas at 120 degrees spacing can be located to provide uninterrupted visibility of a given relay satellite on a single pass for the normal attitude modes, this is not true for the artificial g mode. As illustrated in Figure 2-3, the addition of the S-II stage as a counter-weight limits any one antenna to hemispherical coverage on either side of the spin plane. There are Station/DRS orbit configurations which cause the spin plane to intersect the visible relay satellite, necessitating a handover during a pass and the attendent interruption of service. This could be avoided by the addition of a fourth high gain antenna to provide two in each hemisphere, but this was not considered justified for an experimental mode.

The VHF and S-band antennas also have unique handover considerations ... artificial g mode which impose some operational constraints involving, ... rly, Space Station-to-ground links. A link to a ground station at local ... mask would lie in the spin plane. The circumferential and axial array ... are then oriented such that switching from one array to the other would ... ired two times per revolution. This could interfere with both the ... cy voice link and a turnaround ranging link in the tracking system ... are not properly designed.* These are not insurmountable difficul- ... t should be considered in the design of this mission and the ground ... t equipment.

... RF COMMUNICATIONS SYSTEM INTERFACES

The system interfaces, shown in Figure 2-4, have been separated ... external and internal systems. The external systems are the relay ... ite (DRS), the shuttle (ALS), the detached experiments module (EM_1), ... Manned Space Flight Network (MSFN). The internal interfaces have ... rouped into baseband communication services, communication sys- ... ntrol, and ancillary systems.

Table 2-4 is a compilation of the communication characteristics of ... external systems. This summarizes the RF characteristics of the ... Station and the assumed characteristics of the interfacing systems. ... MSFN characteristics are not included as they are not a limiting ... tor.

Notice that in general, complementary, orthogonal circular polariza- ... n is employed except for the VHF link where all right-hand circular polar- ... tion is specified. This permits both the ALS and the Space Station to com- ... nicate to the ground through the DRS and directly to each other without ... ne to change antenna polarization. (The transmit and receive frequency ... ration is sufficient to use frequency diplexing for isolation.) Notice also ... at the transmit and receive channels in the ALS and Space Station can be ... interchanged as required to establish direct or relay links. The required ... power per carrier (P_c) is specified as are the antenna gains. Effective ... ation power (ERP) is the product of these parameters. The digital modu- ... tion rates shown are the encoded rates which occur at the interface point ... RF carrier) and should not be interpreted as the information rates; ... were previously listed in Table 2-2.

The internal interfaces are listed in Table 2-5. The number of ... ts are the number of discrete terminations either single-ended or ... d to ground. As mentioned earlier in the discussion of the system ... gram, the voice and TV signals are processed within the RF com- ... nications system; therefore, only a single interface is required for each

---

... would require either incoherent demodulation techniques, (e.g., an ... discriminator for emergency voice), or coherent demodulators which ... through a drop-out period or, alternately, demodulators ... reacquire very rapidly.

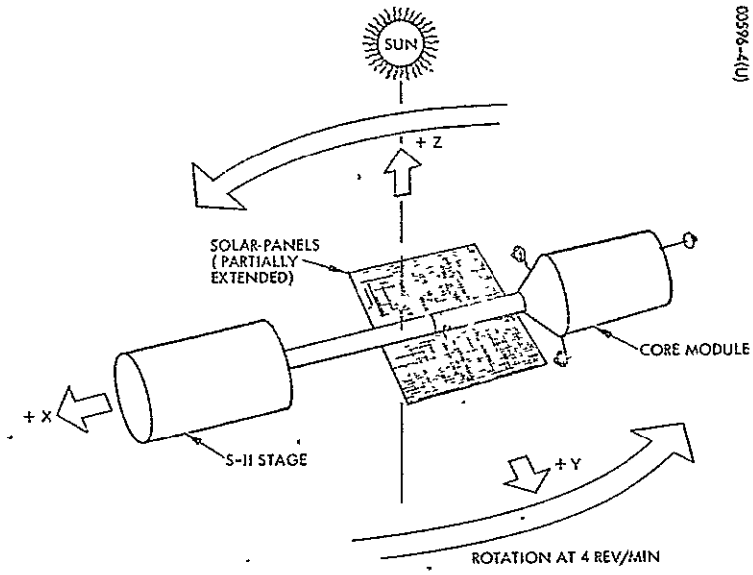

Figure 2-3. Space Station Artificial Gravity Mode

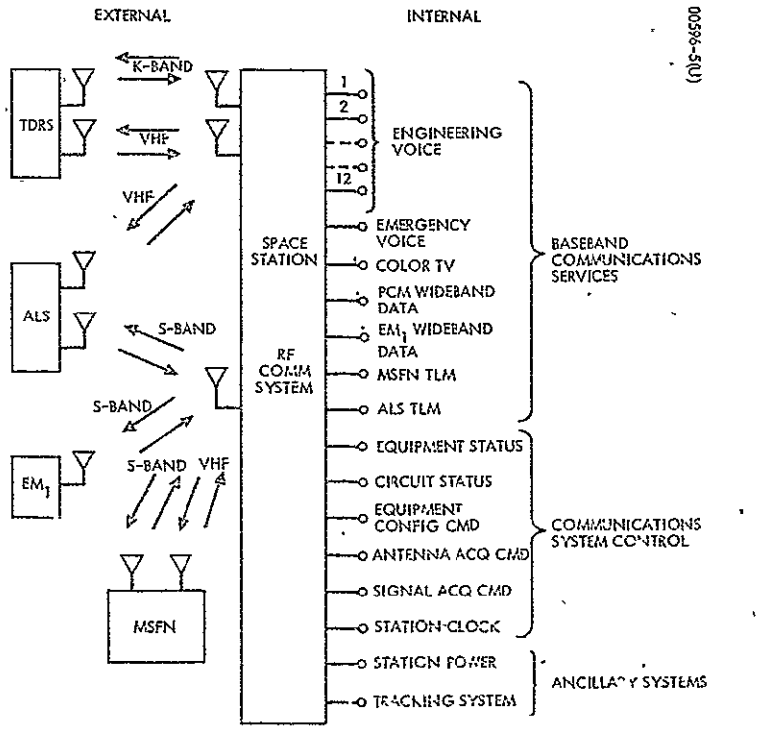

Figure 2-4. RF Communications System Interface

TABLE 2-4. EXTERNAL INTERFACE DESCRIPTION

System	Frequency Band	Carrier Frequency		Polarization		P_c, dBw	T_s, °K	RF Bandwidth	Modulation		Antenna Gain dB	
		Transmit	Receive	Transmit	Receive				Type	Rate, Chips/Sec	Transmit	Receive
Space Station	K-band (Comm)	14.85 - 15.35 GHz	13.70 - 14.26 GHz	RHCP	LHCP	15.0	391	85 MHz	2ϕ PSK	40.4×10^6	42.5	41.9
	K-band (beacon)	15.35 GHz	14.26 GHz	RHCP	LHCP	-12.0	391	6.3 KHz	2ϕ PSK	1.5×10^3	42.3	41.7
	S-band (EM_1)	2100 - 2300	2100 - 2300	RHCP	LHCP	19.4	438	15 MHz	4ϕ PSK	7.38×10^6	-3.0	-3.0
	S-band (ALS)	2100 - 2300	2100 - 2300	RHCP	LHCP	19.4	438	244 KHz	2ϕ PSK	115.2×10^3	-3.0	-3.0
	VHF	149.22 - .32 MHz 135.60 - .70 MHz	135.60 - .70 MHz 149.22 - .32 MHz	RHCP	RHCP	18.1	723	43 KHz	FM $\beta = 5$	3 KHz	-3.0	-3.0
DRS	K-band (comm)	13.70 - 14.2 GHz	14.85 - 15.35 GHz	LHCP	RHCP	7.0*	1200	85 MHz	2ϕ PSK	40.4×10^6	41.9	42.5
	K-band (beacon)	14.26 GHz	15.35 GHz	LHCP	RHCP	-16.5	1200	6.3 KHz	2ϕ PSK	1.5×10^3	15.0	15.0
	VHF	135.60 - .70 MHz	149.22 - .32 MHz	RHCP	RHCP	12.7**	800	43 KHz	FM $\beta = 5$	3 KHz	15.0	15.0
ALS	S-band	2100 - 2300	2100 - 2300	LHCP	RHCP	18.4	800	244 KHz	2ϕ PSK	115.2×10^3	-3.0	-3.0
	VHF	135.60 - .70 MHz 149.22 - 32 MHz	149.22 - .32 MHz 135.60 - .70 MHz	RHCP	RHCP	20.1	800	43 KHz	FM $\beta = 5$	3 KHz	-3.0	-3.0
EM_1	S-band	2100 - 2300	2100 - 2300	LHCP	RHCP	19.4	438	15 MHz	4ϕ PSK	7.38×10^6	20	20

Transmitted C/N ≥ 15.0 dB at K-band

** Transmitted C/N ≥ 12.5 dB at VHF

TABLE 2-5. INTERNAL INTERFACE DESCRIPTION

Interface Group	Circuit Descriptor	Number of Circuits		Signal Description
		Input	Output	
Baseband communications services	Engineering voice	12	12	300 to 3000 Hz delta-mod voice, inband signalling
	Emergency voice	1	1	300 to 3000 Hz analog voice; dedicated
	Color TV	1	1	NTSC video
	PCM wideband data	2	2	Synchronous data in 2.4576 megabit increments to 17.2032 megabit; 2 increments maximum simultaneous with TV
	EM_1 wideband data	1	1	Synchronous data, 7.3728 megabits maximum
	MSFN telemetry ALS telemetry	22	22	Two pairs each; four 19.2 kilobits and 7, 307.2 kilobits synchronous data channels
Communication system control	Equipment status	--	A.R.*	Continuous monitoring (AGC, RF power out, etc.) 0 to 5 volts, Z = 1000 ohms; discrete (command confirmation, etc.) circuit closure to ground

* A.R.: As Required

Interface Group	Circuit Descriptor	Number of Circuits		Signal Description
		Input	Output	
Communication system control (continued)	Circuit status	---	A.R.	Digital channel sync word errors (5 to 10 bit word); subframe assignments (8 bit word); frame buffer register count
	Equipment configuration command	A.R.	---	Redundancy selection, parallel circuit closure to ground; antenna selection, parallel circuit closure to ground
	Antenna ACQ command	A.R.	---	Parallel, axis I.D., 10 to 20 bit word
	Signal acquisition command	A.R.	---	Parallel, channel I.D., ± 1 volt scaled
	Station clock	1	---	19.6608 megabits/sec clock pulse
Ancillary systems	Station power	A.R.	---	56 volts dc and 400 Hz per NAR
	Tracking system	2	2	S-band; compatible channel assignment; omni coverage @-3 dB by two overlapping patterns

* A.R.: As Required

channel. The PCM data, however, is externally processed, so two interfaces are provided for both transmit and receive to enable continuous handover operations. The MSFN and ALS telemetry circuits are similarly externally generated, and so duplicate terminations are provided for each channel.

The detailed communication system control interface cannot be defined at this point as it is intimately related to the baseband and communication control equipment design. Typical signal descriptions are provided, however, to give an understanding of the scope and nature of this interface. The power system interface is straightforward, but as in the instance of the control interface, the specific voltages required by each subsystem can only be determined by considering detailed equipment designs. The tracking system interface has dual transmit and receive ports corresponding to the circumferential and axial arrays.

2.5 SYSTEM COMPATIBILITY

The need was recognized during the design phase for maintaining compatibility between the various portions of the baseline system. Incompatibility was prevented wherever possible simply by minimizing the number of interconnections and interdependences. Design decisions were also influenced by reports of certain problems which have been discovered during operational use of the Apollo communications system. The Apollo tracking system is particularly susceptible to amplitude modulation at frequencies of 50 Hz and 100 Hz, the error signal multiplexing frequencies. Incidental amplitude modulation is caused by subcarrier oscillator imperfections, carrier amplitude modulation, and intermodulation between the range code and the subcarriers (References 2-1 and 2-2). And, in the wide-beam acquisition mode, the Apollo command module high gain antenna occasionally acquires a multipath signal reflected from the spacecraft surface. (Reference 2-3)

The baseline autotrack antenna system was especially designed to avoid these problems and to minimize the possibilities of incompatibilities. The system normally tracks on a beacon signal provided by the DRS. This beacon originates at the DRS, and the communication signal cannot interfere with either its generation or reception. No significant tracking errors should occur due to "incidental amplitude modulation" of the beacon; its biphase PSK signal structure is quite simple and easily implemented. The antenna error signals generated by the autotrack system are demodulated within the RF-IF subsystem by an (incoherent) envelope detector. This type of detector was recommended for Apollo after studies of certain autotrack system difficulties, due to up-link modulation. The Space Station autotrack system will also not acquire signals reflected from the spacecraft surface. This is achieved by the use of precise initial pointing, a narrow (1 degree) acquisition beamwidth, and careful antenna placement on the vehicle.

Ranging for orbit determination can cause no degradation in antenna tracking or communications performance because it is accomplished by a separate system. Input/output ports to the Space Station S-band antenna system are provided at RF for a turnaround transponder compatible with the TDRSS.

Because the ranging and antenna tracking functions are separated from the data transmission function, the signal structures at both K-band and S-band are optimized only for the communications function. The signal format used for the DRS link is biphase PSK directly on the carrier. Time division multiplexing (TDM) is used rather than frequency division multiplexing with subcarriers. In Apollo, intermodulation between the baseband voice and the telemetry subcarrier may cause significant degradation. In the baseline system, the presence of nonlinearities will not generate significant intermodulation noise in the signal structure. The multiplexed data types are generated by source encoders which produce highly random bit streams. Furthermore, a convolutional encoder is used which will tend to randomize the data stream. Therefore, the signal structure between the convolutional encoder and decoder will appear to have few prominent spectral components. Any intermodulation products will be at very low levels.

In the FDM structure of the Apollo Unified S-Band, a residual component is present at the carrier frequency for receiver tracking, however, the receivers have shown a tendency to lock on spurious components near the carrier at frequencies related to the telemetry bit rate. The telemetry rate on the 1.024 MHz subcarrier is 51.2 kilobits/sec (Reference 2-4). False acquisition by the various digital receivers of the baseline system presented here will not occur. The carrier phase tracking loops track a replica of the carrier obtained by squaring the communications signal. (For the quadriphase link, a X4 loop is used.) This straightforward implementation will not generate components that the tracking loop might falsely acquire.

No incompatibilities are forseen between the communications electronics and the Space Station power conditioning system. For example, the frame synchronization scheme was designed to accommodate the power transients. Furthermore, the various electronics units are packaged for protection against EMI and are separated physically from other systems.

As stated above, no attempt was made to design a unified communications system of the Apollo Unified S-Band type. The opposite approach was used in order that the individual functions could be accomplished by units optimized for that purpose. It remains the responsibility of the communications control facility to operate the system in a coordinated manner either by automatic or manual control.

2.6 REFERENCES

2-1. "Tracking Effect due to IAM on the Uplink Mode Containing both S-Band Subcarriers," TRW Systems Group, under Contract NAS 9-4810, to the Manned Spacecraft Center, 18 March 1968.

2-2. "Electronic System Test Program, CSM Block II Unified S-Band System Compatibility and Performance Final Report (Section 11)," EB 68-3119 (u) NASA MSC/ISD, February 1969.

2-3. "An Investigation of the Multipath Problems Associated with the Apollo CSM and LM S-Band High Gain Communication Antenna Tracking Systems," TRW Systems Group, under Contract NAS 9-8166 to the Manned Spacecraft Center, 16 December 1968.

2-4. "Electronic System Test Program, CSM Block II Unified S-Band System Compatibility and Performance Final Report (Section 10)," EB 68-3119 (u) NASA MSC/ISD, February 1969.

3. ANTENNA SUBSYSTEM

3.1 INTRODUCTION

The antenna subsystem block diagram is shown in Figure 3-1. The K-band section contains the high gain antennas, the antenna masts and erection mechanisms, the pedestal and servo systems, and the associated RF gear, such as preamplifiers and power amplifiers. The S-band section consists of two broad-beam arrays and preamplifiers. The VHF section also consists of two arrays and their preamplifiers. The S-band and VHF power amplifiers are part of the RF-IF subsystem because they are physically colocated with the IF equipment.

Figure 3-2 shows the NAR Space Station configuration and the location of the various antennas, and Table 3-1 summarizes the physical characteristics of the antenna subsystem. The weight figures are detailed in Table 3-2. The power required assumes a typical operating condition with only one K-band power amplifier active. The volume requirements are specified for the electronics components only.

3.2 K-BAND SECTION

Three K-band antenna groups are employed. The antennas and pedestals are mounted on masts spaced 120 degrees about the circumference of the station. The two masts at the forward end of the station are folded down to the conical section during launch. These are arranged so that their azimuth axes are collinear for despinning in the artificial g mode. The third mast folds into the inner-stage area at the aft end. The masts are erected and locked after normal station operations are begun.

A 48-inch parabolic reflector is used with a five-horn Cassegrain feed. Table 3-3 summarizes the characteristics of the K-band antenna. The detailed gain and loss budget is given in Table 3-4. Its physical dimensions appear in Figure 3-3. Note that an equipment compartment at the rear of the dish contains the monopulse circuitry and preamplifier.

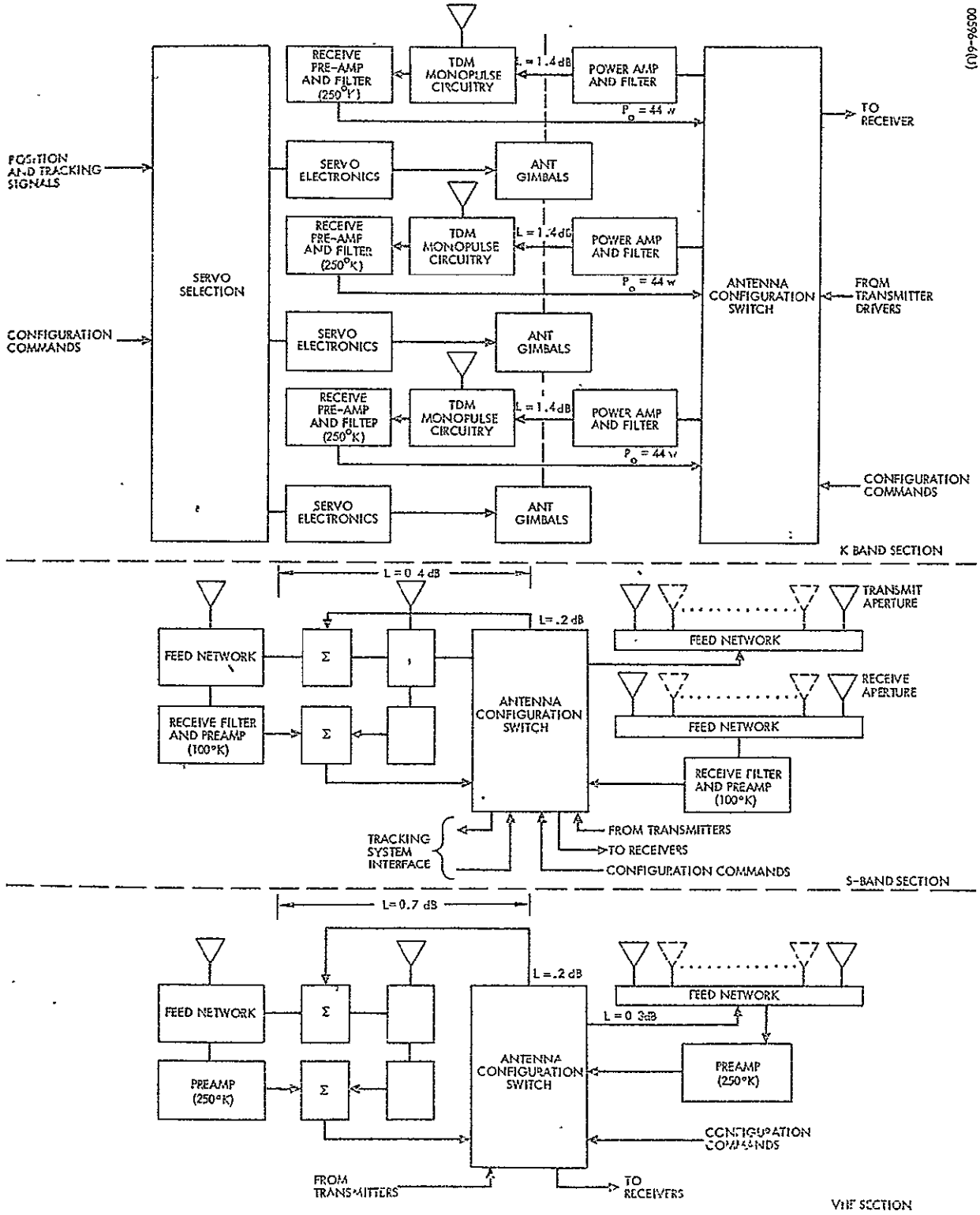

Figure 3-1. Antenna Subsystem Block Diagram

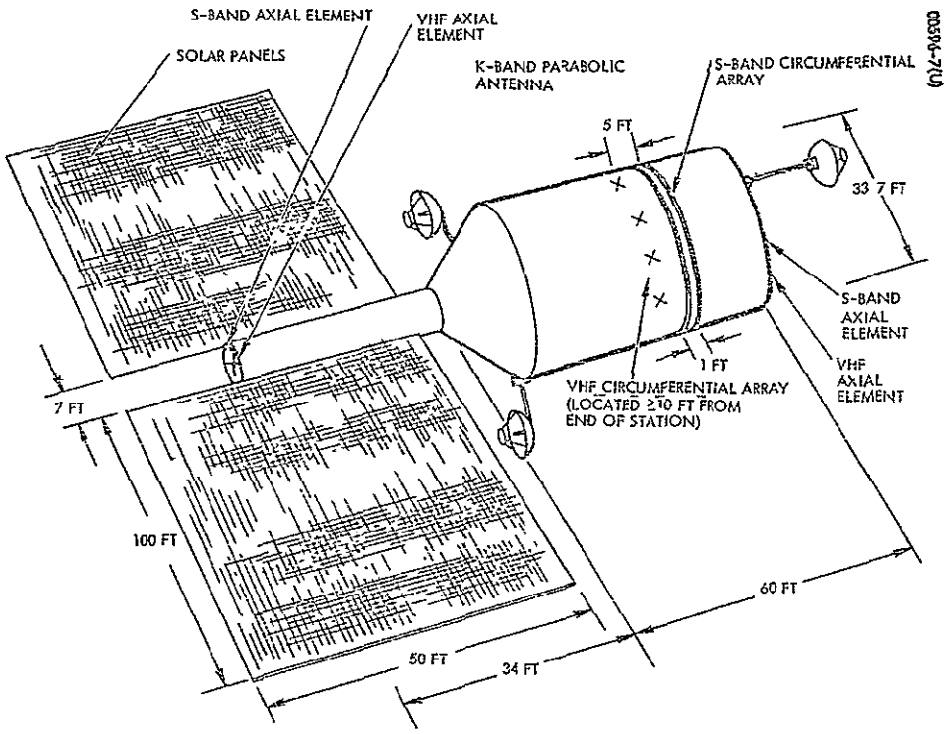

Figure 3-2. Space Station Configuration (North American Rockwell)

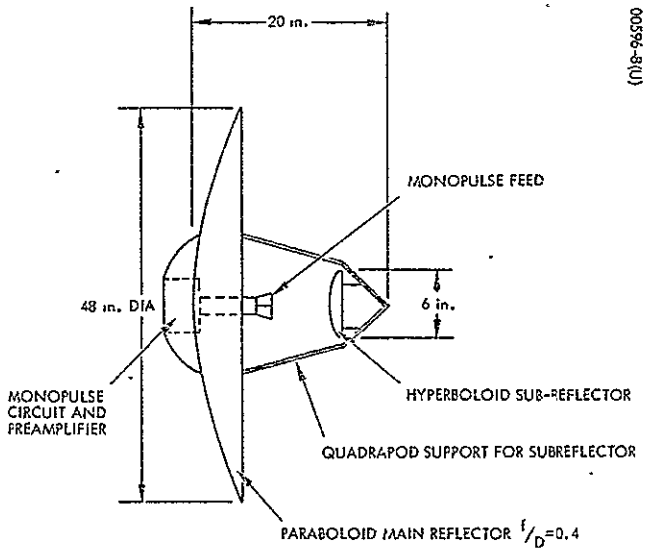

Figure 3-3. Cassegrain Reflector Antenna

Item	Weight, Pounds	Power, Watts	Volume, Cubic Inches	Location
K-Band				
Reflector and feed package	11.2	6.0	---	A
Servo electronics	2.5	5.0	50	B
Pedestal	39.0	14.0	---	A
Mast and mechanism	22.0	---	---	A
RF power amplifier	24.0	220.0	300	B
Configuration switch	1.0	---	10	C
One Antenna Group	99.7	245.0	360	
K-Band Section*	299.1	245.0	1,080	
S-Band				
Circumferential array and feed	350.0	---	---	---
Axial array and feed	62.0	---	---	---
Preamp and filters (3)	9.0	18.0	120	A
Configuration switch	2.0	---	300	C
S-Band Section	423.0	18.0	420	
VHF				
Circumferential array and feed	66.0	---	---	---
Axial array and feed	24.0	---	---	---
Preamp and filters (3)	3.0	0.3	30	A
Configuration Switch	1.0	---	30	C
VHF Section	94.0	0.3	60	
TOTAL	816.1	263.3	1,560	

*Assumes one antenna group active
**Electronics only

TABLE 3-2. ANTENNA WEIGHT ESTIMATES

	Weight, Pounds
S-Band	
Circumferential Array (1/16-inch aluminum)	
Two radiating apertures (TX and RY)	88
Two corporate feeds (TX and RY)	262
Total	350
Axial Array	
Two radiating elements and feed	5
100 foot waveguide (20-mil aluminum)	32
100 foot cable (coax and power)	25
Total	62
S-Band Total	412
VHF	
Per radiating element	
Dipole, balun, and hybrid	1
Pop-up mast and base	1
Element Total	2
Circumferential Array	
Aperture (18 elements)	36
Corporate feed	30
Total	66
Axial Array	
Aperture (two elements)	4
100 foot cable (coax and power)	20
Total	24
VHF Total	90

TABLE 3-3. K-BAND ANTENNA SUMMARY CHARACTERISTICS

Design	Cassegrain, 5 Horn Time Division Monopulse
Reflector Diameter:	48 Inches
Wideband Gain:	
Transmit:	42.5 dB @ 14.825 GHz
Receive:	41.9 dB @ 13.725 GHz
Polarization (4 db Axial Ratio)	
Transmit:	RHCP
Receive:	LHCP
Beamwidth (-3 dB)	1.25 Degree
Gimbal Design:	Three Axis, Hemispheric Coverage Without Tracking Interruption
Servo Design:	Torque Motor Drive With Digital Position Feedback
Signal Inputs:	Monopulse Tracking Errors, Manual Slew and Digital Positioning Commands

Figure 3-4 shows the three-axis antenna gimbal design. The addition of the cross-axis gimbal to the conventional elevation/azimuth mount permits tracking without interruption over a viewing area greater than a hemisphere. During auto-track operation, the cross-axis and elevation axes are controlled by the monopulse error signals. The azimuth axis is slaved in such a manner as to maintain orthogonality between the elevation and cross-axis using the cross-axis angle transducer as a signal source. As the line of sight to the DRS approaches the zenith region of the control system (that is, along the azimuth axis), the azimuth gimbal tracking loop gradually becomes ineffective in maintaining this orthogonality. The tracking loop is eventually disabled by the zenith logic unit. The antenna then tracks through the zenith region as an X-Y mount. The highest tracking rate required of this system is 4.5 deg/min on any axis. In the tracking mode, the communications control facility provides a constant velocity command input to the azimuth axis at the Space Station relay.

TABLE 3-4. CASSEGRAIN REFLECTOR ANTENNA GAIN AND LOSS BUDGET, dB.

Center Frequency, GHz	13.725		14.825	
Area gain, dB		44.9		45.6
Losses, dB				
Illumination efficiency	0.5		0.7	
Spillover efficiency	1.0		0.8	
Hyperboloid blockage	0.2		0.3	
Hyperboloid support blockage	0.5		0.5	
Reflector surface error (σ_n = 0.015", σ_s = 0.005")	0.2		0.2	
Feed, ohmic	0.3*		0.3	
Cross-polarized power	0.3		0.3	
Total	3.0		3.1	
Expected gain at center frequency		41.9		42.5
Additional loss over 0.950 GHz band	0.2		0.2	
Gain at band edge		41.7		42.3

*Contributes to system noise temperature

Figure 3-5 illustrates the antenna servo system. The power amplifiers, torque motors, tachometers, and resolvers are located on the gimbal structure. The servo electronics shown is located in the equipment shelf. The monopulse feed network generates signals $\Delta 1$ and $\Delta 2$ in proportion to the pointing error in two orthogonal planes. The signals are amplitude modulated onto the sum channel after time division multiplexing. The resulting signal is passed through a single preamplifier and then sent to the RF-IF subsystem for further processing. This subsystem recovers the tracking signals and forwards them to communications control. Normal operation entails tracking on the DRS beacon; the design also permits track-on-comm as a backup capability with negligible degradation. The time multiplexed $\Delta 1$ and $\Delta 2$ signals are sent to the servo electronics unit by communications control (at the bottom of Figure 3-5) and after multiplexing, they are passed through shaping circuits and used to control

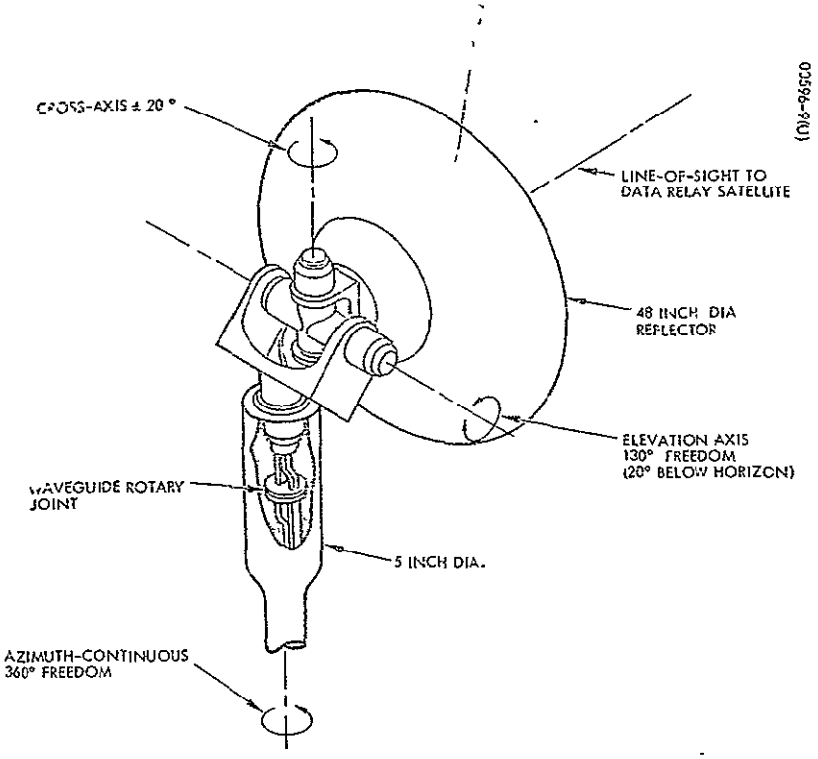

Figure 3-4. K-Band Antenna Gimbal System

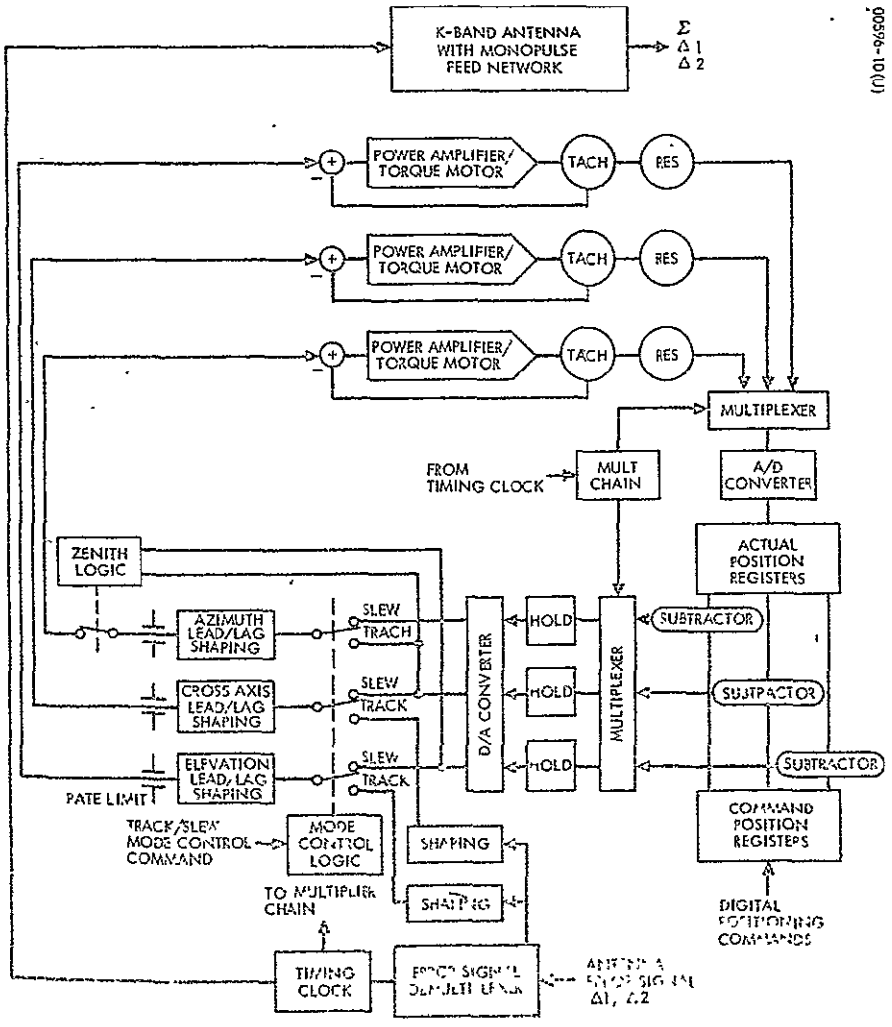

Figure 3-5. K-Band Antenna Servo Block Diagram

the cross-axis and elevation drive motors. The repositioning of the antenna boresight by these motors completes the autotrack feedback loop.

The antenna servo system also functions in a slew mode for automatic prepositioning of the antenna at handover or for manually assisted prepositioning. When the mode control logic selects the slew mode, the control loop detailed in Figure 3-5 becomes active. The loop error signals are formed by subtracting the contents of the command position register and the actual position register. Slewing continues until the loop error is zero on all axes. A rate limit is included to prevent excessive slew rates.

The sum channel of the monopulse feed network is initially processed in a unit placed directly behind the reflector. A receiver filter is provided and a 250°K uncooled, parametric amplifier is used. The receive K-band waveguide is separated at a coaxial rotary joint just below the azimuth drive and then is routed within the antenna mast to the equipment shelf at the base.

The transmitter includes a K-band traveling-wave tube amplifier (TWTA) located within the equipment shelf. The TWTA output is 44 watts with a 25 percent efficiency; the associated high voltage power supply is 80 percent efficient. Passive thermal control is used within the equipment shelf containing the amplifier. A loss of 1.4 dB is budgeted for the signal path from the output of the TWTA to the antenna feed port. The transmit signal is inserted through the coaxial rotary joint in the azimuth axis and through a rotary joint in the gimbal opposite the receive channel at the elevation axis.

3.3 S-BAND SECTION

The S-band antenna system consists of two separate arrays. The general coverage provided by these arrays is shown in Figure 3-6. The circumferential array provides a toroidal pattern centered about the Station's longitudinal axis. When the Station is in the X-POP (X-axis perpendicular to the orbit plane) attitude mode, this antenna provides good coverage to vehicles approaching the Station for rendezvous, and to ground tracking stations. The axial array provides coverage in the +X and -X directions. With the X-axis oriented along the velocity vector during Y-POP operations, the axial array is utilized for the S-band links to the ALS and EM_1.

The circumferential array has separate transmit and receive apertures spaced 1 foot apart, center-to-center (see Figure 3-2). Figure 3-7 illustrates the power division network used for the feed. Each radiating element is 6.47 feet long and has 18 slots and loops of the type shown in Figure 3-8. The system transmits at S-band with left-hand circular polarization (LHCP) and receives with right-hand circular polarization (RHCP). A section of the transmit/receive patterns is shown in Figure 3-9.

The axial array uses one element at either end of the Station (see Figure 3-2). The axial element design is shown in Figure 3-10. This

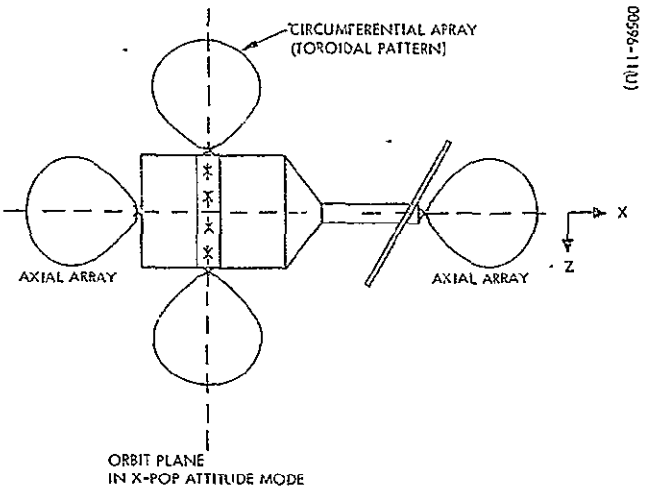

Figure 3-6. Omnidirectional Antenna Placement and Coverage S-band and VHF

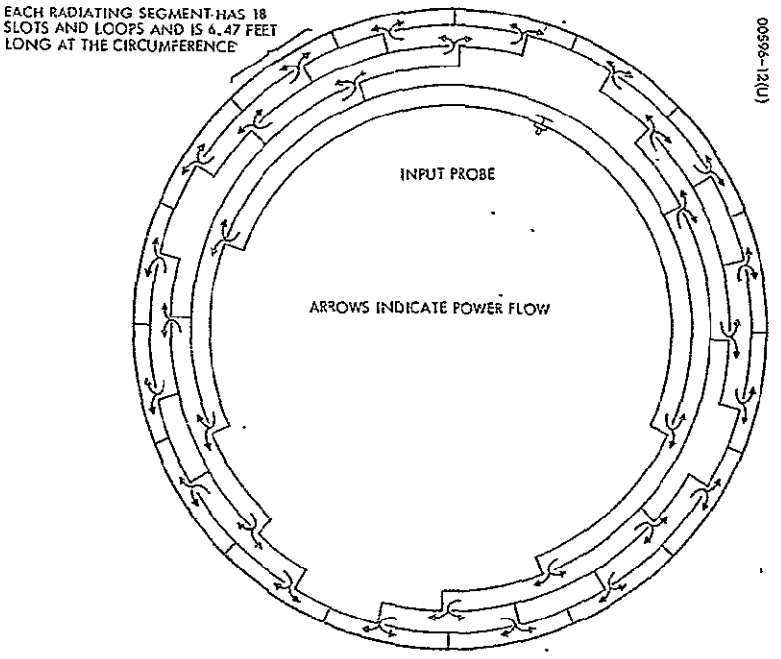

Figure 3-7. S-Band Circumferential Array Feed Network

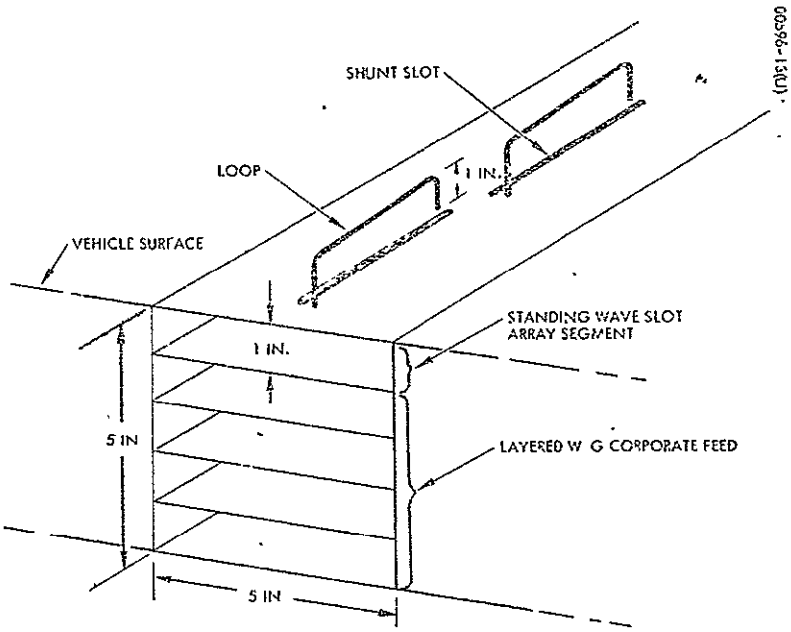

Figure 3-8. S-Band Circumferential Array Element

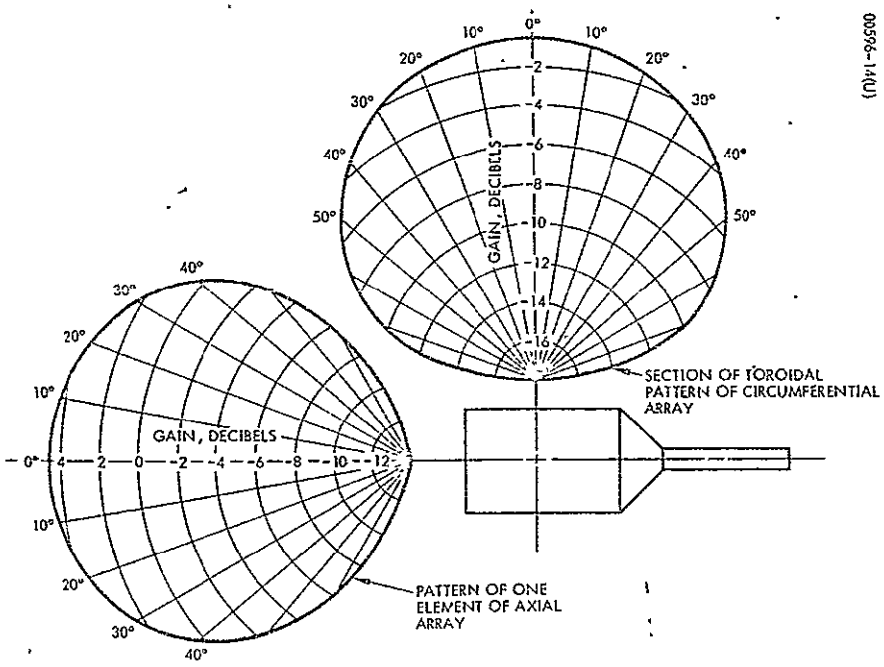

Figure 3-9. Gain Patterns of S-Band Arrays

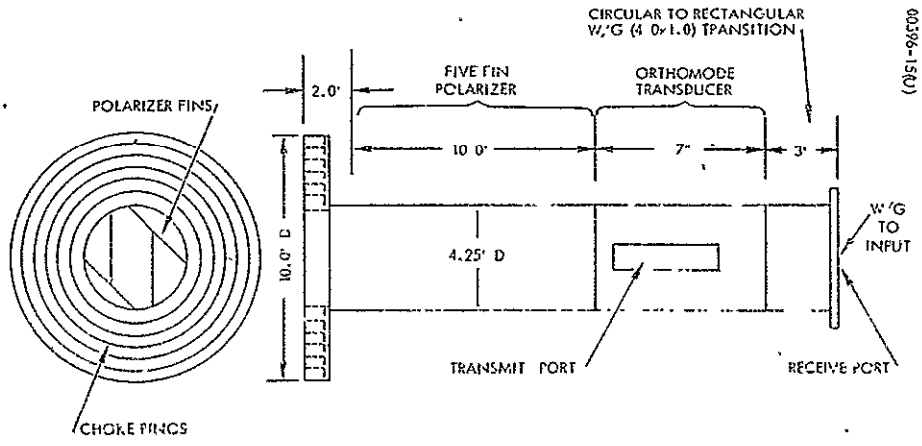

Figure 3-10. S-Band Axial Element

element provides both RHCP and LHCP for transmit/receive isolation and, in addition, the element design provides a high degree of isolation from surrounding structure. For this reason, the element may either be mounted flush with the skin surface or it may be permitted to protrude. The pattern of one element is shown in Figure 3-9. Table 3-5 summarizes the performance of the two arrays.

Three 100°K uncooled parametric amplifiers and associated filters are used in the receive channels. One is positioned at the output port of the circumferential array and the other two are colocated with the two axial array elements.

TABLE 3-5. PERFORMANCE OF S-BAND ARRAYS

Circumferential Array**			Axial Array*	
Degrees Off Axis	G	Ellipticity, dB	G	Ellipticity dB
0	-0.5	1	+4.5	1
10	-0.8		+4.3	
20	-1.3		+3.5	
30	-2.2		+2.3	
40	-3.5		+0.3	
45	-4.3	5	-1.0	3
50	-5.2		-2.5	
60	-7.3	10	-6.5	6
70	-9.6		-10.5	
80	-13.5		-14.5	

Ohmic loss (per element) = 0.3 dB
Ripple = ±1 dB at 0 degree, ohmic loss = 1.2 dB

The configuration switch shown within the S-band section permits connection of the desired antenna array and IF units and the input/output interface with the MSFN tracking system.

3.4 VHF SECTION

The VHF antenna system consists of two separate arrays. The coverage these patterns provide is very similar to the coverage of the S-band arrays. (See Figure 3-6.) The patterns are optimized to provide coverage in the directions defined by the principal axes of the spacecraft. The circumferential array consists of 18 crossed-dipole elements. The feed network is shown in Figure 3-11. Because the antenna must provide RHCP on both transmit and receive, transmit/receive isolation is achieved by the use of a frequency diplexer. A typical element is shown in Figure 3-12. After launch, the mast telescopes out to the full 10-inch length, which the design requires. A section of the transmit/receive patterns is shown in Figure 3-13.

The axial array uses one of the crossed-dipole elements at each end of the Station. The pattern of one element is shown in Figure 3-13. Assuming a requirement for only -3 dB gain, a useful beamwidth of 100 degrees was attained. Table 3-6 summarizes the performance of both VHF arrays. Three 250°K tunnel diode preamplifiers are used. One is located at the output port of the circumferential array. The other two are located at each end of the Space Station near the axial array elements.

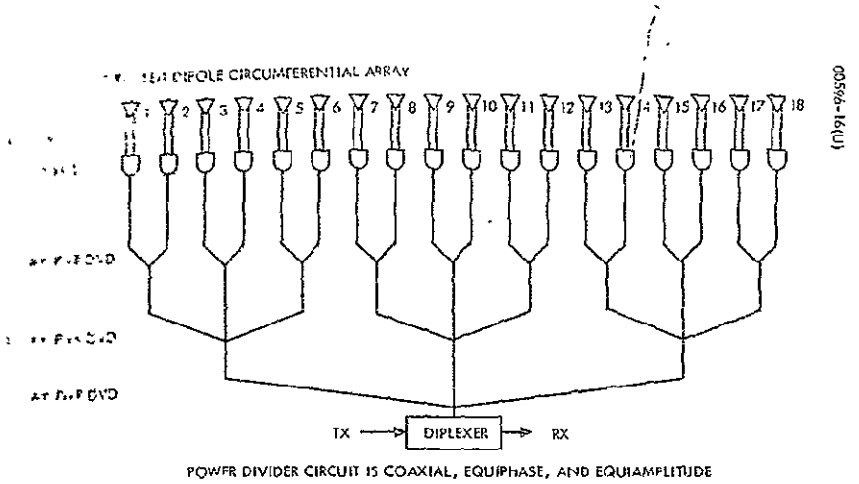

Figure 3-11.
VHF Feed Network

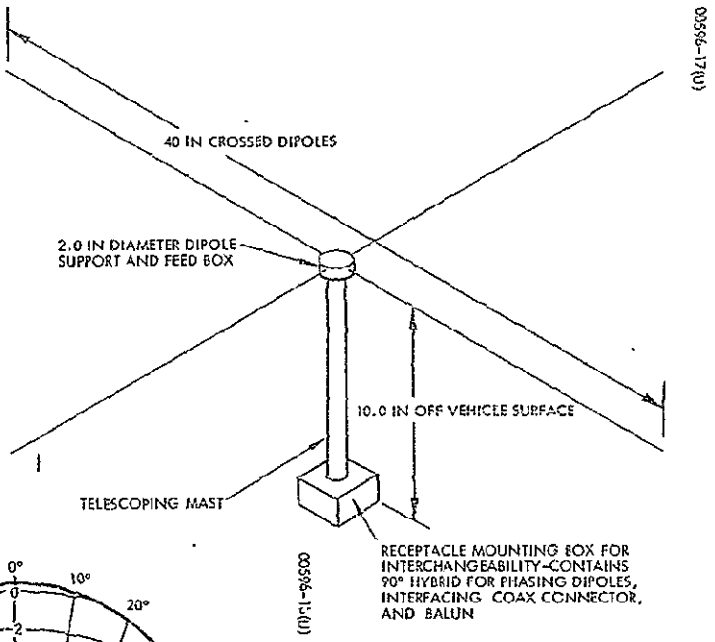

Figure 3-12.
VHF Array Element

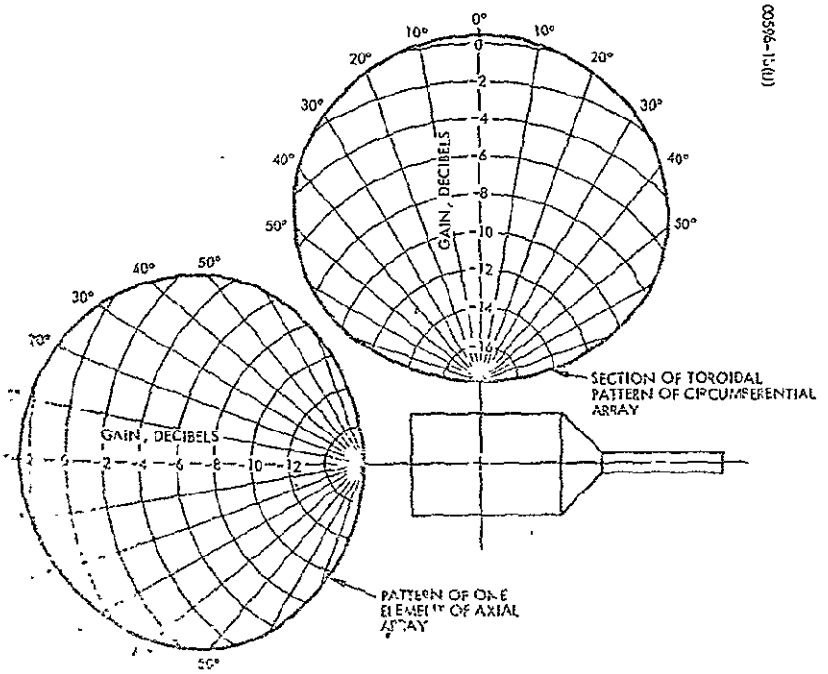

Figure 3-13.
Gain Patterns of VHF Arrays

TABLE 3-6. PERFORMANCE OF VHF ARRAYS

VHF Antenna Performance

Circumferential Array**			Axial Array*	
Degrees Off Axis	G	Ellipticity, dB	G	Ellipticity dB
0	+0.5	1	+2.5	1
10	+0.1		+2.2	
20	-0.5		+1.5	
30	-1.6		+0.5	
40	-3.0		-1.1	
45	-4.0	5	-2.0	5
50	-5.0		-3.0	
60	-7.5	10	-5.5	10
70	-10.5		-8.5	
80	-14.5		-12.5	

*Ohmic Loss (per element) = 0.4 dB
**Ripple = ±1 dB at 0 Degree, Ohmic Loss = 1.5 dB

4. RF-IF SUBSYSTEM

4.1 INTRODUCTION

The RF-IF subsystem block diagram is shown in Figure 4-1, where the units indicated actually occur in triplicate. The subsystem consists basically of receive and transmit IF stages and the power amplifiers. The K-band power amplifiers are not included because excessive line losses forced their placement at the base of the antenna masts. The DRS beacon demodulator is included in this subsystem because it interfaces only with communications control -- it does not require a baseband interface with a communication system user. Because of the simplicity of the VHF emergency voice equipment, the modem is packaged with the RF-IF gear. The RF-IF subsystem is actually defined (as shown in Figure 4-1) as that hardware located between the configuration switches in the antenna and baseband subsystems. Figure 4-2 summarizes the physical characteristics of the subsystem. Note that the power indicated is a typical load not a peak load.

4.2 K-BAND SECTION

A single stage upconverter is used on the transmit side. The data, modulated on a 270 MHz source is up-converted to one of the satellite communication channel frequencies (14.85 to 15.35 GHz) by a channel selection command to the frequency synthesizer. This stage also upconverts the Space Station beacon to 15.35 GHz.

The receiver downconverter uses two stages in the parallel communication and beacon channels. The first stage of the communication channel downconverter permits selection of the appropriate DRS communications channel. The intermediate frequency of both the beacon and communication channel is 750 MHz. The second conversion generates a beacon second IF at 30 MHz and a communication channel second IF at 270 MHz. Frequency acquisition and tracking is accomplished at these second stages. Acquisition is aided by a doppler compensating offset based on computer generated estimates. Automatic frequency control (AFC) for both the communication and beacon channels is normally accomplished by tracking of the beacon. Communications signal AFC is used as a backup.

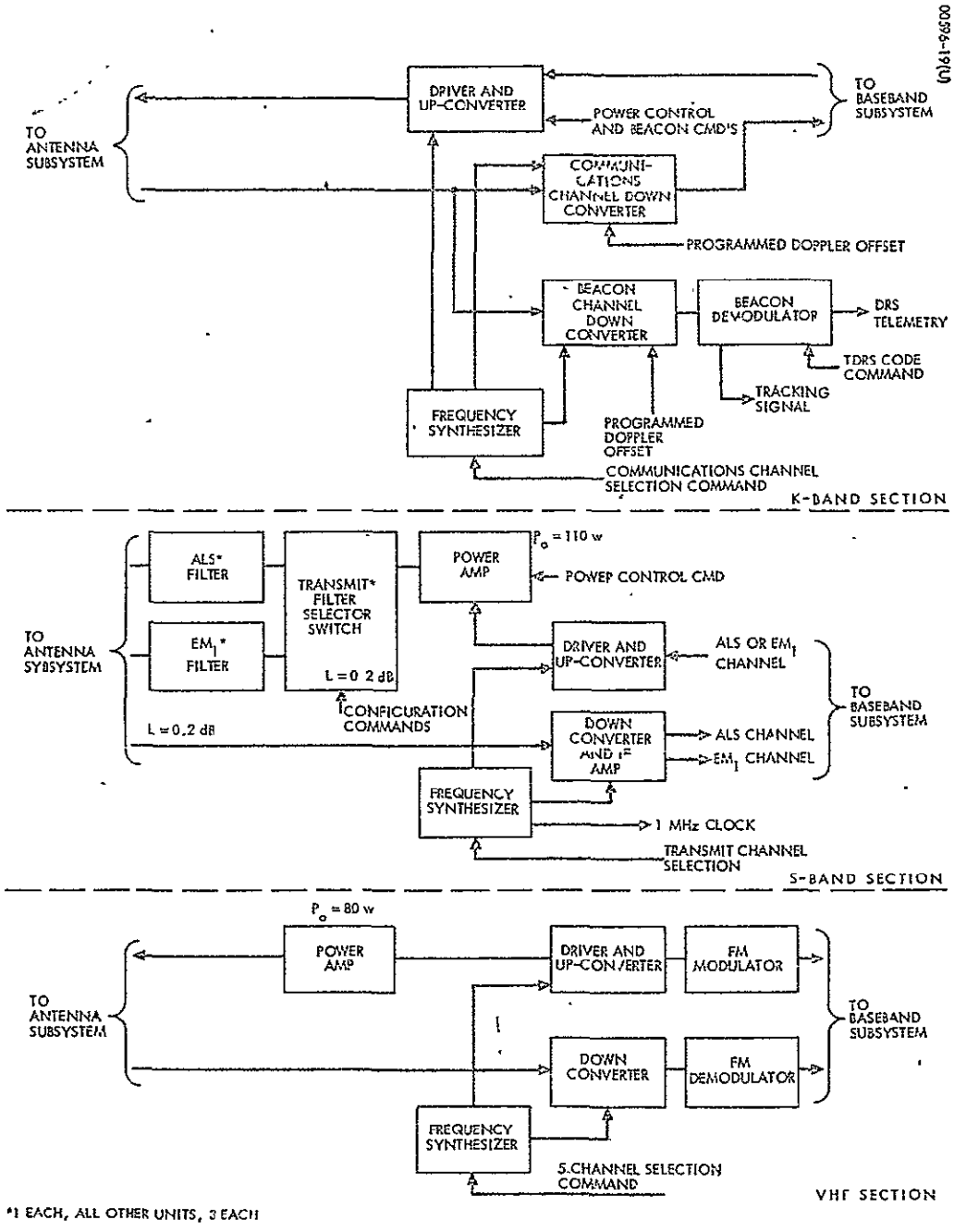

Figure 4-1. RF-IF Subsystem Block Diagram

The beacon demodulator is detailed in Figure 4-3. The device is a digital implementation of a delay lock PN code tracking loop and a biphase data demodulator. The generation of the inphase (I) and quadrature (Q) components occurs in mixers 1 and 2. The feedback connection of the data demodulation loop is seen at the bottom of the diagram. The code tracking error is generated by taking the difference of correlations of the incoming signal with an advanced and retarded replica of the reference code. The code of the desired DRS must be loaded into the PN reference generator by communications control. The beacon demodulator outputs 150 bits/sec PCM telemetry to communications control when beacon acquisition is established.

4.3 S-BAND SECTION

A double stage upconverter is used in the transmitter. The signal to be transmitted enters the RF-IF subsystem at either 3 MHz (ALS data) or at 50 MHz (EM_1 data). After the first upconverters, these signals are positioned within parallel IF's centered at 120 MHz. The second mixer in each channel generates an S-band output which is then passed to one of the power amplifiers. The power amplifier is a medium scale integrated circuit device; it generates 110 watts with 50 percent efficiency. The appropriate transmit filter is selected by commands from communications control.

The first mixers of the receiver are followed by parallel IF's for the ALS and EM_1 signals. Each is centered at 120 MHz; the bandwidth of the ALS amplifier is 1 MHz and that of the EM_1 is 16.2 MHz. The second stage in each of the IF's performs the AFC function. The second IF frequencies are 3 MHz for the ALS and 50 MHz for the EM_1.

4.4 VHF SECTION

The 3 kHz voice signal is frequency modulated on a 30 MHz carrier. This is up-converted to either 149 or 136 MHz. The power amplifier is a 60 percent efficient solid-state device, capable of 80 watts output at VHF. The receive side uses two stages of conversion (either 136 or 149 MHz to 30 to 3 MHz). Automatic gain control is performed at both IF stages; the bandwidth of each is 43 kHz. The demodulator is a threshold extension device.

ITEM	WEIGHT (LBS)	POWER (W)	VOLUME (IN^3)	LOCATION
[illegible] ELECTRONICS	10.0	20.0	700	C
[illegible] SECTION* (3)	30.0	20.0	2,100	C
[illegible] AMPLIFIER	10.0	220 0	200	C
[illegible] SWITCHES & FILTERS	2.0	---	24	C
[illegible] ELECTRONICS	20.0	18.0	700	C
ONE GROUP	32.0	238.0	1,124	C
S-BAND SECTION ** (3)	96.0	476.0	3,372	C
POWER AMPLIFIER	4 0	160 0	100	C
HF ELECTRONICS	5.0	6.0	700	C
ONE GROUP	9.0	166.0	800	C
VHF SECTION* (3)	27 0	166.0	2,400	C
TOTAL	153.0	496***	7,872	

* ASSUMES ONE GROUP ACTIVE
** ASSUMES TWO GROUPS ACTIVE
*** ASSUMES K-BAND AND S-BAND ACTIVE

Figure 4-2. RF-IF Subsystem Physical Characteristics

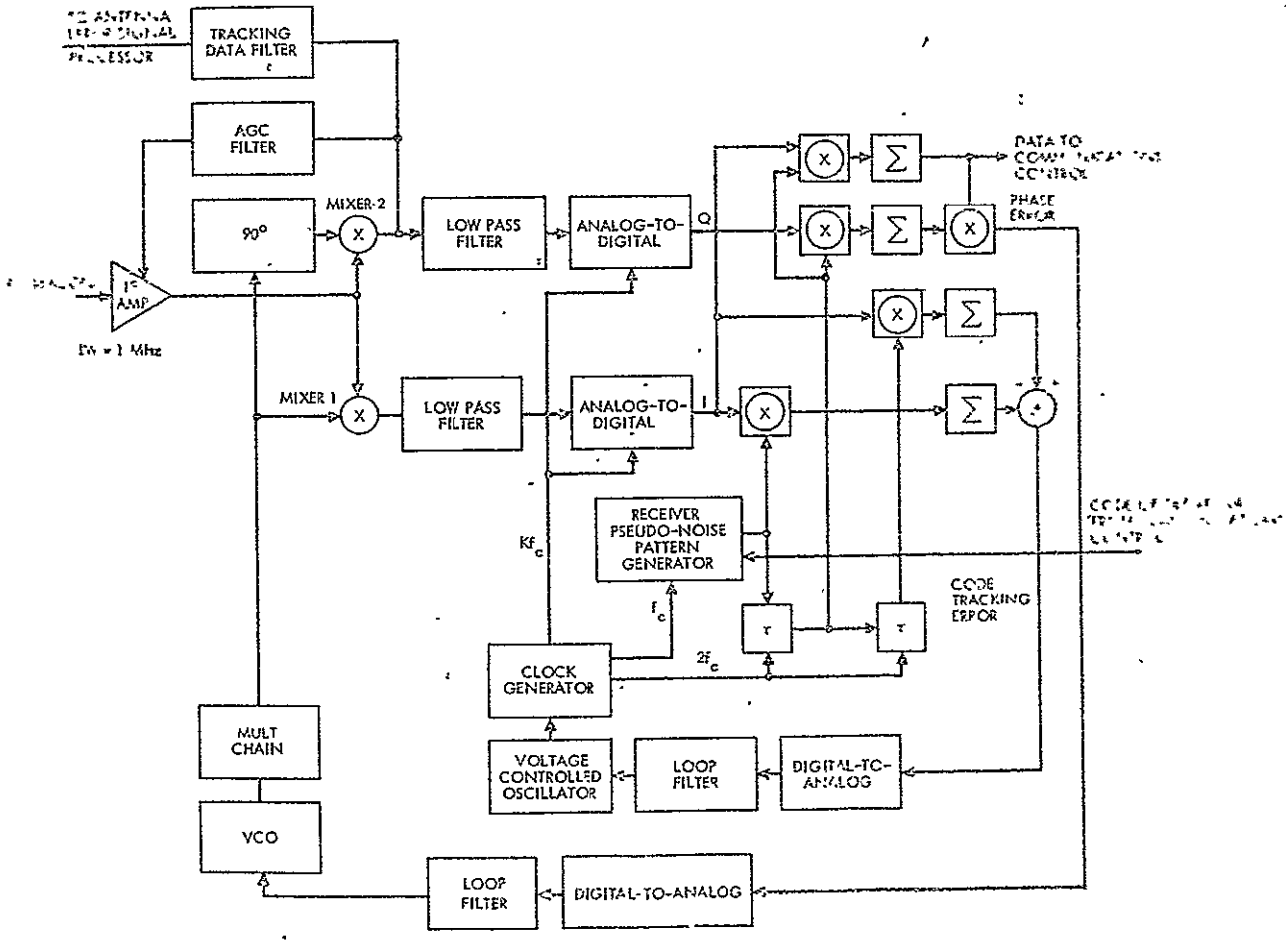

Figure 4-3. DRS Beacon Demodulator
Delay lock PN-code tracking loop

5. BASEBAND SUBSYSTEM

5.1 INTRODUCTION

The baseband subsystem block diagram is shown in Figure 5-1. As before, the units shown actually occur in triplicate for purposes of link continuity during handover and for redundancy. The subsystem consists basically of modulator/demodulators, digital channel encoder/decoders, and time division multiplex equipment. In the K-band section, digital source encoder/decoders are also provided which process the analog video and voice signals. Only digital data streams are passed across the S-band section interface; source encoder/decoders were not required. The VHF section contains little baseband equipment, as the FM modem is contained within the RF-IF subsystem. The baseband subsystem is delineated with respect to the other subsystems in Figure 2-1. Figure 5-2 summarizes the physical characteristics of the subsystem. Note that the power indicated is a typical load, not a peak load.

5.2 K-BAND SECTION

Modem

The modem consists of digital and analog portions. The convolutional encoder (K = 5, V = 2) accepts a data stream at approximately 20.2 megabits/sec and generates 40.4×10^6 subbits per second. The biphase modulation is accomplished at 270 MHz; the data is then passed to the configuration switch for routing to the proper RF-IF units. The biphase demodulator recovers a coherent carrier reference and subbit timing information. A filter and sample approach is used in the detection operation, but rather than a "hard decision" on the subbit, an analog to digital (A/D) converter quantizes the detector output and generates a 3-bit word. This digital output is processed by a parallel Viterbi decoder and the result is a 20.2 megabits/sec data stream. All the K-band gear can operate at 307.2 kilobits/sec in a fall-back mode.

TDM System

The transmit portion of the time division multiplex unit is shown in Figure 5-3. The unit accepts standardized Station-clock-synchronous data streams. The rates of either the TV or PCM data can vary from zero to 17.2032 megabits/sec in increments of 2.4576 megabits/sec with the

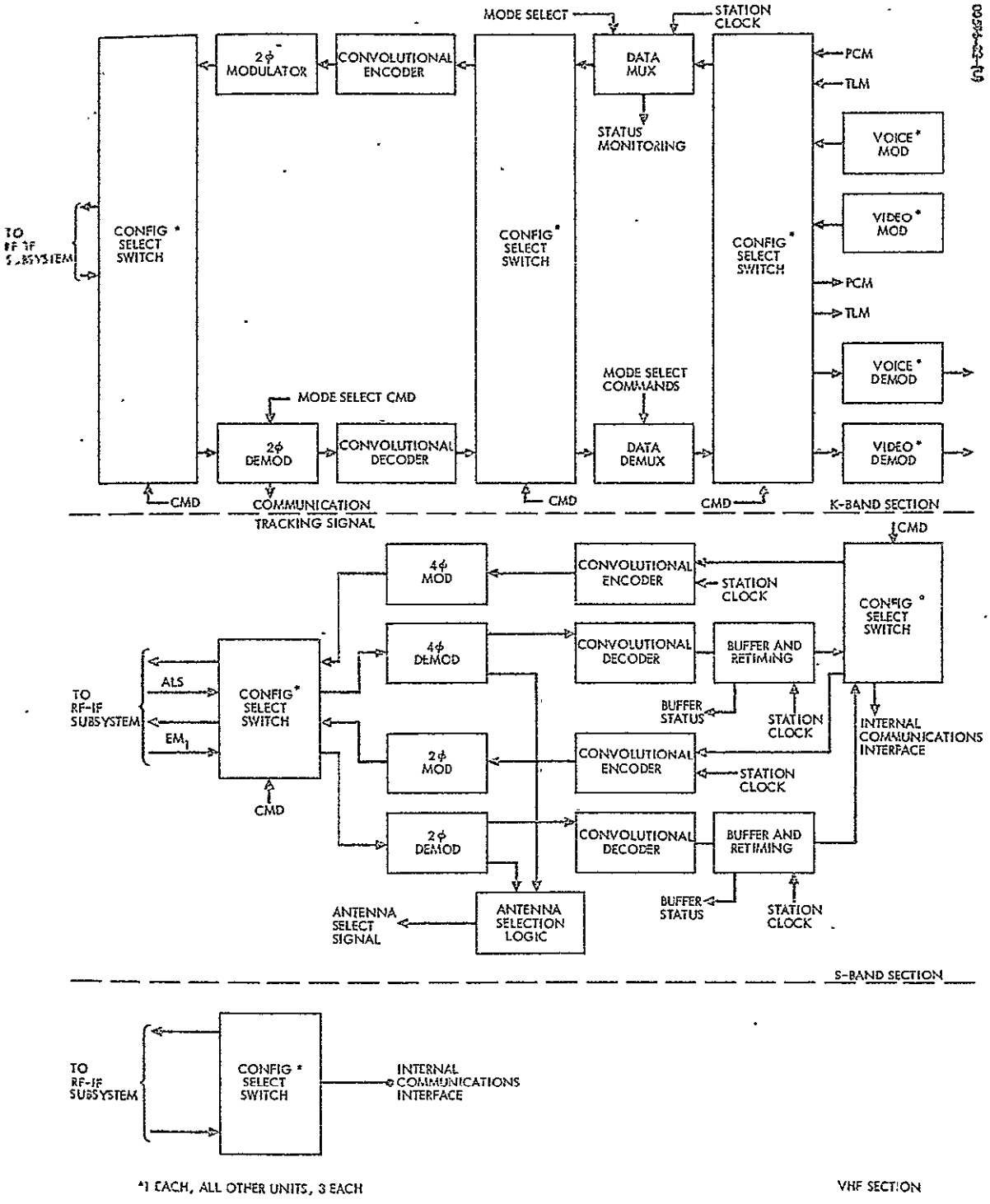

Figure 5-1. Baseband Subsystem Block Diagram

	ITEM	WEIGHT (LBS)	POWER (W)	VOLUME (IN^3)	LOCATION
K-BAND	MODEM	17.0	44.0	800	D&E
	TDM	62.0	100.0	2,000	D&E
	CONFIGURATION SWITCHES	3.0	---	1,000	D&E
	VOICE MODEM	16.0	12.0	800	D&E
	VIDEO MODEM	54.0	61.0	800	D&E
	ONE GROUP	152.0	217.0	5,400	
	K-BAND SECTION	410.0	217.0	11,000	D&E
S-BAND	ALS MODEM	12.0	19.0	400	D&E
	EM, MODEM	21.0	40.0	800	D&E
	CONFIGURATION SWITCHES	3.0	---	1,000	D&E
	ONE GROUP	36.0	59.0	1,840	D&E
	S-BAND SECTION *	102.0	59.0	4,600	D&E
	VHF CONFIGURATION SWITCH	2.0	---	400	D&E
	TOTAL	514.0	276.0	16,000	

* ASSUMES ONE BASEBAND GROUP ACTIVE.

00596-23(U)

Figure 5-2. Baseband Subsystem Physical Characteristics

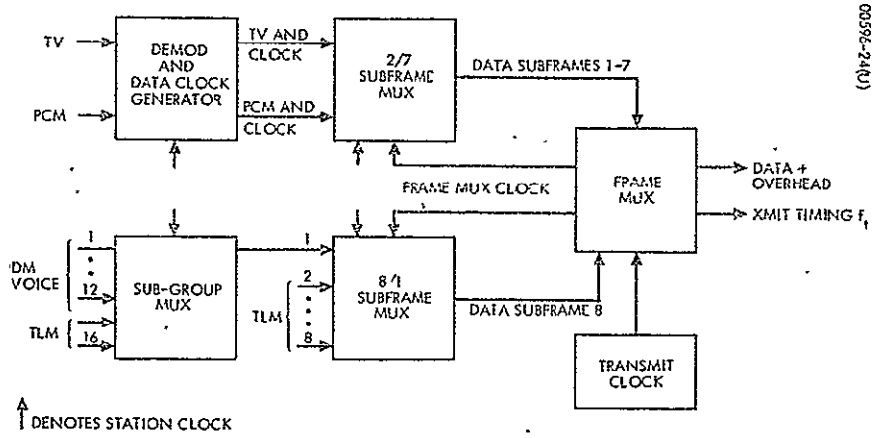

Figure 5-3. Transmit Block Diagram

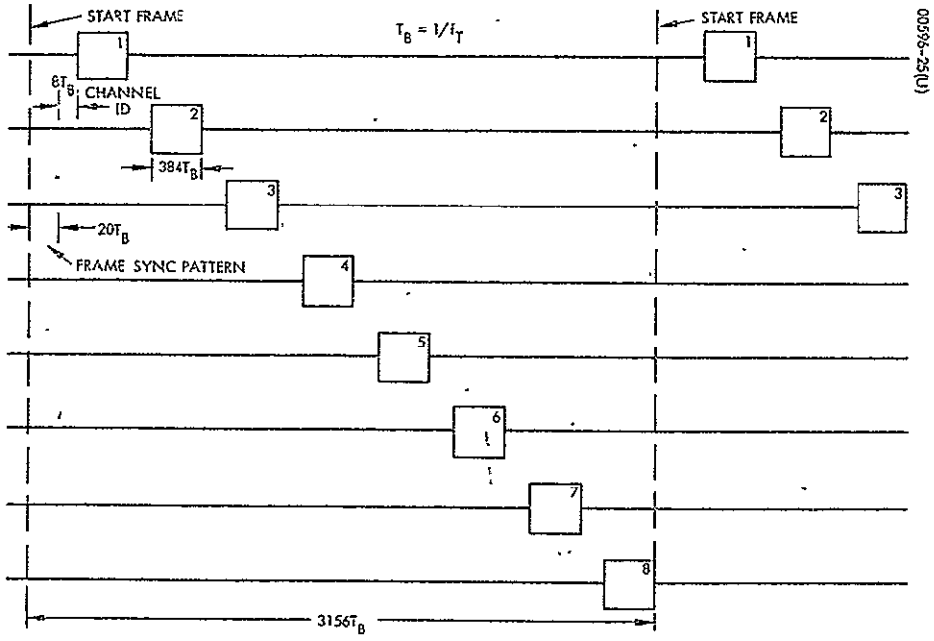

Figure 5-4. Frame Timing Diagram

...struction that the total TV and PCM rate can be no greater than 17.2032 ...bits/sec. The twelve voice channels are each 19.2 kilobits/sec and ...n of the four priority telemetry channels are 19.2 kilobits/sec. Seven ...2 kilobits/sec telemetry channels are also provided. The total avail... data capacity without overhead is 19.6608 megabits per second. Fig... ...-4 shows the frame timing diagram for the multiplexing process, includ... the addition of the channel ID words and the frame synchronization word.

Figure 5-5 details the more complex of the subframe multiplexers. ...mmunications control commands the configuration logic device to gener... the appropriate shift register logic (SRL). These commands indicate ... data rates being received in the PCM and TV channels. In the PCM ...nel logic unit, the pulse stream is gated successively into subframe ...rough 7 storage according to the clock rate. The TV channel logic unit ...ultaneously gates data into these same storage devices beginning with ..., 7 and progressing upward toward No. 1. If the PCM channel is oper... at 12.2880 megabits/sec, subframe 1 is used for PCM data and sub... ...es 7, 6, 5, 4, and 3 are used for TV data. The SRL configures the ..., 2 storage unit into a linear-feedback shift register and outputs a ...udo-random code. The signals from the parallel frame multiplex ...s to the storage units are generated by the frame mux device. These ...als cause the storage devices to output their data in appropriate time ...quence.

The frame mux diagram is given in Figure 5-6. Driven by the ...ansmit clock at 20.1984 MHz, this unit clocks out the data from the sub... ...me registers and inserts the synchronization pattern and the channel ... at the appropriate times (according to the timing sequence given in ...ure 5-4).

The receive portion of the TDM gear is diagrammed in Figure 5-7. ...cause the K-band link is full-duplex, the overall structure of the receive ...r is very similar to the transmit unit shown in Figure 5-3. However, ...en data is first received, the "start frame" time is unknown and further... ...re, during operation, the received clock frequency may vary (doppler ...ts or clock drift). Frame synchronization and receive clock buffering ... accomplished by the frame demux diagrammed in Figure 5-8. The ...ived data stream and received clock is accepted from the modem. The ...-bit counter then clocks out successive 20-bit words which the sync word ...ognizer cross-correlates with a reference pattern and also with the ...rn's complement. A search for the complementary pattern must be ...rmed because of the 180 degree ambiguity in the recovered carrier. ...ecessary, the data stream is re-inverted in the data channel logic unit. ... 5-9 describes the scanning operation and manner in which the main... ...e mode is attained. Once synchronization is achieved, the remaining ...nal is enabled and the demultiplexing operation can be initiated. ... received data and the associated clock can be buffered by the frame ... unit up to one full frame time of 0.149 ms. It is assumed that the ...tation adjusts its transmission rate such that the rate seen by the ... within this buffering capability.

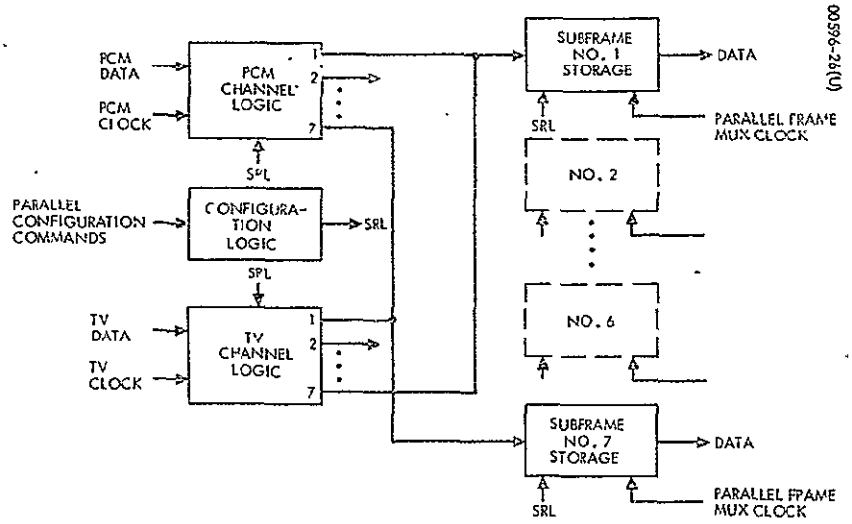

Figure 5-5. 2/7 Subframe Multiplexer Diagram

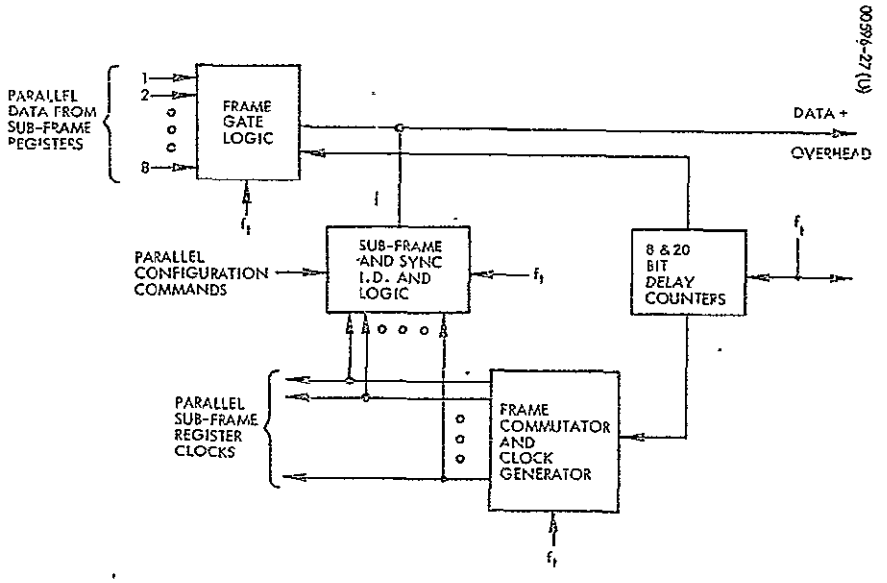

Figure 5-6. Frame Multiplexer Diagram

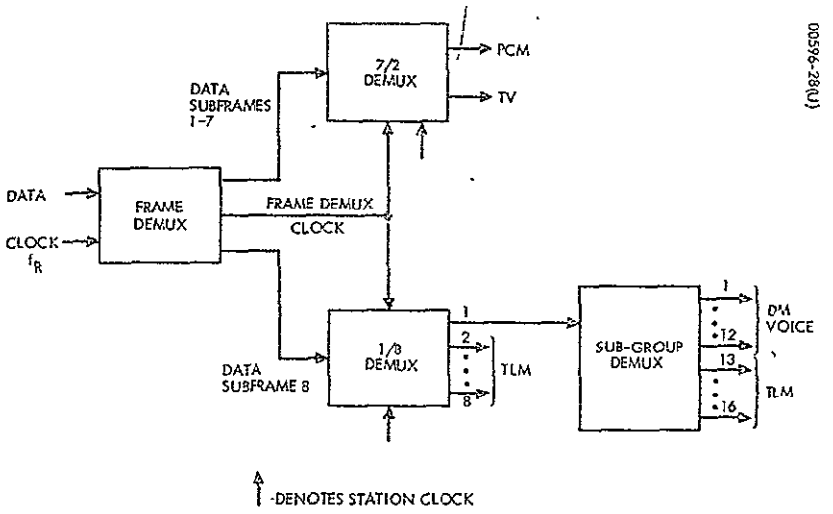

Figure 5-7. Receive Block Diagram

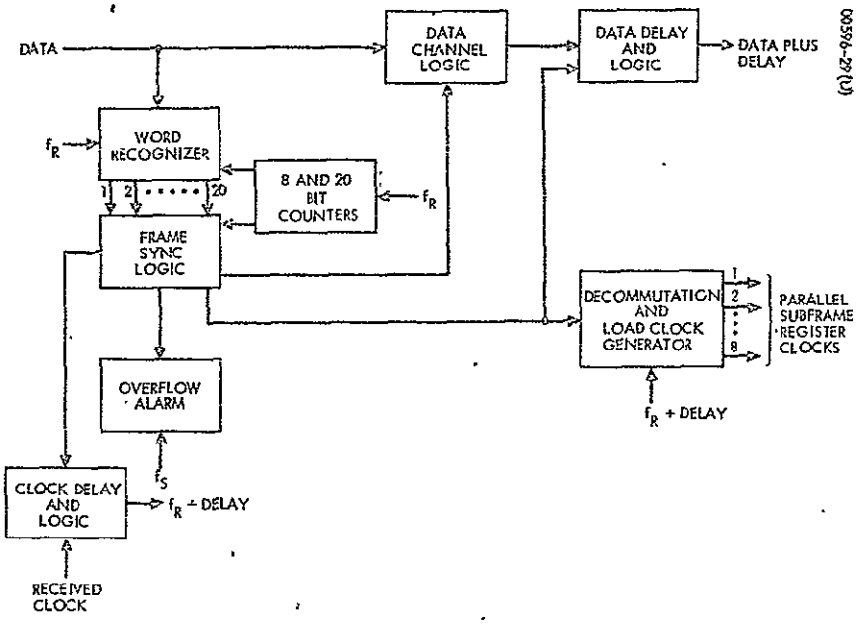

Figure 5-8. Frame Demultiplexer Diagram

SCANNING (RECOGNIZER SEARCHES FOR THE 20 BIT SYNC PATTERN AND ITS COMPLEMENT. NO ERRORS PERMITTED.)

- AFTER THE INITIATION OF SCANNING, A PATTERN RECOGNITION WILL BE MADE WITHIN ONE FRAME TIME WITH A PROBABILITY GREATER THAN 0.9998
- THE PROBABILITY THAT THIS SYNC IS FALSE IS LESS THAN 6×10^{-3}
- ANOTHER FRAME WORD IS EXAMINED BEFORE SYNC IS CONSIDERED ESTABLISHED. THE PROBABILITY THAT FALSE SYNC IS NOT DISCOVERED AFTER THIS SECOND FRAME IS GIVEN BY 9.5×10^{-7}. THE PROBABILITY THAT CORRECT SYNC IS REJECTED IS 2×10^{-4}

MAINTENANCE (TWO OR MORE ERRORS MUST OCCUR IN TWO SUCCESSIVE SYNC WORDS BEFORE RETURN TO SCANNING.)

- THE PROBABILITY OF SYNC LOSS DUE TO CHANNEL NOISE = 1.4×10^{-15}

005596-30(U)

Figure 5-9. Data Synchronizer Characteristics

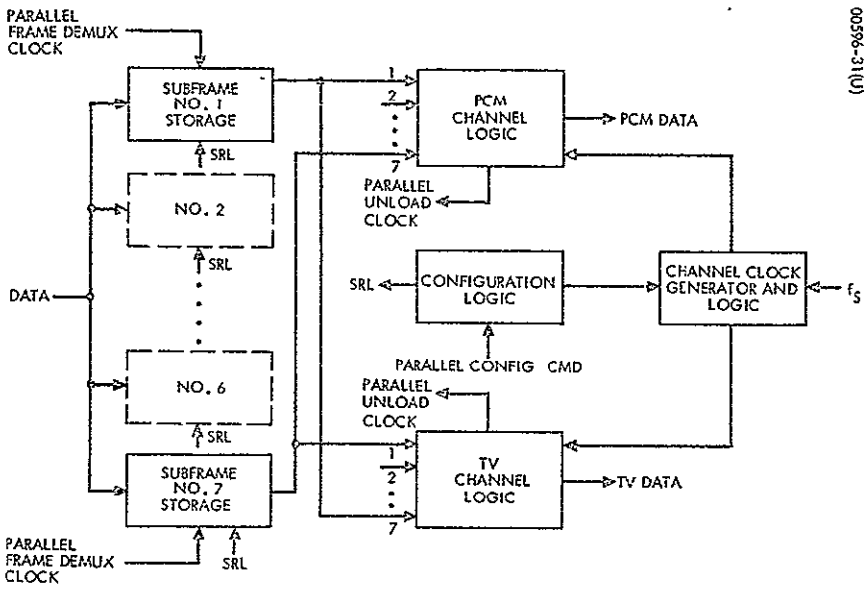

Figure 5-10. 7/2 Demultiplexer Diagram

The 7/2 demux diagram in Figure 5-10 shows that this unit is very similar to the 2/7 mux unit of Figure 5-5. The 7/2 demux accepts seven data subframes and outputs the data in two channels. The parallel frame demux signals gate the data into subframe storage registers 1 through 7. The data is then unloaded at synchronous rates into either the PCM channel or TV channel according to the configuration commands. Registers containing PN bits are ignored during this process.

Source Encoder/Decoder

At the time of DRS link handover, two TDM units will be operating. The propagation delay difference in the links will cause the data streams from these units to have a significant differential delay. Since the PCM channel user may require uninterrupted data flow, he is provided the outputs of both operating units. The user may then buffer as required. Momentary data dropout will occur in the voice and television channels during handover. The twelve 19.2 kilobits/sec outputs from a single TDM are switched into a bank of delta modulators which generate the analog voice waveforms. These units also encode the 3 kHz voice signals for transmission. The 12.2880 megabits/sec television data is switched from one TDM into a data expander which regenerates the commercial quality analog waveform. A data compressor encodes the TV originating at the Space Station and generates a 12.2880 megabits/sec bit stream.

5.3 S-BAND SECTION

The S-band section of the baseband subsystem provides modems for the EM_1 and ALS links. It also provides a means of automatic antenna selection for transmissions to these vehicles. Figure 5-1 shows the arrangement of the S-band section. The equipment shown is provided in triplicate. Two ALS demodulators and two EM_1 demodulators are active, with another set as standbys. Each active pair is continually receiving data from both of the two antennas. Within each modem a measurement is made on the power received via a particular antenna. The antenna logic unit determines through which antenna the received ALS signal power is greater and through which antenna the received EM_1 signal power is greater. The communication control then configures the system to receive and transmit both ALS and EM_1 data through the appropriate antennas. A particular antenna may be used for both ALS and EM_1 data simultaneously. A particular power amplifier may be used for either link, but not simultaneously.

Figure 5-11 shows the more complex of the two modems. The EM_1 modem accepts data at a 7.3728 megabits/sec rate synchronous with the station clock. The convolutional K = 5, V = 2 encoder consists of a 5-bit shift register with tap connections to two adders. For each bit into the encoder, one subbit is generated at each adder -- that is, each adder outputs 7.3728×10^6 subbits per second. The data stream from adder No. 2 is biphase modulated on a 50 MHz source. The data stream from adder No. 1 is biphased modulated on the same source in phase quadrature.

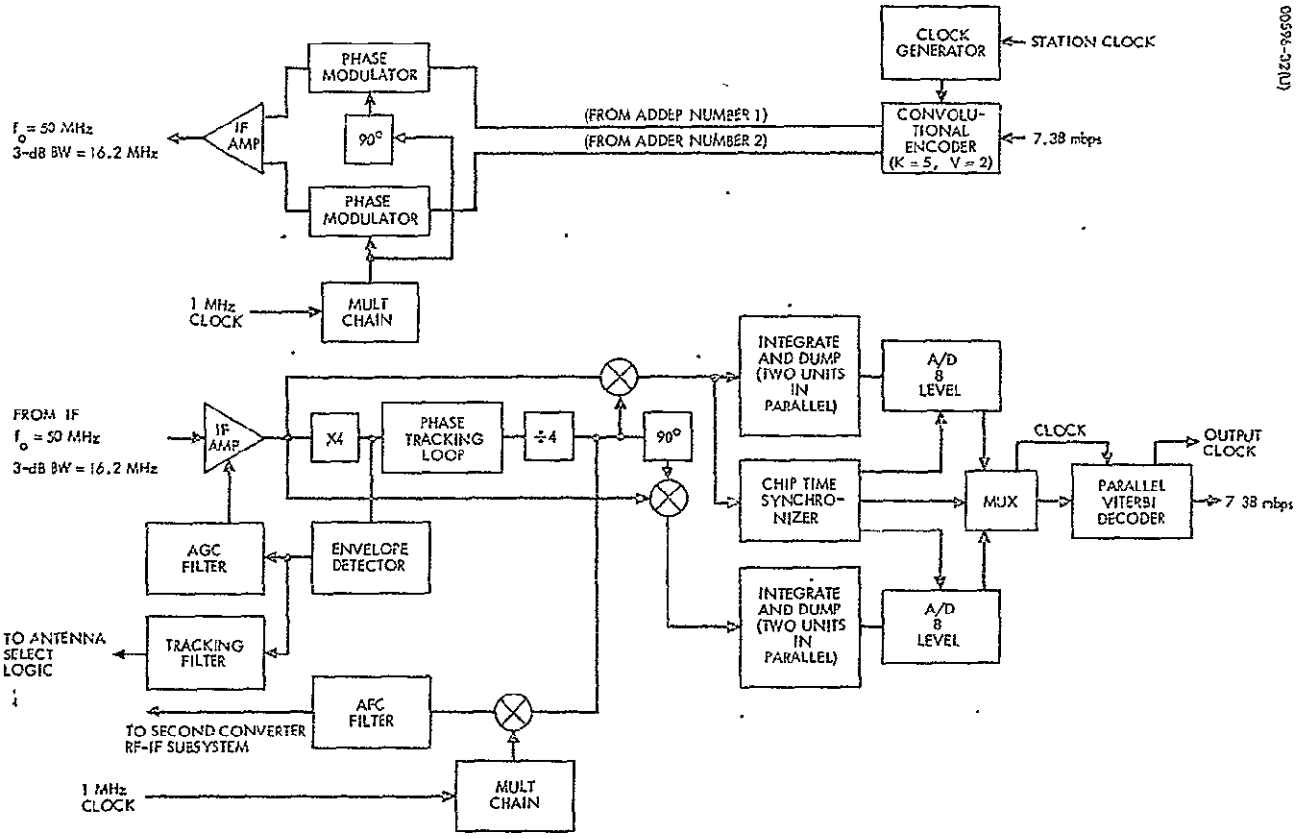

Figure 5-11. EM_1 Modem

The summation of the two biphase channels generates a quadriphase signal with 7.3728×10^6 chips per second. The receive side of the modem sees the same signal format that the transmit side generates. The modem recovers a coherent reference from the signal itself by a X4 phase tracking loop. This reference and its 90 degree phase shift is used to translate the two biphase channels down to baseband. The integrate and dump operation is accomplished by the use of two units in parallel (for each channel) which are used alternately. The chip time synchronizer determines the zero crossings in the received data. The chip time clock determines the integrator sampling times and the timing of the multiplexing of the eight-level digital samples. The samples from the two channels are processed by a parallel implementation of the Viterbi decoding algorithm. This decoder outputs data which is nominally 7.3728 megabits/sec. Note that the modem also provides an AGC signal and a signal to the antenna selection logic. Furthermore, multiplying the recovered carrier with the local clock generates an error signal for the AFC loop which controls the VCO at the second stage of the downconverter.

The ALS modem accepts data at 57.6 kilobits/sec, uses a K = 5, V = 2 convolutional code, and performs a biphase modulation of a 3 MHz source. The demodulator employs optimum integrate and dump detection. An eight-level quantization of the integrator's output is processed by the serial Viterbi decoder. This device then outputs a data stream at the received clock rate at a nominal 57.6 kilobits/sec. Buffering of the EM_1 and ALS received data permits the interface data rates to be synchronous with the Station clock.

5.4 VHF SECTION

The configuration select switch permits the user to select a particular transmit/receiver unit. The interface with the internal communications system consists of two wire pairs for the full-duplex 3-kHz voice.

PART II

PARAMETRIC ANALYSIS

Part II of this report documents the analyses and parametric trades performed during this study. Many of the sections discuss design studies performed in support of the Space Station communication system design. Several sections provide data of a parametric nature which can be used in the development of communication system designs employing alternate implementation techniques. Where applicable, the results of these analyses were used to evaluate alternate designs and implementations prior to the baseline selections. The analyses included in this report will aid in evaluating modifications to the baseline system and will provide a basis for the design of communication systems with requirements differing from those of the baseline.

6. COMMUNICATIONS GEOMETRY AND ANTENNA POINTING ANALYSIS

6.1 INTRODUCTION

An in-depth analysis of the geometry associated with the Space Station links was begun early in the study. It was concluded that three high gain antennas were required on the Station for uninterrupted DRSS communication. This effort also developed the need for a three-axis antenna gimbal system. Computer analysis allowed a quantitative description of the required gimbal system performance. A second computer program was developed to analyze the performance of the selected cross-axis/azimuth design. Various types of parametric data were generated during the communications geometry study and are summarized below.

Subsection 6.2 consists of a collection of curves giving range and range-rate for the various links. These results are of sufficient accuracy that they can be used for preliminary design studies. Subsection 6.3 provides a mathematical analysis for determination of the line of sight angles between two earth-orbiting spacecraft. Although the results are applicable to Station/ALS communication, the application of special interest is the Space Station to DRS link. The analysis permits determination of the required motions of a Space Station antenna which must track the DRS. Subsection 6.4 describes the geometrical considerations involved in placement of an antenna on the Space Station which is to be used for DRS communication. Subsection 6.5 considers the problem of predicting DRS occultation and of anticipating the need for handover. Subsection 6.6 considers the basic Space Station high gain antenna pointing problem. Both two and three gimbal approaches are discussed. The final subsection gives an analysis of the baseline three-gimbal antenna positioning system.

6.2 PRELIMINARY RANGE AND DOPPLER SHIFT DATA

Figures 6-1 through 6-6 present the maximum range and doppler shift data for the various communication link geometries that may be encountered by low earth orbit manned spacecraft. The data is based on circular orbits and simple geometrical relationships, but is useful for preliminary link analyses. The equations used to produce these curves are summarized briefly below.

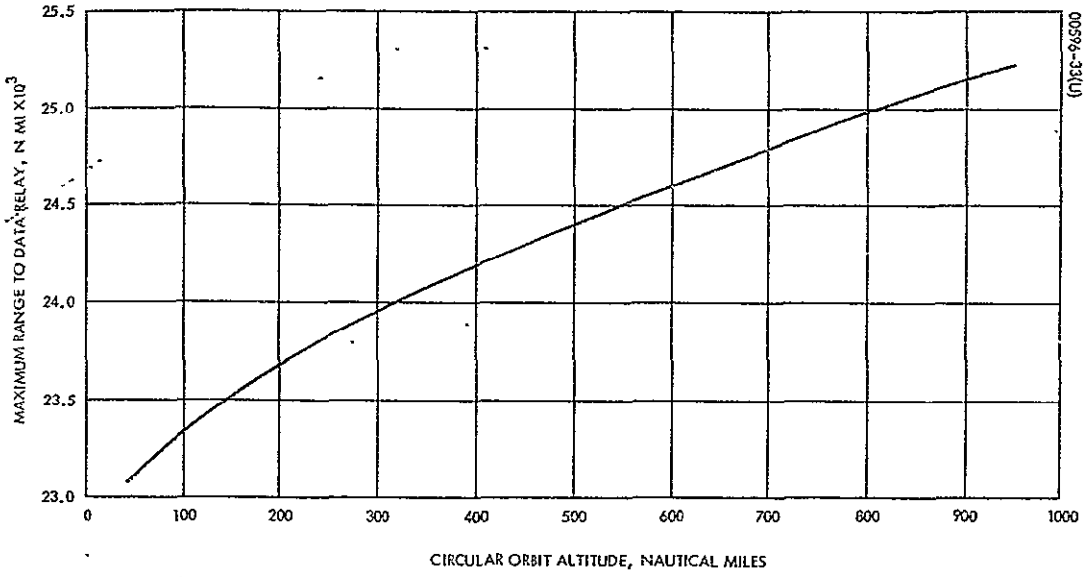

Figure 6-1. Maximum Range Between Space Station and Synchronous Data Relay

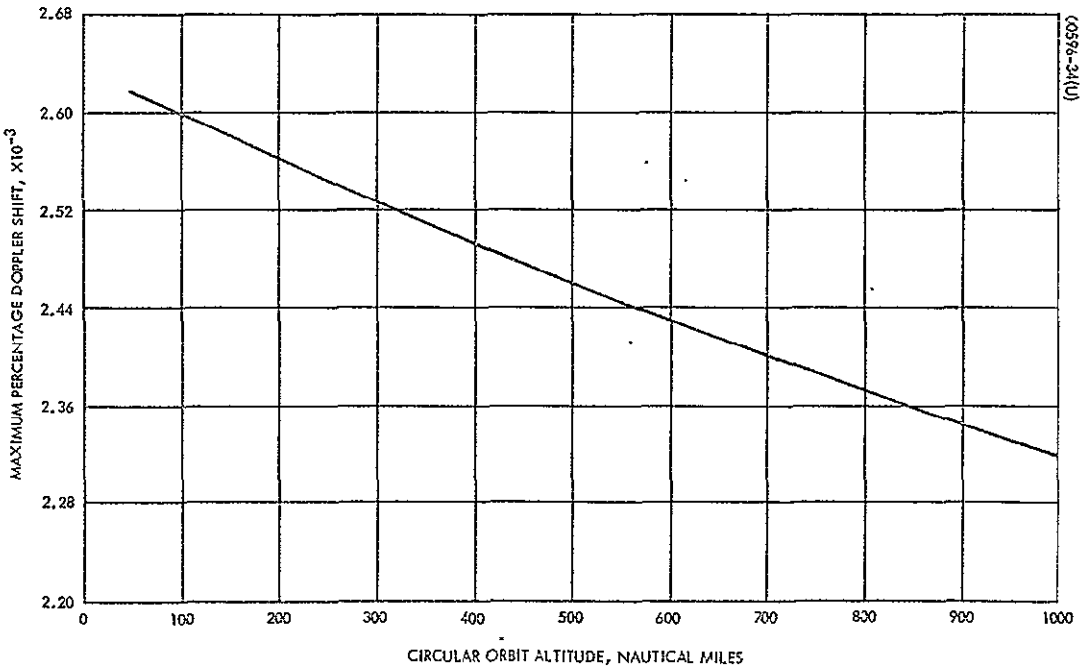

Figure 6-2. Maximum Percentage Doppler Shift Between Space Station and Synchronous Data Relay

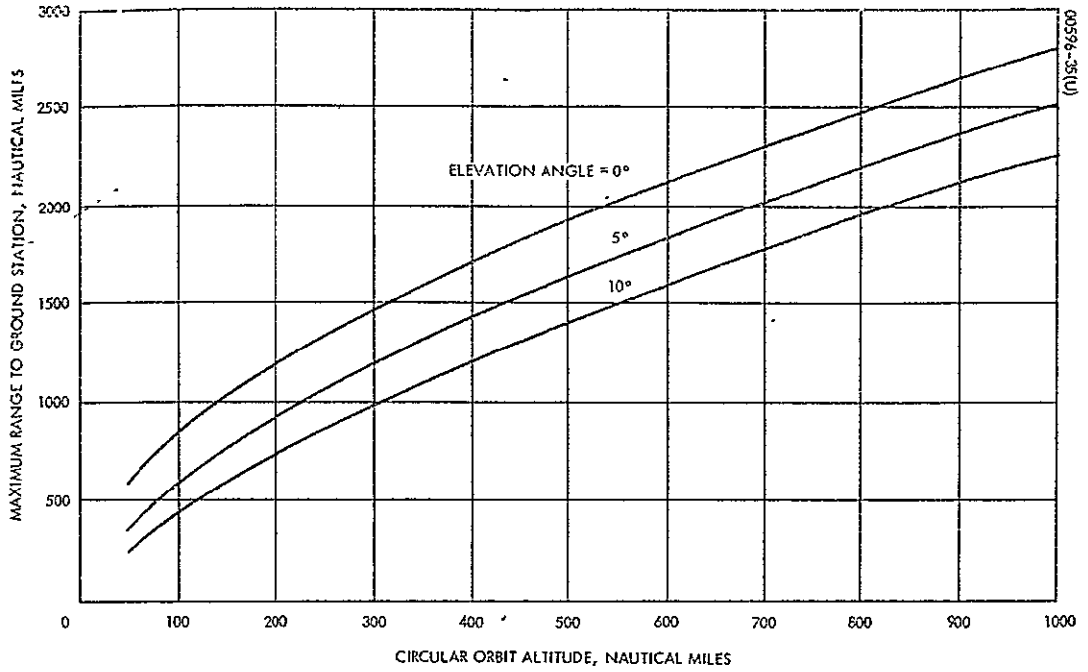

Figure 6-3. Maximum Range Between Space Station and Ground Station

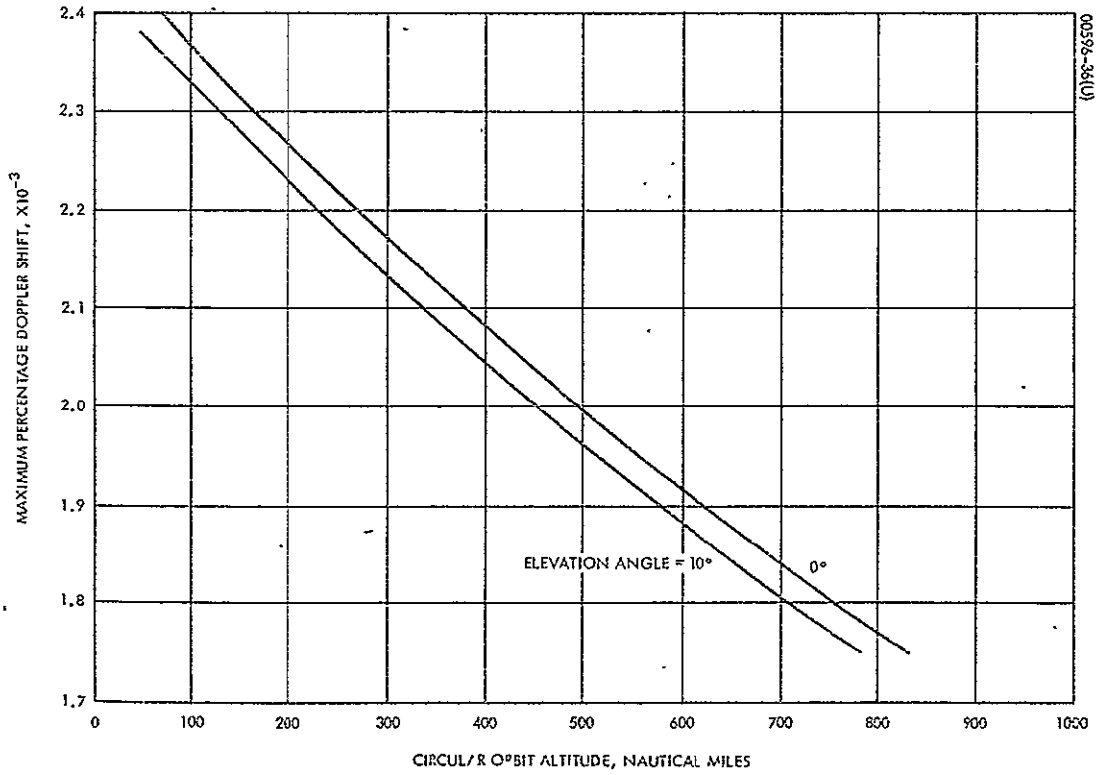

Figure 6-4. Maximum Percentage Doppler Shift Between Space Station and Ground Station (Equatorial Orbit)

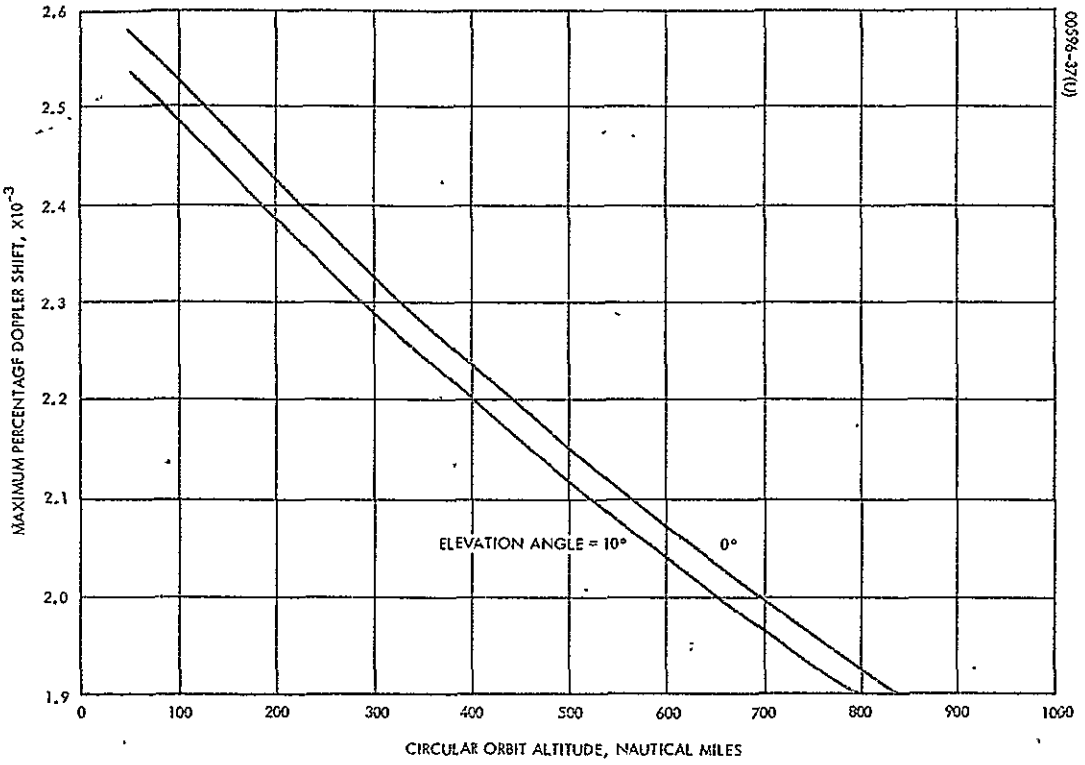

Figure 6-5. Maximum Percentage Doppler Shift Between Space Station and Ground Station (Polar Orbit)

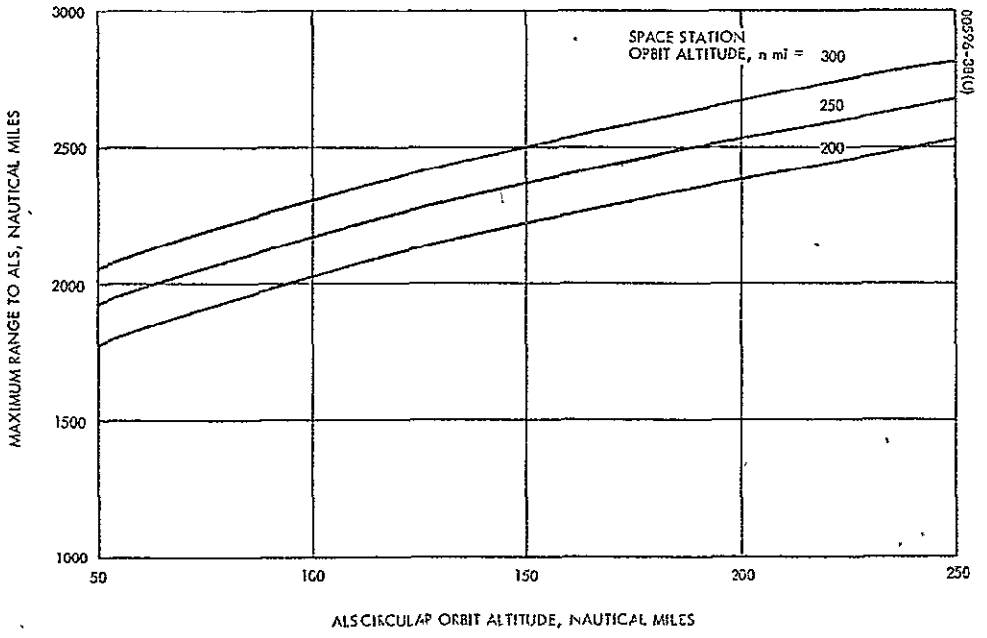

Figure 6-6. Maximum Range Between Space Station and ALS

Space Station ⇋ Data Relay Satellite Link

$$d_r = \left(R_{DRS}^2 - R_E^2\right)^{1/2} + \left(2R_E h + h^2\right)^{1/2} \qquad \text{(See Figure 6-1)}$$

where

d_r = maximum range between Space Station and DRS

h = circular orbit attitude of Space Station

R_E = radius of earth (3440 n. mi.)

R_{DRS} = geocentric range of data relay

$$\Delta f = \frac{v_c}{c}\left(\frac{R_E}{R_E + h}\right)^{1/2} \qquad \text{(See Figure 6-2)}$$

where

Δf = maximum fractional doppler shift between Space Station and DRS

v_c = velocity of body in circular orbit at earth's surface (2.595×10^4 fps)

c = velocity of light (9.85×10^8 fps)

Space Station ⇋ Ground Station Link

$$d_g^2 = R_E^2 + \left(h + R_E\right)^2 - 2R_E\left(h + R_E\right)\left[\sin\theta \cos\delta + \cos\theta \sin\delta\right]$$

$$\sin\delta = \frac{R_E}{h + R_E}\cos\theta \qquad \text{(See Figure 6-3)}$$

$$\cos\delta = \left(1 - \sin^2\delta\right)^{1/2}$$

where

d_g = maximum range between Space Station and ground station

h = circular orbit altitude of Space Station

θ = ground station elevation angle

R_E = radius of earth (3440 n. mi.)

$$\Delta f_e = \frac{v_c}{c}\left(\frac{R_E}{h + R_E}\right)^{3/2} \cos\theta - \frac{v_e}{c} \cdot \frac{1}{\cos\theta} \quad \text{(See Figure 6-4)}$$

where

Δf_e = maximum fractional doppler shift between Space Station and ground station for equatorial orbits.

v_e = tangential velocity of body at earth's equator (1.52×10^3 fps)

$$\Delta f_p = \frac{v_c}{c}\left(\frac{R_E}{h + R_E}\right)^{3/2} \cos\theta \quad \text{(See Figure 6-5)}$$

where

Δf_p = maximum fractional doppler shift between Space Station and ground station for polar orbits.

Space Station ⇋ ALS Link

$$d_s = \left(2R_E\, h_{ALS} + h_{ALS}^2\right)^{1/2} + \left(2R_E\, h_{SS} + h_{SS}^2\right)^{1/2}$$

(See Figure 6-6)

where

d_s = maximum range between Space Station and ALS

h_{SS} = circular orbit altitude of Space Station

h_{ALS} = circular orbit altitude of ALS

R_E = radius of earth (3440 n. mi.)

6.3 MATHEMATICAL ANALYSIS OF SPACE STATION/DRS GEOMETRY

Quantitative data concerning antenna pointing geometry for the Space Station/DRS link requires that the line of sight (LOS) between the two vehicles be related geometrically to the Space Station and the antenna positioning mechanisms. Of interest are the look-angles with respect to coordinates referenced to the Station and the requirements of an antenna positioning mechanism. Specifically, gimbal freedom, total angular movement and

angular rates are quantities to be determined. Look-angle data is required in making mounting decisions, and the antenna positioner requirements may be determined for several implementations to provide a basis for a choice.

This subsection develops mathematical expressions for look-angles, gimbal angles, and gimbal rates. The development is general and is oriented toward machine computation. The matrices defined and equations developed may be readily implemented in a computer program, allowing variation of attitude mode and gimbal system mechanization. The following subsection defines coordinate systems useful in the analysis and defines transformations between these systems. Later, notation is discussed under that heading, and Definitions defines several vector quantities essential to the analysis. The mathematical expressions for look-angles, gimbal angles, and gimbal rates are developed under the subheading Analysis.

Coordinate Systems

Before analysis of antenna pointing can be initiated, coordinate systems and associated notation must be defined. There are five sets of coordinates which prove useful in developing mathematical expressions for quantities of interest.

Inertial Coordinates (I_1 I_2 I_3)

This system is shown in Figure 6-7. The origin lies at the earth's center. I_1 coincides with the vernal equinox vector, I_3 coincides with the earth's polar axis, and I_2 lies in the equatorial plane, completing the right-handed system.

Space Station Orbit Coordinates (S_1 S_2 S_3)

This system is also shown in Figure 6-7. S_3 is perpendicular to the orbit plane, S_1 coincides with the line of nodes and lies in the direction of the ascending node, and S_2 lies in the orbit plane, completing the right-handed system.

A vector, $\bar{V}$, expressed in S_1 S_2 S_3 coordinates, is denoted by V_S and can be expressed in I_1 I_2 I_3 coordinates when operated on by the linear transformation, A_{IS}, given by

$$A_{IS} = \begin{pmatrix} \cos\lambda_s & -\sin\lambda_s & 0 \\ \sin\lambda_s & \cos\lambda_s & 0 \\ 0 & 0 & 1 \end{pmatrix} \begin{pmatrix} 1 & 0 & 0 \\ 0 & \cos i_s & -\sin i_s \\ 1 & \sin i_s & \cos i_s \end{pmatrix} \tag{6-1}$$

$$A_{IS} = \begin{pmatrix} \cos\lambda_s & -\sin\lambda_s \cos i_s & \sin\lambda_s \sin i_s \\ \sin\lambda_s & \cos\lambda_s \cos i_s & -\cos\lambda_s \sin i_s \\ 0 & \sin i_s & \cos i_s \end{pmatrix}$$

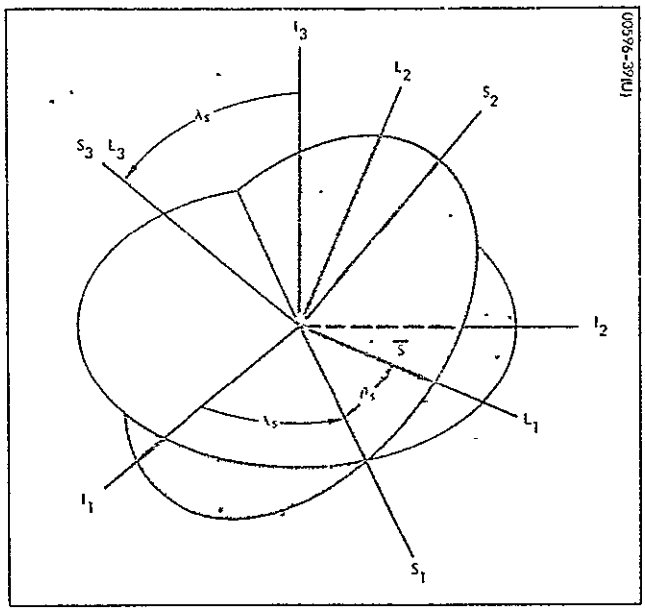

Figure 6-7. Inertial, Space Station Orbit and Local Space Station Coordinates

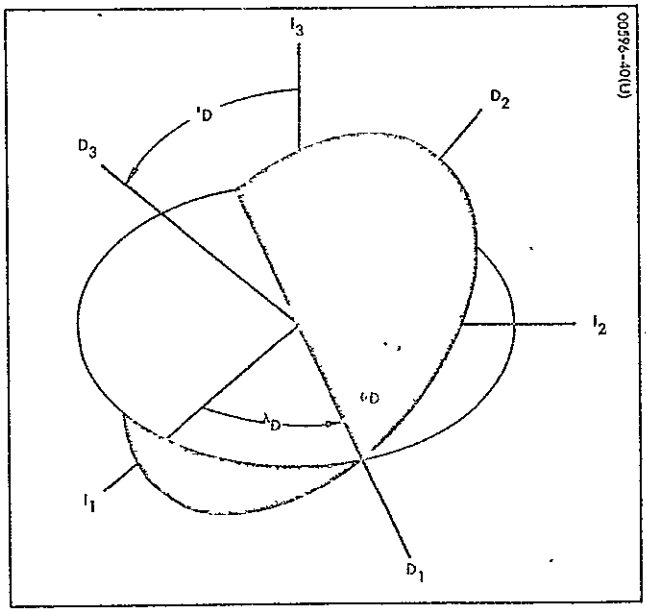

Figure 6-8. Inertial and Data Relay Orbit Coordinates

Thus, denoting $\bar{V}$ in $I_1\ I_2\ I_3$ coordinates by V_I:

$$V_I = A_{IS}\ V_S \tag{6-2}$$

Data Relay Orbit Coordinates ($D_1\ D_2\ D_3$)

This system is shown in Figure 6-8, and is conceptually the same as the $S_1\ S_2\ S_3$ system. D_3 is perpendicular to the orbit plane, D_1 coincides with the ascending node direction, and D_2 completes the system. The transformation from $D_1\ D_2\ D_3$ coordinates to $I_1\ I_2\ I_3$ is denoted by A_{ID} and is the same as A_{IS}, but with the subscripts changes, i.e.,

$$A_{ID} = \begin{pmatrix} \cos\lambda_D & -\sin\lambda_D \cos i_D & \sin\lambda_D \sin i_D \\ \sin\lambda_D & \cos\lambda_D \cos i_D & -\cos\lambda_D \sin i_D \\ 0 & \sin i_D & \cos i_D \end{pmatrix} \tag{6-3}$$

Denoting V in $D_1\ D_2\ D_3$ coordinates by V_D,

$$V_I = A_{ID}\ V_D \tag{6-4}$$

Local Space Station Coordinates ($L_1\ L_2\ L_3$)

This system is shown in Figure 6-7, where L_3 coincides with S_3, the orbit normal. L_2 lies along the velocity vector, and L_1 coincides with the vector from the earth's center toward the space station. The transformation from $L_1\ L_2\ L_3$ coordinates to $S_1\ S_2\ S_3$ coordinates is denoted by A_{LS} which is expressed as the matrix

$$A_{SL} = \begin{pmatrix} \cos\theta_s & -\sin\theta_s & 0 \\ \sin\theta_s & \cos\theta_s & 0 \\ 0 & 0 & 1 \end{pmatrix} \tag{6-5}$$

Thus,

$$V_S = A_{SL}\ V_L \tag{6-6}$$

Space Station Coordinates (X Y Z)

These coordinates have been adopted from the North American Rockwell Space Station Phase B Definition Program and are illustrated in Figure 6-9. Different attitude modes for the Station result in different transformations from the XYZ system to the L_1 L_2 L_3 system, but the general transformation will be denoted by A_{LX}. Four candidate attitude modes are treated below.

Earth Pointing, X-POP. The X coordinate is perpendicular to the orbit plane, Y lies along the velocity vector, (L_2), and Z coincides with the radius vector, (L_1). Thus,

$$A_{LX1} = \begin{pmatrix} 0 & 0 & 1 \\ 0 & 1 & 0 \\ 1 & 0 & 0 \end{pmatrix} \tag{6-7}$$

and

$$V_L = A_{LX1} V_X \tag{6-8}$$

where V_X denotes a vector in the XYZ coordinates.

Earth Pointing, Y-POP. X lies along the velocity vector, Y is perpendicular to the orbit plane, and Z coincides with the radius vector.

$$A_{LX2} = \begin{pmatrix} 0 & 0 & 1 \\ 1 & 0 & 0 \\ 0 & 1 & 0 \end{pmatrix} \tag{6-9}$$

Inertial, X-POP. The Space Station's attitude is held constant in inertial space with the X-axis perpendicular to the orbit plane.

$$A_{LX3} = \begin{pmatrix} 0 & \sin(\theta_o - \theta_s) & \cos(\theta_o - \theta_s) \\ 0 & -\cos(\theta_o - \theta_s) & \sin(\theta_o - \theta_s) \\ 1 & 0 & 0 \end{pmatrix} \tag{6-10}$$

where θ_o is the angle between Z and L_1 at $\theta = 0$ (where $L_1 = S_1$) in the direction of orbital angular motion. Note that the transformation from XYZ coordinates to S_1 S_2 S_3 coordinates is given by

$$A_{SX3} = A_{SL}\, A_{LX3} = \begin{pmatrix} 0 & \sin\theta_o & \cos\theta_o \\ 0 & -\cos\theta_o & \sin\theta_o \\ 1 & 0 & 0 \end{pmatrix} \qquad (6\text{-}11)$$

Inertial, Y-POP. The Space Station attitude is held constant in inertial space with the Y-axis perpendicular to the orbit plane.

$$A_{LX4} = \begin{pmatrix} -\sin(\theta_o - \theta_s) & 0 & \cos(\theta_o - \theta_s) \\ \cos(\theta_o - \theta_s) & 0 & \sin(\theta_o - \theta_s) \\ 0 & 1 & 0 \end{pmatrix} \qquad (6\text{-}12)$$

and

$$A_{SX4} = A_{SL}\, A_{LX4} = \begin{pmatrix} -\sin\theta_o & 0 & \cos\theta_o \\ \cos\theta_o & 0 & \sin\theta_o \\ 0 & 1 & 0 \end{pmatrix} \qquad (6\text{-}13)$$

where θ_o is the angle between L_1 and Z at $\theta = 0$ in the direction of orbital angular motion.

Gimbal Reference Coordinates (G_1 G_2 G_3). In a two-gimbal system, one axis is fixed rigidly to the vehicle. This axis is called the primary axis. A second rotating mechanism is attached to it, usually in an orthogonal arrangement. This second axis of rotation, called the secondary axis, is positioned by the primary axis. The gimbal reference system is a coordinate system representing the "zero" position of the two rotating axes. This system may be referenced go the Space Station coordinate system (XYZ) or the orbital coordinate system (S_1 S_2 S_3). That is, a vector V in the G_1 G_2 G_3 system is expressed in XYZ or S_1 S_2 S_3 coordinates by transformations A_{XG} or A_{SG}, respectively. These matrices will be further defined in the subsequent analysis.

The angular orientation of the antenna boresight can be easily referenced to the G_1 G_2 G_3 system. Referring to Figure 6-10, the primary axis

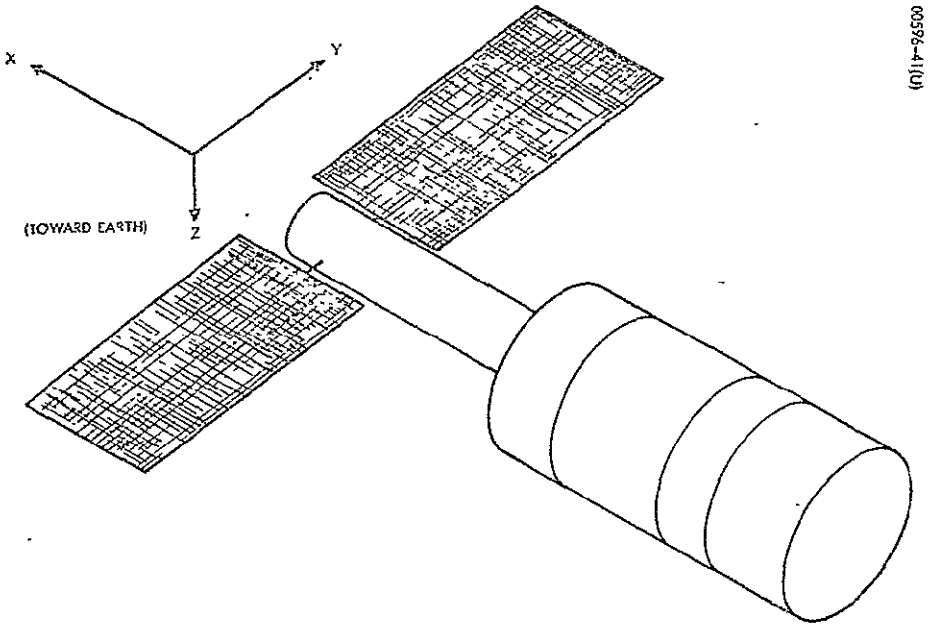

Figure 6-9. Space Station Coordinates

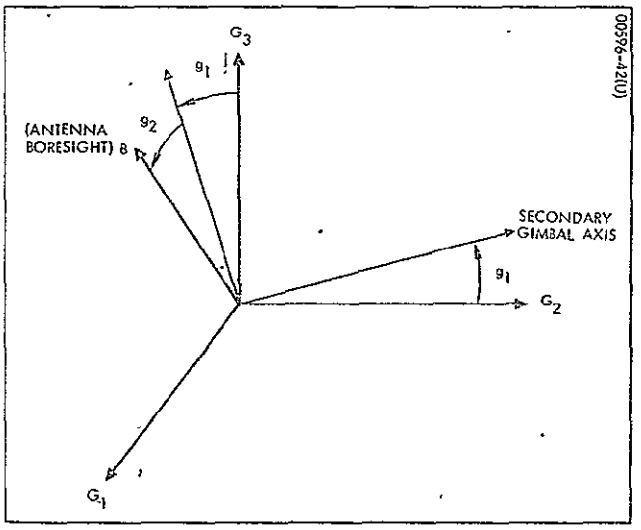

Figure 6-10. Gimbal System Coordinates

coincides with G_1, and in the zero position, the secondary axis and antenna boresight coincide with G_2 and G_3, respectively. Denoting angular rotation about the primary and secondary axes by g_1 and g_2, respectively, the antenna boresight unit vector, $\bar{B}$, is expressed in $G_1\ G_2\ G_3$ coordinates by

$$B_G = \begin{pmatrix} \sin g_2 \\ -\sin g_1 \cos g_2 \\ \cos g_1 \cos g_2 \end{pmatrix} \quad . \tag{6-14}$$

Notation

As may already be noted, letter subscripts refer to coordinate systems. Matrix transformations have two subscripts, the first referring to the coordinate system to which the vector is being transformed and the second referring to the coordinate system from which the vector is being transformed. Thus, A_{SG} represents a transformation from $G_1\ G_2\ G_3$ coordinates to $S_1\ S_2\ S_3$ coordinates.

A_{SG}^{-1} is the inverse of A_{SG}, and it can be shown that

$$A_{SG}^{-1} = A_{SG}^{T} = A_{GS} \tag{6-15}$$

where A_{SG}^{T} is the transpose of the matrix A_{SG}. This property is true of all the transformations defined earlier because they are orthonormal transformations.

Components of a vector are denoted by a number in addition to the coordinate system letter subscript. Thus, V_{S2} is the component of the vector $\bar{V}$ along the S_2 coordinate axis. Since the magnitude of a vector is simply a number and does not depend on any coordinate system, it will be denoted by the letter used for the vector but with no subscript. Thus, $|V_S| = |V| = V$. Also, a vector not referred to a coordinate system will have a "bar" above it, e.g., $\bar{V}$.

Definitions

The vectors to the Space Station and DRS are denoted by $\bar{S}$ and $\bar{D}$, respectively, and are defined in $S_1\ S_2\ S_3$ coordinates by

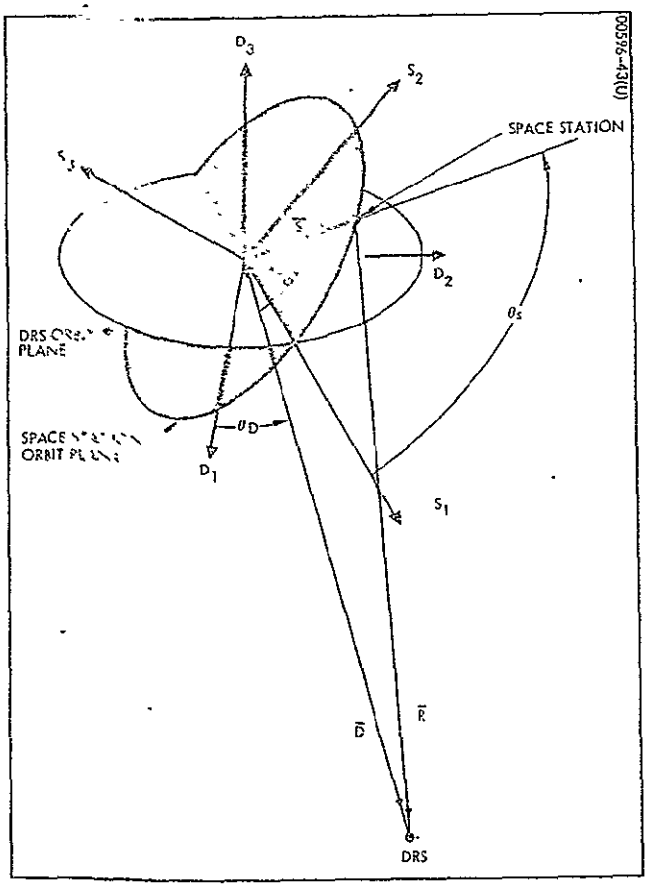

Figure 6-11. Range Vector and Space Station/DRS Geometry

$$\dot{S}_S = A_{SL} \begin{pmatrix} 1 \\ 0 \\ 0 \end{pmatrix} = S \begin{pmatrix} \cos \theta_s \\ \sin \theta_s \\ 0 \end{pmatrix} \tag{6-16}$$

$$D_D = D \begin{pmatrix} \cos \theta_D \\ \sin \theta_D \\ 0 \end{pmatrix} \tag{6-17}$$

These two vectors are shown in Figures 6-7 and 6-8, respectively. Their derivatives are given by

$$\dot{S}_S = \omega_s S \begin{pmatrix} -\sin \theta_s \\ \cos \theta_s \\ 0 \end{pmatrix} \tag{6-18}$$

$$\dot{D}_D = \omega_D D \begin{pmatrix} -\sin \theta_D \\ \cos \theta_D \\ 0 \end{pmatrix} \tag{6-19}$$

where $\omega_s = \frac{d\theta_s}{dt}$ and $\omega_D = \frac{d\theta_D}{dt}$.

The range vector is defined to be directed from the Space Station to the DRS and is denoted by $\bar{R}$. The geometry is illustrated in Figure 6-11. Thus,

$$\bar{R} = \bar{D} - \bar{S} \tag{6-20}$$

Analysis

The analysis of antenna pointing amounts to expressing the range vector in appropriate coordinate systems for determining look angles, gimbal angles, etc. In particular, the range vector must be expressed in Space Station coordinates (XYZ) and gimbal reference coordinates. This is accomplished using the transformations defined under Coordinate Systems and the definitions under Definitions, specifically Equations 6-16, 6-17, and 6-20.

The range vector in inertial coordinates is given by

$$R_I = D_I - S_I = A_{ID}\, D_D - A_{IS}\, S_S \tag{6-21}$$

Then, using property (Equation 6-15),

$$\begin{aligned} R_S &= A_{SI}\, R_I = A_{IS}^T\, R_I \\ R_S &= A_{IS}^T\, A_{ID}\, D_D - S_S \end{aligned} \tag{6-22}$$

The magnitude of $\bar{R}$ is defined by

$$\begin{aligned} R^2 &= \bar{R}^T \bar{R} = R_I^T\, T_I \\ &= D_D^T\, A_{ID}^T\, A_{ID}\, D_D + S_S^T\, A_{IS}^T\, A_{IS}\, S_S - D_D^T\, A_{ID}^T\, A_{IS}\, S_S \\ &\quad - S_S^T\, A_{IS}^T\, A_{ID}\, D_D \\ R^2 &= D^2 + S^2 - 2\left[(A_{IS}\, S_S)^T\, (A_{ID}\, D_D)\right] \end{aligned} \tag{6-23}$$

The angle between D and S is denoted by φ and is shown in Figure 6-11. By the law of cosines, it can be shown that

$$\cos\varphi = \frac{(A_{IS}\, S_S)^T\, (A_{ID}\, D_D)}{SD} \tag{6-24}$$

Space Station Look Angles

The range vector can be expressed in spacecraft coordinates by transforming R_S:

$$R_X = A_{XL}\, A_{LS}\, R_S$$

where $A_{SL} = A_{LX}^T$ and $A_{LS} = A_{SL}^T$.

Substituting from Equation 6-22

$$R_X = A_{LX}^T A_{SL}^T (A_{IS}^T A_{ID} D_D - S_S) \tag{6-25}$$

Define the unit vector in the $\bar{R}$ direction, expressed in XYZ coordinates, by

$$R_{UX} = \frac{R_X}{R} \tag{6-26}$$

Then the X component of R_{UX} is the cosine of the angle, α_X, between the X axis and $\bar{R}$. Denoting the direction cosines by α_X, α_Y, and α_Z

$$\begin{aligned} \cos \alpha_X &= R_{UX1} \\ \cos \alpha_Y &= R_{UX2} \\ \cos \alpha_Z &= R_{UX3} \end{aligned} \tag{6-27}$$

Calculation of these angles for different attitude modes will provide useful for making mounting choices and studying structural interference.

Gimbal Angles

For proper communication, the antenna boresight axis, $\bar{B}$, must nominally coincide with the range vector. Transforming $\bar{R}$ to G coordinates

$$\begin{aligned} R_G &= A_{XG}^T RX \\ R_G &= A_{XG}^T A_{LX}^T A_{SL}^T (A_{IS}^T A_{ID} D_D - R_S) \\ \text{or} \quad R_G &= A_{XG}^T A_{SX}^T (A_{IS}^T A_{ID} D_D - R_S) \end{aligned} \tag{6-28}$$

Since $\bar{B}$ is a unit vector, correct antenna pointing requires that

$$B_G = \frac{R_G}{R} = \begin{pmatrix} \sin g_2 \\ -\sin g_1 \cos g_2 \\ \cos g_1 \cos g_2 \end{pmatrix} \tag{6-29}$$

Thus,

$$\tan g_1 = -\frac{R_{G2}}{R_{G3}} \tag{6-30}$$

$$\tan g_2 = \frac{R_{G1}}{R_{G3}} \cos g_1 \tag{6-31}$$

or equivalently

$$g_1 = \tan^{-1}\left(\frac{-R_{G2}}{R_{G3}}\right) \tag{6-32}$$

$$g_2 = \tan^{-1}\left(\frac{R_{G1}}{R_{G3}} \cos y_1\right) \tag{6-33}$$

If g_2 is expected to lie between +90 and -90 degrees, then from Equation 6-24

$$g_2 = \sin^{-1}\left(\frac{R_{G1}}{R}\right) \tag{6-34}$$

The rate of change of the gimbal angles may be derived from Equations 6-32 and 6-33 above.

$$\frac{dg_1}{dt} = \dot{g}_1 = \frac{R_{G2}\dot{R}_{G3} - \dot{R}_{G2}R_{G3}}{R_{G2}^2 + R_{G3}^2} \tag{6-35}$$

$$\frac{dg_2}{dt} = \dot{g}_2 = \frac{(\dot{R}_{G1} R_{G3} - \dot{R}_{G1} R_{G3}) \cos \dot{g}_1 - g_1 R_{G1} R_{G3} \sin g_1}{R_{G3}^2 + (R_{G1} \cos g_1)^2} \quad (6\text{-}36)$$

where the derivative of $\bar{R}_G$ is given by

$$\begin{aligned} \dot{R}_G = {} & A_{XG}^T A_{SX}^T (A_{IS}^T A_{ID} \dot{D}_D - \dot{S}_S) \\ & + A_{XG}^T \dot{A}_{SX}^T (A_{IS}^T A_{ID} D_D - S_S) \end{aligned} \quad (6\text{-}37)$$

where $\dot{D}_D$ and $\dot{S}_S$ are given by Equations 6-18 and 6-19.

$$A_{SX} = A_{SL} A_{LX}$$

Thus

$$A_{SX}^T = A_{LX}^T A_{SL}^T$$

and so

$$\dot{A}_{SX}^T = \dot{A}_{LX}^T A_{SL}^T + A_{LX}^T \dot{A}_{SL}^T \quad (6\text{-}38)$$

For earth-pointing modes, A_{LX} is constant; thus,

$$\dot{A}_{SX}^T = A_{LX}^T \dot{A}_{SL}^T \quad \text{(earth pointing modes)} \quad (6\text{-}39)$$

and from Equation 6-5

$$\dot{A}_{SL} = \omega_s \begin{pmatrix} -\sin \theta_s & -\cos \theta_s & 0 \\ \cos \theta_s & -\sin \theta_s & 0 \\ 0 & 0 & 0 \end{pmatrix} \quad (6\text{-}40)$$

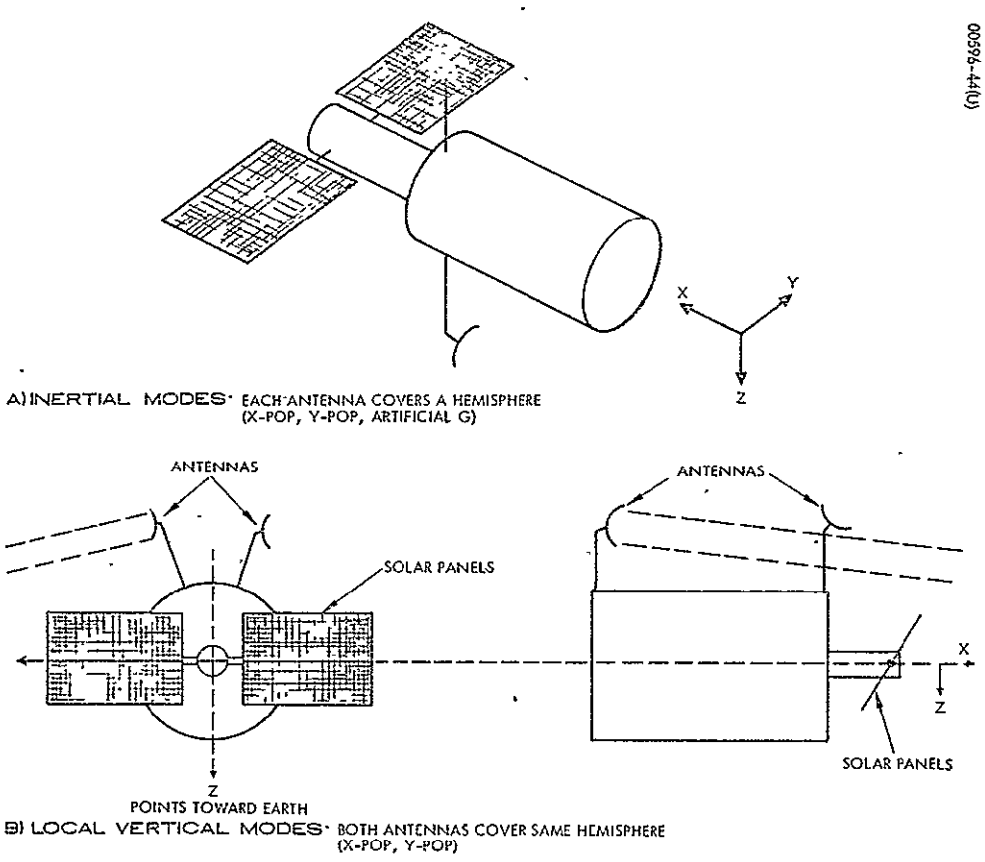

Figure 6-12. Mounting of Two DRS Link Antennas

For inertial modes, A_{SX} is constant, and so

$$\dot{R}_G = A_{XG}^T A_{SX}^T (A_{IS}^T A_{ID} \dot{D}_D - \dot{S}_S) \quad \text{(inertial modes)} \qquad (6\text{-}41)$$

6.4 ANTENNA PLACEMENT

Introduction

The discussion below is directed toward the factors determining the proper placement of the DRS high gain antennas on the Space Station. Many of the results also will aid in locating omni antennas used for DRS communication or for links direct to ground.

The relay link antennas should be placed so as to accomplish the following:

1) Permit stowage at the fore or aft end of the Station during launch,

2) Minimize obstruction of the LOS by the Station structure

3) Minimize the number of handovers and time required for each handover (and therefore, minimize data loss).

Antenna Placement Schemes

One Antenna

If only one relay link antenna were to be used, it would be placed so as to look in the -Z direction relative to the Station. In the local vertical attitude modes, this direction is along the local vertical away from the earth, thus providing good coverage of the DRS System (DRSS). In the artificial-g mode, this single antenna could provide coverage to the DRSS on one side of the spin plane. For the inertial modes, there is no preferred LOS direction to the DRSS relative to the spacecraft. Therefore, there is also no preferred location for the antennas.

Two Antennas

Figure 6-12 shows two different schemes for mounting two antennas. One is designed for the inertial attitude modes and the other is intended to be used with an earth-oriented spacecraft.

In the inertial modes, complete spherical coverage must be provided, consequently, the antennas are placed 180 degrees apart. They are placed out along the +Z and -Z axes to permit their azimuth gimbals to

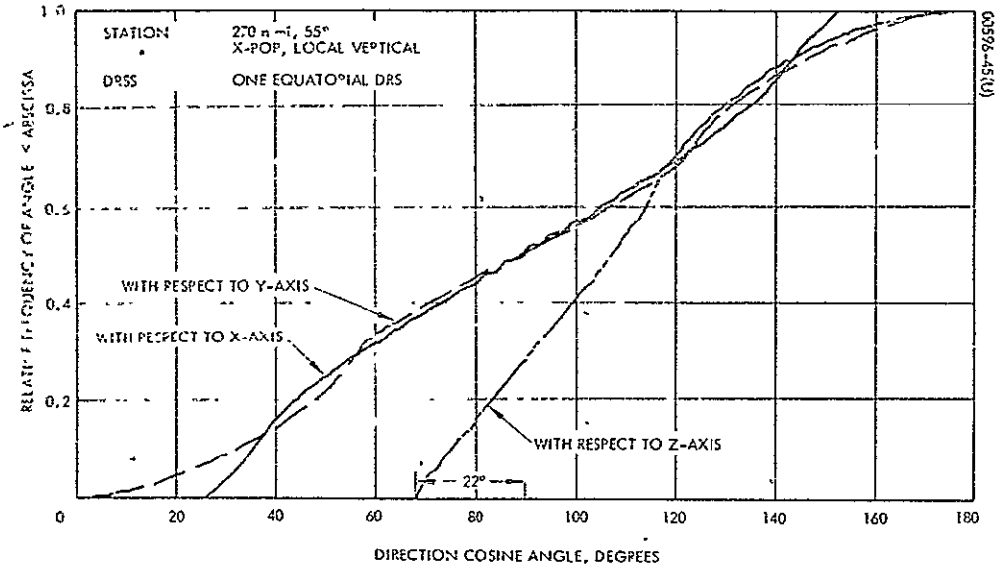

Figure 6-13. Distribution of Direction Angles

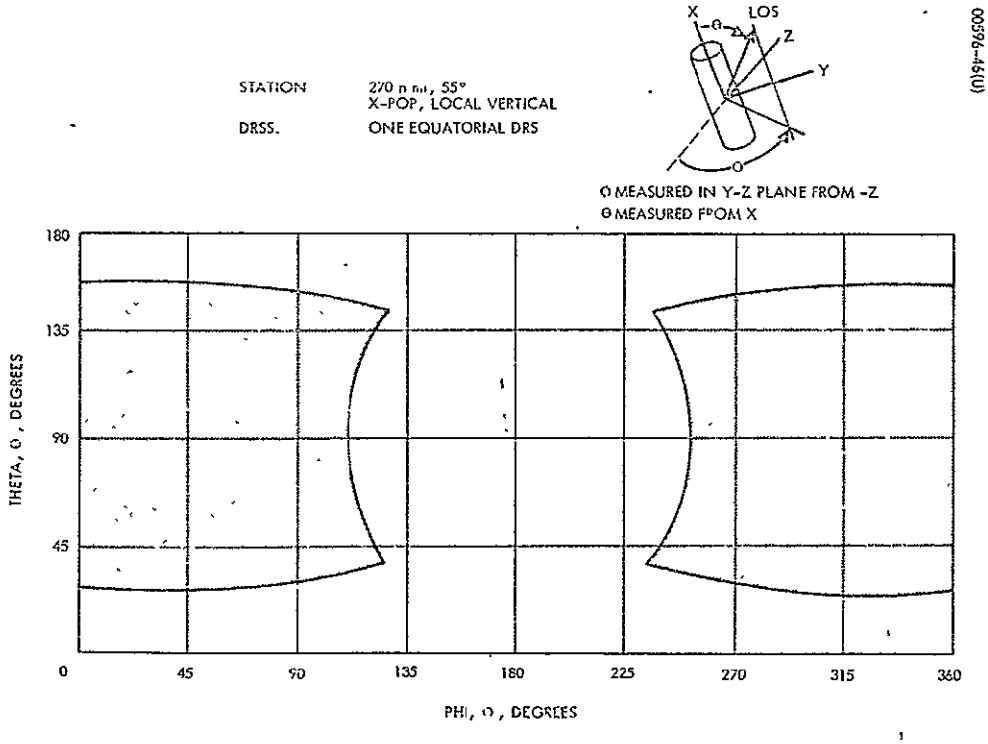

Figure 6-14. Line of Sight Angles θ and ϕ Required for Uninterrupted Communication with a Single DRS.

to spin the antennas when the Station operates in the artificial gravity mode. Note that with this two-antenna configuration, a handover is required whenever the LOS to the visible DRS passes between the hemispheres seen by the two antennas. Furthermore, if the antennas are separated by 180 degrees, the solar panels may block both at the same time because the two solar panels are co-planar and are gimbaled about two axes.

If the Station were only to be used in the local vertical modes, the antennas should be mounted out away from the earth. In this configuration, an antenna tracks a particular DRS from horizon to horizon. Handover is only required when a DRS becomes occulted by the earth. Assuming that the deployment of the DRSS is such that periods of dual coverage will exist, the two antennas can provide essentially uninterrupted communication. While one antenna is tracking a DRS, the other antenna is automatically positioned toward the DRS just appearing above the horizon. Note that the antenna masts are not oriented exactly in the -Z direction and that they are on opposite ends of the Station. In the X-POP local vertical mode, the antennas would interfere with one another if placed on the same end of the Station. If they were both out in the -Z direction, problems might also arise in the Y-POP LV mode when the LOS is generally along the length of the spacecraft. Mounting the antennas on opposite ends of the space station also gives the system the capability for "looking" past rendezvousing vehicles such as the EM_1 or ALS.

Baseline Design: Three Antennas

The Space Station may be used in any of the various attitude modes mentioned above according to the latest mission plans of NASA. The placement of three antennas in the manner suggested in the baseline design combines the desirable characteristics of the two schemes described just above. As shown in Figure 3-2 the three antennas are placed 120 degrees apart about the spacecraft. The two antennas on the -Z side of the spacecraft are used during the local vertical modes. The two antennas on the forward end of the station are used during artificial gravity operations. They have their azimuth axes oriented parallel to the Z-direction so that the gimbal system can remove the artificial-g spin by a counter-rotation about this axis. All three antennas can be used during one of the other inertial modes when the spacecraft is not spinning.

Computer Results

In the local vertical attitude modes, the LOS to the DRS is generally "away from the earth." To quantitatively describe the possible pointing directions of an antenna mounted on the Space Station, a computer program was developed based on the analysis of Subsection 6.3. The program computes LOS angles to a DRS relative to Space Station coordinates. The program requires inputs on the station's attitude mode and its orbital parameters. Orbital parameters of the DRSS are also required. Figures 6-13 and 6-14 are outputs from the "relative frequency" version of the

program. This version calculates the amount of time gimbal angles and their rates can be expected to occur during a long duration mission. The relative frequency of a quantity is the ratio of this occurrence time to the total mission time.

Figure 6-13 shows a plot of the relative occurrence of a LOS direction defined by direction angles relative to the Station's X, Y, and Z axes. The curves correspond to a cumulative probability function -- that is, the ordinate gives the relative frequency of occurrence of a value less than or equal to the abscissa. For the Station's attitude shown, the earth is always "down" in the +Z direction and the Station's XY plane is always at 90 degrees to this reference. Note that the plot indicates that the LOS can approach to within 68 degrees of the +Z direction or 22 degrees below the XY plane. An antenna on the Station is never required to look closer than 26 degrees to either the +X or -X directions.

Figure 6-14 contains the same basic data as is shown in the previous figure. The data here is in the form of a "scatter plot" on a θ and ϕ grid. The areas delineated are those portions of space, relative to the Station, in which a DRS may be found. For a more complete analysis, this plot could be used in conjunction with a program for determination of blockage by the spacecraft structure. Figure 6-14 shows the LOS angles required for uninterrupted communication when the DRS's are above the horizon. The additional program would determine those LOS angles which result in an unobstructed view by the antenna. In Figures 6-13 and 6-14, only one DRS was assumed because this constitutes a "worst case" situation. The required coverage is significantly less when utilizing a DRSS with many satellites.

6.5 DRS HANDOVER GEOMETRY

Introduction

Communication with a particular DRS must be discontinued whenever the LOS is occulted by the earth (or effectively occulted by the earth's atmosphere). DRS handovers may also be desired for operational reasons (such as to permit DRSS access by multiple users).

Determination of Effective Occultation

Figure 6-15 shows the algorithm included in the Space Station/DRSS Geometry Program for determination of effective occultation. The DRS is assumed to be effectively occulted when the LOS vector passes within an altitude, h_a, of the earth. This parameter is determined by the atmospheric effects and CCIR requirements on RFI that exist at the link frequency. At frequencies above S-band, the signal will be severely attenuated if it passes through rain storms in the lower atmosphere. At frequencies below K-band, the CCIR has placed restrictions on the power density which may graze the earth at various angles. (See Figure 6-16.) At X-band, for example, the power density is limited because terrestrial microwave relay systems utilize these frequencies and could be jammed if the satellite's antenna beam viewed the earth. This condition can be prevented by stipulating that the

LOS (and consequently, the main beam) should pass no closer than h_a miles from the surface of the earth (see Figure 6-17).

At the 14-GHz band chosen for the Space Station baseline design, no CCIR requirement currently exists. An h_a = 10 n. mi. was chosen in order that the beam will pass above the most severe weather. This value also allows for anomalies of the nonspherical earth.

Determination of Handover Times

DRSS deployment may provide for dual coverage of certain portions of the user's orbit. Handover from DRS to DRS can occur at any time during this dual coverage period. Handover initiation near the beginning of this period permits the most time for antenna and receiver acquisition. However, during the middle of the dual coverage period, the LOS geometry to the two satellites is approximately the same and the LOS is well above the horizon. In a "late" handover, communication with the "setting" DRS must be maintained down very close to the effective atmosphere limit. Determination of handover times will ultimately be fixed by operational needs. A particular DRSS user may require uninterrupted service during certain periods when performing important experiments.

The first step in developing an operational DRSS user schedule is a computer analysis of the geometry for the time period of interest (perhaps 24 hours). The Space Station/DRSS Communications Geometry Program developed during the study performs these basic calculations for spacecraft in circular orbits. Two mathematical algorithms for handover scheduling were written for this program. The first algorithm causes communication to continue until just before the DRS is occulted; the next DRS utilized is the first vehicle to the east which is visible. This algorithm is shown pictorially in Figure 6-18. The second algorithm causes communication to be passed to whatever DRS is closest to the user spacecraft. Figure 6-19 shows the use of the algorithm for an equatorial space station orbit. For polar orbits, the "shortest-range" algorithm is a poor choice. Figure 6-20 shows that this scheme can cause two unnecessary handovers during that period in which the user passes through the triple coverage region at the poles.

6.6 ANTENNA POINTING GEOMETRY

Introduction

Articulation of an antenna for DRS communication requires a mechanical system with at least two degrees of freedom. The discussion below centers on the possible use of a two-gimbal system. This discussion is the basis of the rationale for selection of a three-gimbal design. The baseline three-gimbal system is discussed in Subsection 6.7.

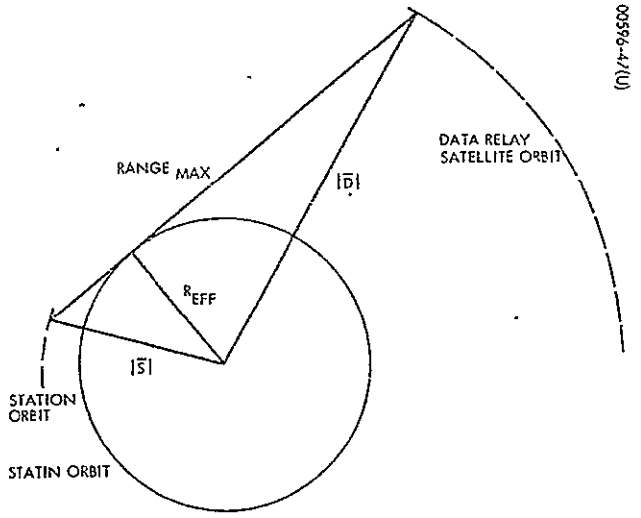

$R_{EFF} = R_{EARTH} + h_{ATMOSPHERE}$

h_A = FUNCTION OF ATMOSPHERIC EFFECTS AND CCIR REQUIREMENTS ON RFI

$|\bar{D}| = R_{EARTH} + h_D$

h_D = ALTITUDE OF RELAY SATELLITE ORBIT

$|\bar{S}| = R_{EARTH} + h_S$

h_S = ALTITUDE OF STATION'S ORBIT

$$RANGE_{MAX} = \sqrt{|S|^2 - R_{EFF}^2} + \sqrt{|D|^2 - R_{EFF}^2} = CONSTANT$$

WHEN THE RANGE > $RANGE_{MAX}$ THE DRS IS OCCULTED.

Figure 6-15. Determination of Effective Occultation by Earth and the Effective Atmosphere

Assumes circular orbits and spherical earth

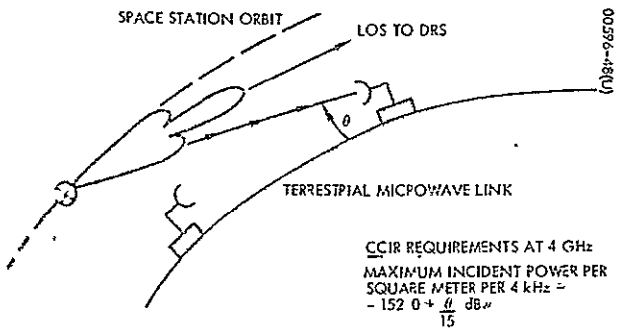

Figure 6-16. CCIR Requirements on RFI

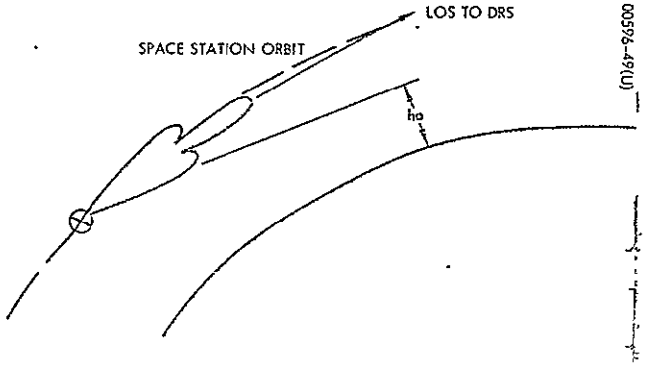

Figure 6-17. Effect of CCIR Requirements on Parameter h_a

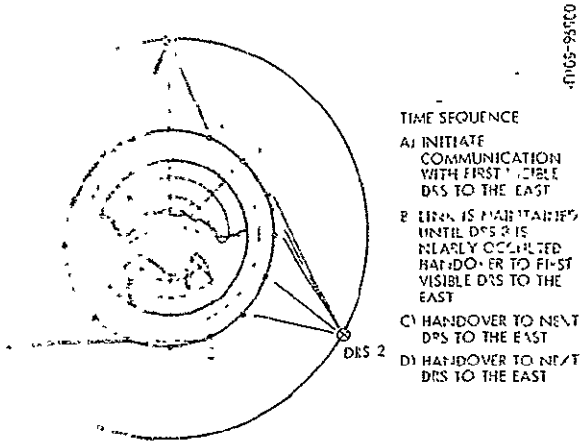

Figure 6-18. DRS Handover Algorithm No. 1 - Space Station in Equatorial Orbit

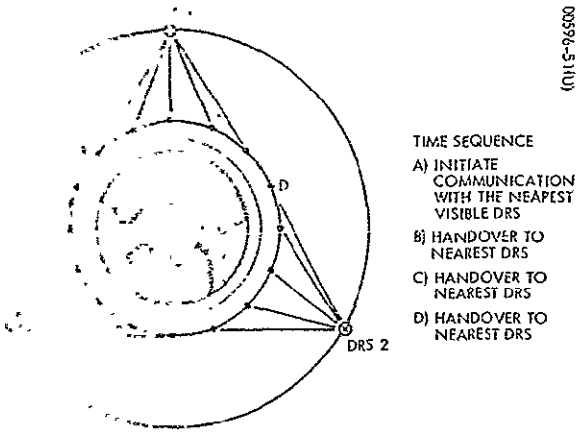

Figure 6-19. DRS Handover Algorithm No. 2 - Space Station in Equatorial Orbit

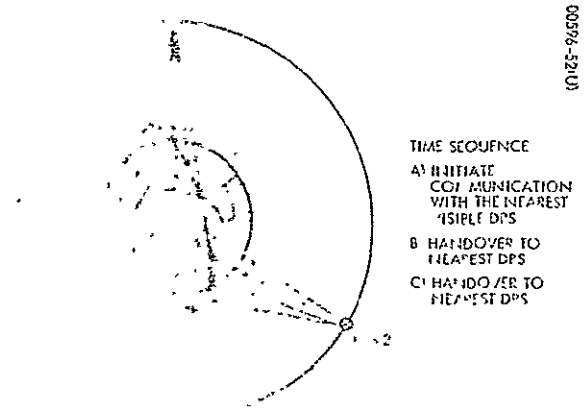

Figure 6-20. DRS Handover Algorithm No. 2 - Space Station in Polar Orbit

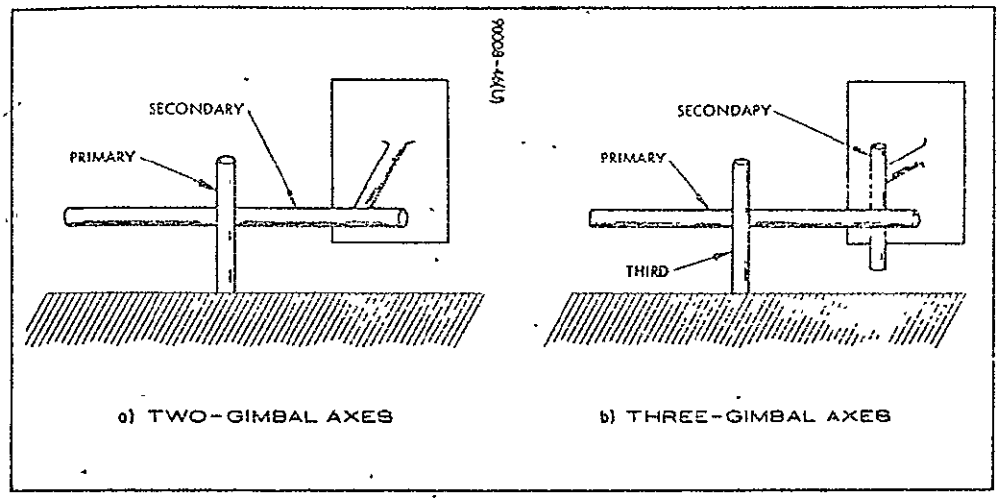

Figure 6-21. Gimbal System Schemes

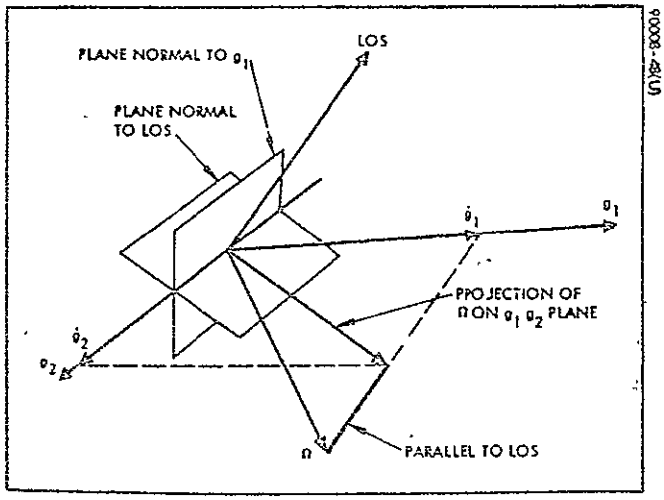

Figure 6-22. Geometric Determination of Gimbal Rates

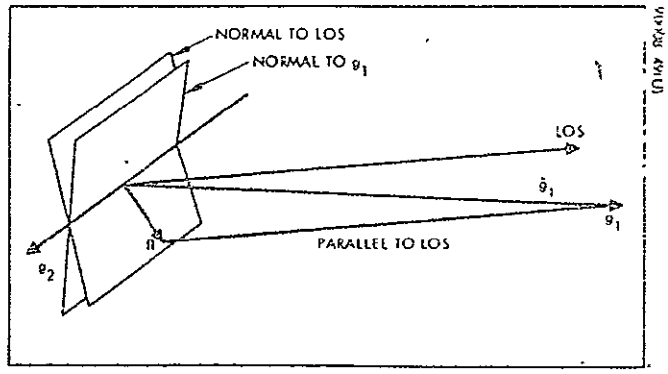

Figure 6-23. Primary Gimbal Axis Rate Increase When LOS and Primary Axis are in Close Proximity

Two-Gimbal Versus Three-Gimbal Designs

To mechanically orient an antenna with respect to the spacecraft, there must be one axis of rotation fixed rigidly to the spacecraft and one axis fixed rigidly to the antenna. For a positioner with only two rotational axes, the axis fixed to the spacecraft will be called the primary axis, and the axis fixed to the antenna will be called the secondary axis. If there are three axes of rotation, the axis attached to the antenna is again called the secondary axis, and the axis that orients the secondary axis is again called the primary. The axis that is attached to the spacecraft and orients the primary axis will be denoted here as the third axis. Thus, for the three-gimbal system, the primary axis is the middle axis that connects the two axes which are attached to the spacecraft and the antenna. These two schemes are illustrated in Figure 6-21. Wherever possible, the two-gimbal scheme is used because of its simplicity.

Theoretically, an antenna can be pointed in any direction if it has two connected axes of rotation -- one fixed in inertial space (the primary) and the other fixed to the antenna (the secondary). One heuristic argument supporting this statement is based on the fact that rotational motion about the axis defined by the LOS is unnecessary and/or unimportant; hence, only two other degrees of rotational motion are required. The major problem with a two-gimbal system is that the angular rate about the primary axis can be very large. To see how and why this occurs, consider the following heuristic discussion.

Denote the primary axis of an orthogonal two-gimbal system by g_1 and the secondary axis by g_2. Orthogonal means that g_1 is perpendicular to g_2. Let the antenna pointing direction be perpendicular to g_2. Such a configuration is shown in Figure 6-21a. Since the pointing direction must coincide with the LOS to the target, g_2 lies in the plane normal to the LOS, but also must lie in the plane normal to g_1 because of the orthogonal design. Thus, the rotation of g_2 about g_1 must be such as to make g_2 coincide with the intersection of these two planes. But, in addition to this positioning requirement about g_1, the relative angular rate of the LOS with respect to the body to which g_1 is fixed must be compensated.

It was mentioned previously that rotational motion about the LOS is unimportant. Thus, the angular rates, $\dot{g}_1$ and $\dot{g}_2$, must compensate for the component of the LOS angular rate, Ω, which is normal to the LOS. As just explained, g_2 is defined by g_1 and the LOS. And consistent with the above argument, $\dot{g}_1$ and $\dot{g}_2$ are defined by the projection of the Ω vector along the LOS onto the $g_1 - g_2$ plane. This geometric interpretation is illustrated in Figure 6-22. The gimballing problem occurs when the LOS and g_1 coincide or nearly coincide. Figure 6-23 indicates geometrically when $\dot{g}_1$ becomes very large; namely, the projection of the LOS angular rate, Ω, along the LOS onto the $g_1 - g_2$ plane results in a large value of $\dot{g}_1$. Theoretically, when the LOS and g_1 coincide, $\dot{g}_1$ must be infinite in order to point the antenna at the target.

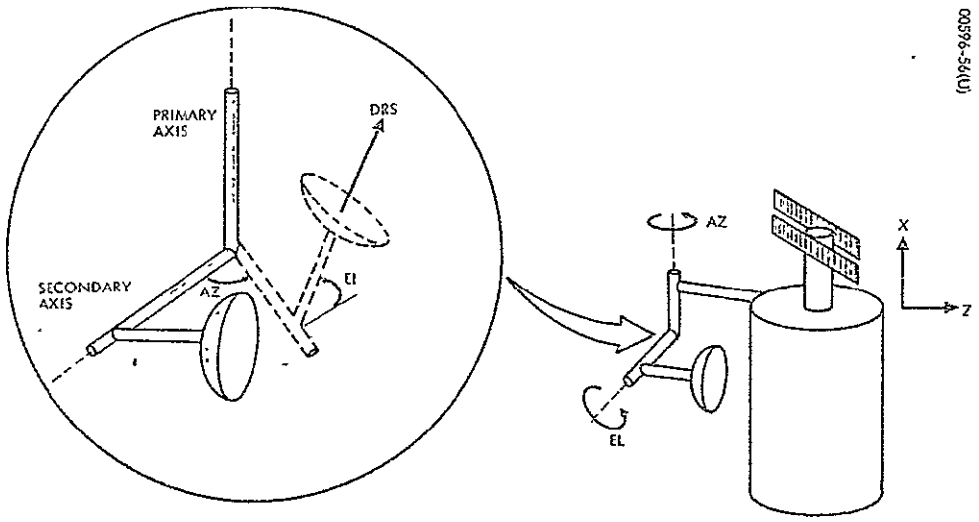

Figure 6-24. Two-Gimbal System on Mast of X-POP Station

Use of Two-Gimbal Designs

Two-gimbal antenna pointing systems can be used successfully under one or more of the following conditions:

1) The gimbal system can be oriented such that the LOS does not pass near the zenith -- that is, the primary or azimuth axis.

2) The system can be designed to track at rates great enough to maintain the target within the beamwidth of the antenna when encountering a zenith condition.

3) Short communications outages can be tolerated when antenna system pointing lags behind the motion of the LOS.

For the Space Station mission, it was assumed that communication outages (condition 3) would not be tolerated. It was also assumed that condition 2 did not apply to the Space Station DRS antenna. During the design phase, narrowing the beamwidth would necessitate servo system redesign to achieve higher tracking rates. Furthermore, the excessive motions of a two-gimbal system during a zenith pass could shorten gimbal life; the system must operate for more than 5 years.

It was discovered that for certain phases of the mission, a two-gimbal system could be oriented such that the LOS to the DRSS would never be near the system zenith. Therefore, condition 1 could be met. Figure 6-24 shows how an AZ/EL system might be mounted on a Station used in an X-POP (X-axis perpendicular to the orbit plane) mode. Figure 6-25 shows pictorially (that with certain inclinations) that this arrangement prevents coincidence of the LOS and the primary axis. Figure 6-26 shows the maximum declination on the celestial sphere of the LOS to the DRSS and (in dashed lines) the declination of the orientation of the primary gimbal axis. This is a worst case geometrical condition. Note that for 80 degrees $\leq i \leq$ 100 degrees, the LOS can pass through the gimbal system zenith. However, the baseline inclination of the Space Station's orbit has been set at 55 degrees. Therefore, a two-gimbal system with the primary axis perpendicular to the orbit plane can be used with the Station in its baseline orbit.

When the station is in the local vertical mode, the principal motion of the azimuth axis is a 1 rev/orbit rotation to remove the earth-pointing rotation of the spacecraft. The antenna motions required to "track-out" Station and DRS orbital motions are very slow. The required motions were determined quantitatively by the use of the computer program discussed previously. Figure 6-27 shows a histogram of the required azimuth and elevation angular rates. (The curves correspond to probability density functions. The computer plot shows that the azimuth rate is centered about 1 rev/orbit 360 deg/90 min. = 4 deg/min. The azimuth rate is always between -4.7 and -2.8 deg/min. The elevation rate is between -0.6 and +0.6 deg/min.)

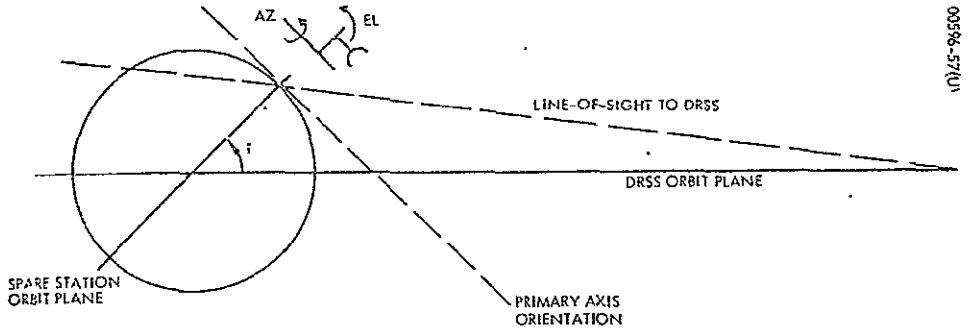

Figure 6-25. LOS/Primary Axis Geometry - Primary Axis Perpendicular to the Orbit Plane

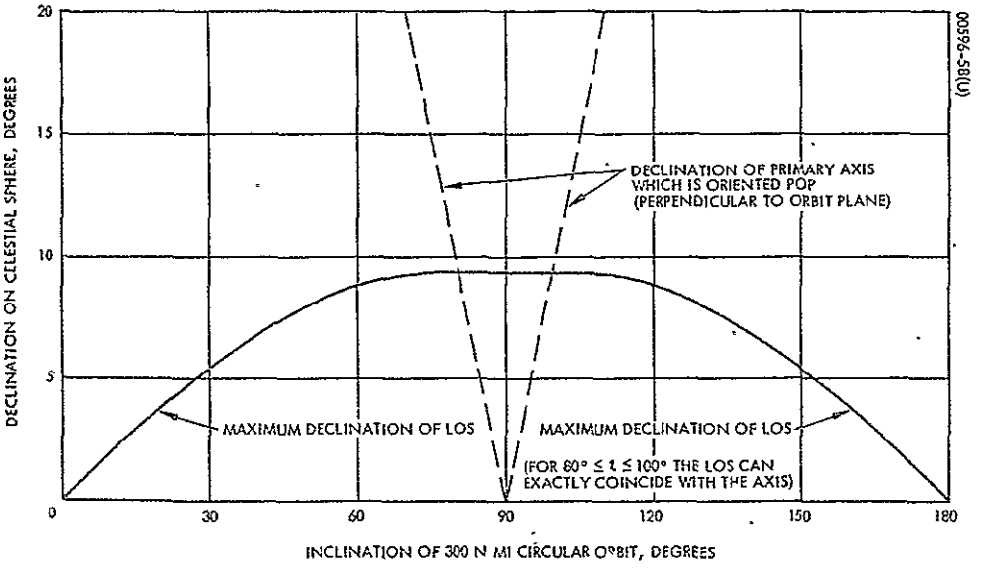

Figure 6-26. Worst Case LOS/Primary Axis Geometry - Primary Axis Perpendicular to the Orbit Plane

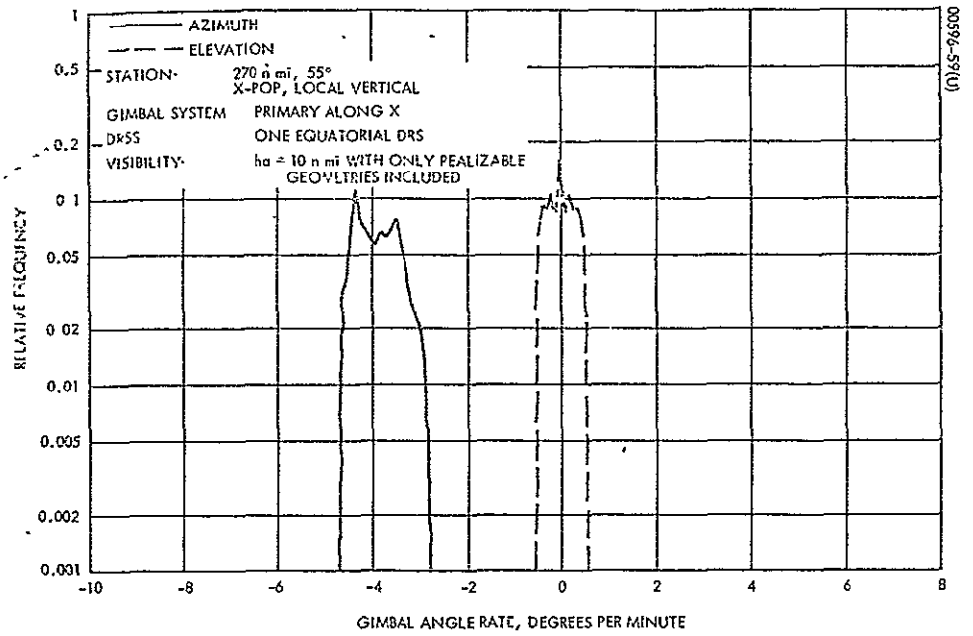

Figure 6-27. Gimbal Rate Data

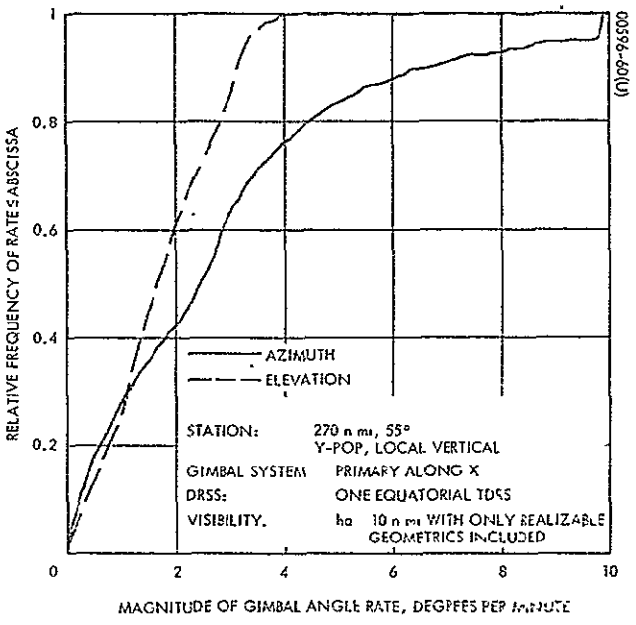

Figure 6-28. Required Gimbal Rates

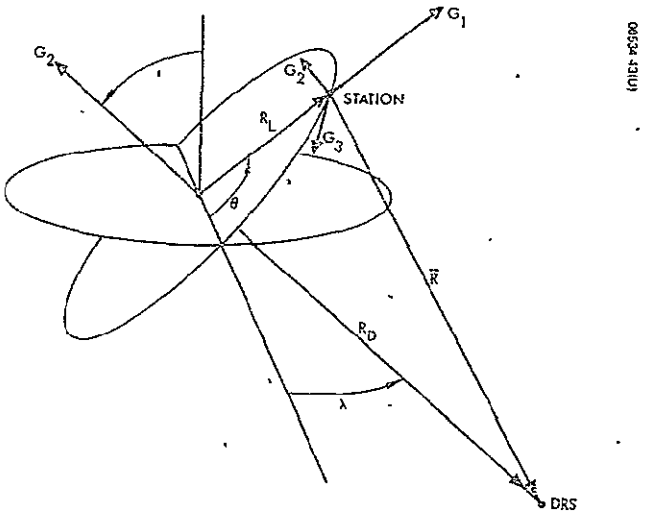

Figure 6-29. Gimbal Coordinates

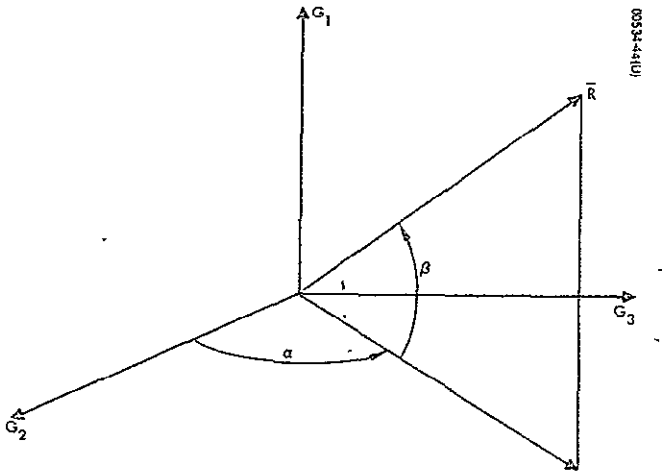

Figure 6-30. Definition of Angles α and β

It has been shown that a two-gimbal system can be mounted on an X-POP Station with an orbit inclination of 55 degrees such that a zenith condition never occurs. However, if the Station can maneuver into other attitude modes, this preferred geometry may no longer exist. Figure 6-28 shows a computer-generated "cumulative probability density" of the required angular rates assuming a change to the Y-POP local vertical mode. Because the antenna must track through its zenith, the azimuth rate is no longer limited to 4.6 deg/min. Approximately 5 percent of the time, the azimuth rate must be greater than 10 deg/min in order for the boresight to be kept coincident with the LOS.

Selection of a Three-Gimbal Design

The two-gimbal system discussed above was considered undesirable because it could only be used over a limited range of the possible mission attitude modes (and it could also be unsatisfactory on a Station placed in a polar orbit). The three-gimbal system discussed in the following section, can be used with any Space Station orbit or attitude mode. This particular design was selected for the baseline system.

6.7 ANALYSIS OF BASELINE GIMBAL SYSTEM

For the three-gimbal system shown in Figure 3-2, a history of the gimbal motion is useful for determining: 1) the limitations of the system, 2) the logic required for three-axis control, and 3) understanding handover. The following analysis does not consider the dynamics of the control system, but only the basic control logic and the Station/DRSS geometry.

Gimbal Coordinate System

Figure 6-29 illustrates a coordinate system for a positioning system mounted on an earth-oriented vehicle. The coordinate unit vector, G_1, is parallel to the local vertical and points away from the earth's center. G_2 is perpendicular to the orbit plane in the direction of the orbit angular velocity; G_3 is parallel to, but in the opposite direction of, the velocity vector.

The time-varying vector, $\overline{R}$, from the Station to the DRS, can be expressed in these coordinates as a function of orbital parameters as is shown in Subsection 6.3. In Figure 6-30, the angles α and β define the direction of $\overline{R}$ with respect to the G_1 G_2 G_3 coordinates.

The angular position of the gimbals is defined by angles g_1, g_2, and g_3, where "1" refers to the azimuth axis (A), "2" refers to the elevation axis (E), and "3" refers to the cross-axis (C). Note that g_1, g_2, and g_3 are not necessarily simply related to the angles α and β. The zero points of the three angles are defined such that $g_1 = 0$ when the elevation axis coincides with G_2 (the orbit normal), $g_2 = 0$ when the antenna boresight is parallel to the $G_2 - G_3$ plane (local horizontal), and $g_3 = 0$ when the boresight is perpendicular to the elevation axis. The baseline mechanical limits on these angles are as follows:

$$-180 \leq g_1 \leq 180 \text{ degrees (unlimited motion)}$$

$$-20 \leq g_2 \leq 110 \text{ degrees}$$

$$-20 \leq g_3 \leq 20 \text{ degrees}$$

Positioning Logic

Gimbal angle motion depends on the time history of the vector, $\bar{R}$, with respect to the G_1 G_2 G_3 coordinate system and the control system logic, which splits the required angular motion into the three gimbal angles. There are three positioner modes with the logic proposed: 1) azimuth-elevation mode, 2) X-Y mode, and 3) transient mode.

Azimuth-Elevation Mode

As an azimuth-elevation mount ($g_3 = 0$) approaches zenith, the azimuth angle rate of change required for perfect tracking approaches infinity. To prevent tracking errors at zenith, the proposed LAS gimbal operates as an az-el mount for low elevation angles and as an X-Y mount for high elevation angles. If a satellite orientation and altitude is assumed, an elevation angle, E, can be chosen below which the maximum required azimuth rate will be within the slewing capability of the azimuth drive. Then, referring to Figure 6-30, when -20 degrees $\leq \beta < E_1$, the positioner behaves as a typical az-el mount with

$$g_1 = \alpha, \; g_2 = \beta, \text{ and } g_3 = 0$$

It was in Subsection 6.3 that

$$g_1 = \tan^{-1}\left(\frac{-R_{G2}}{R_{G3}}\right) = \alpha$$

$$g_2 = \tan^{-1}\left(\frac{R_{G1}}{R_{G3}} \cos g_1\right) = \sin^{-1}\left(\frac{R_{G1}}{R}\right) = \beta$$

$$g_3 = 0$$

$$\dot{g}_1 = \frac{R_{G2}\,\dot{R}_{G3} - \dot{R}_{G2}\,R_{G3}}{R_{G2}^2 + R_{G3}^2}$$

$$\dot{g}_2 = \frac{\left(\dot{R}_{G1} R_{G3} - R_{G1} \dot{R}_{G3}\right) \cos g_1 - \dot{g}_1 R_{G1} R_{G3} \sin g_1}{\dot{R}_{G3}^2 + \left(R_{G1} \cos g_1\right)^2}$$

$$\dot{g}_3 = 0$$

For the proposed system, $E_1 = 80$ degrees.

X-Y Mode

In the X-Y mode, the elevation axis and cross-axis are used to track the DRS. When the elevation angle exceeds E_1, the azimuth angle, g_1, ceases tracking, and remains at the value, α_o, which it attained at $g_2 = E_1$. And, it remains at this position for as long as the gimbals are in the X-Y mode. To prevent the elevation and cross-axis gimbals from hitting their stops, thresholds are set on the angles g_2 and g_3, which are sufficiently far below the mechanical limits that a return to az-el mode can be effected without reaching the limits. The proposed thresholds are 95 and 10 degrees, respectively. Thus, for

$$80° < g_2 < 95° \quad \text{and} \quad -10° < g_3 < 10°$$

the positioner behaves as an X-Y mount. It can be shown that the gimbal angles and gimbal angle rates are given by the following equations:

$$g_1 = \alpha_o \tag{6-42}$$

$$g_2 = \tan^{-1}\left(\frac{R_{H1}}{R_{H3}}\right) \tag{6-43}$$

$$g_3 = \sin^{-1}\left(\frac{R_{H2}}{R}\right) \tag{6-44}$$

$$\dot{g}_1 = 0$$

$$\dot{g}_2 = \frac{R_{H3}\,\dot{R}_{H1} - R_{H1}\,\dot{R}_{H3}}{R_{H3}^2 + R_{H1}^2} \tag{6-46}$$

$$\dot{g}_3 = \frac{\left(\dot{R}_{H3}\,R_{H2} - R_{H3}\,\dot{R}_{H2}\right)\cos g_2 + \dot{g}_2\,R_{H2}\,R_{H3}\sin g_2}{R_{H3}^2 + R_{H2}^2\cos^2 g_2} \tag{6-47}$$

$$R_H = A_{HG}\,R_G \tag{6-48}$$

$$A_H = \begin{pmatrix} 1 & 0 & 0 \\ 0 & \cos g_1 & \sin g_1 \\ 0 & -\sin g_1 & \cos g_1 \end{pmatrix} \tag{6-49}$$

where α_o is the value of g_1 when g_2 reached E_1.

Transient Mode

When the gimbal system is in the X-Y mode, and the thresholds for g_2 or g_3 are reached, the azimuth axis is reactivated. Typically, g_1 will be different from α, and this error must be nulled while g_2 and g_3 adjust to maintain the boresight unit vector, $\bar{B}$, equal to $\bar{R}/R$. When $\dot{g}_1 = \alpha$, the gimbal system resumes the az-el mode. Figure 6-31 illustrates a simplified control system error response that is useful for this preliminary analysis. This response amounts to a constant rate slew of the azimuth axis in the proper direction to minimize the error nulling time. The baseline value for r, the azimuth slewing rate, is 36 deg/min. For this mode, the gimbal angles and rates can be found from Equations 6-42 through 6-49 with the following azimuth gimbal rate

$$g_1 = \begin{cases} -r & (\alpha - g_1) < 0 \quad \text{or } > 180^\circ \\ 0 & (\alpha - g_1) = 0 \\ r & (\alpha - g_1) > 0 \quad \text{or } < -180^\circ \end{cases} \tag{6-50}$$

In performing the computation, g_1 is found from $\dot{g}_1$ and the initial value, $g_1(t) = \alpha_o$, where t = 0 when starting the transient mode.

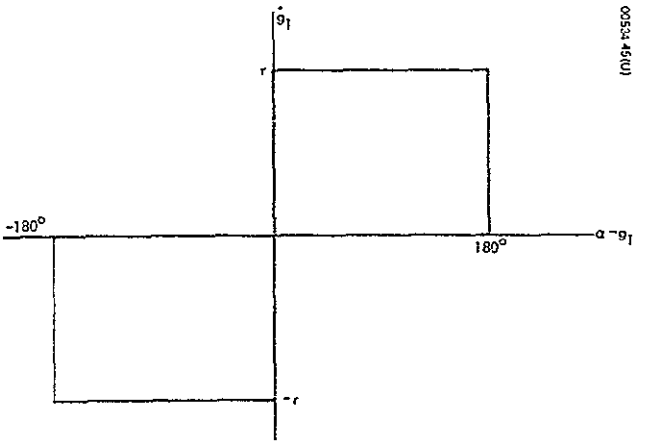

Figure 6-31. Simplified Error Response for Nulling Azimuth Error During Transient Mode

Computer-Generated Time History

Using the logic and equations described above, a computer program was developed to compute the gimbal angles and gimbal rates as a function of time. For an illustrative example, the Station is assumed to be in a 55 degree inclined orbit at 250 n. mi. Three equatorial synchronous DRS are also assumed. The Station's initial position is such that at 24 minutes after t = 0, the spacecraft passes directly under one of the DRS's. The particular K-band system analyzed here is that with its azimuth axis pointing out along the +Z axis with the station in a local vertical mode. Note that only the tracking behavior of the antenna system is generated by the program. Slewing and acquisition by the antenna is not included. "Instantaneous handover" between DRS's is shown in Figures 6-32 and 6-33. Note in the first figure that as the Station passes under the DRS (at about t = 0.5 hours), the antenna must track through its zenith and the Y-axis become active. Figure 6-33 shows the rates which occur on the three axes during this transient mode and during normal AZ-EL mode.

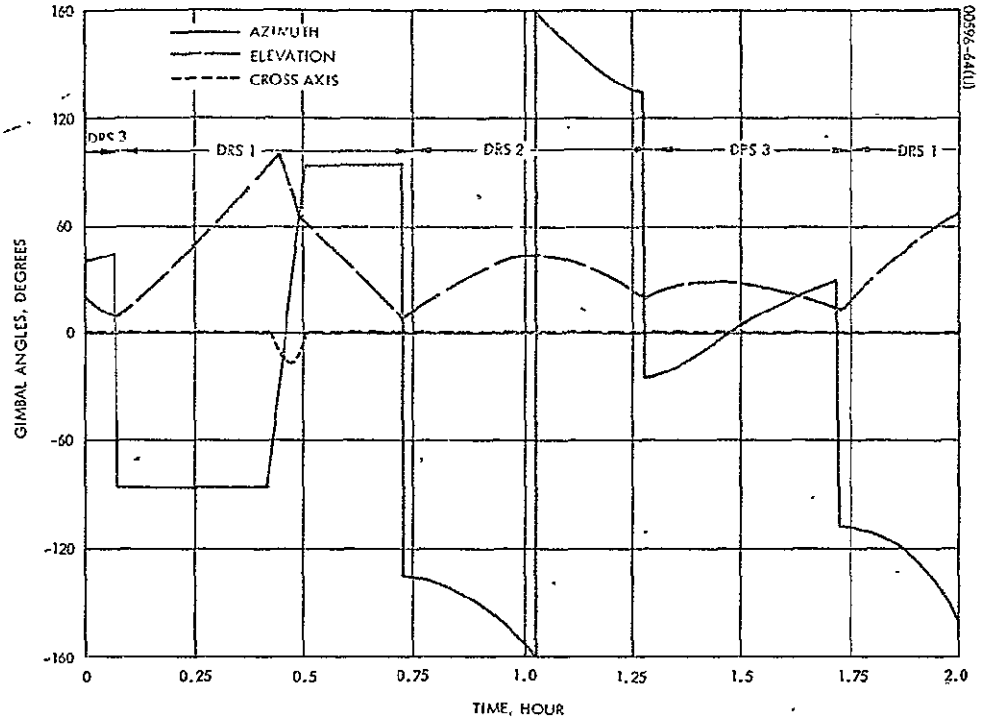

Figure 6-32. Gimbal Angle Time History - Baseline Three-Gimbal System

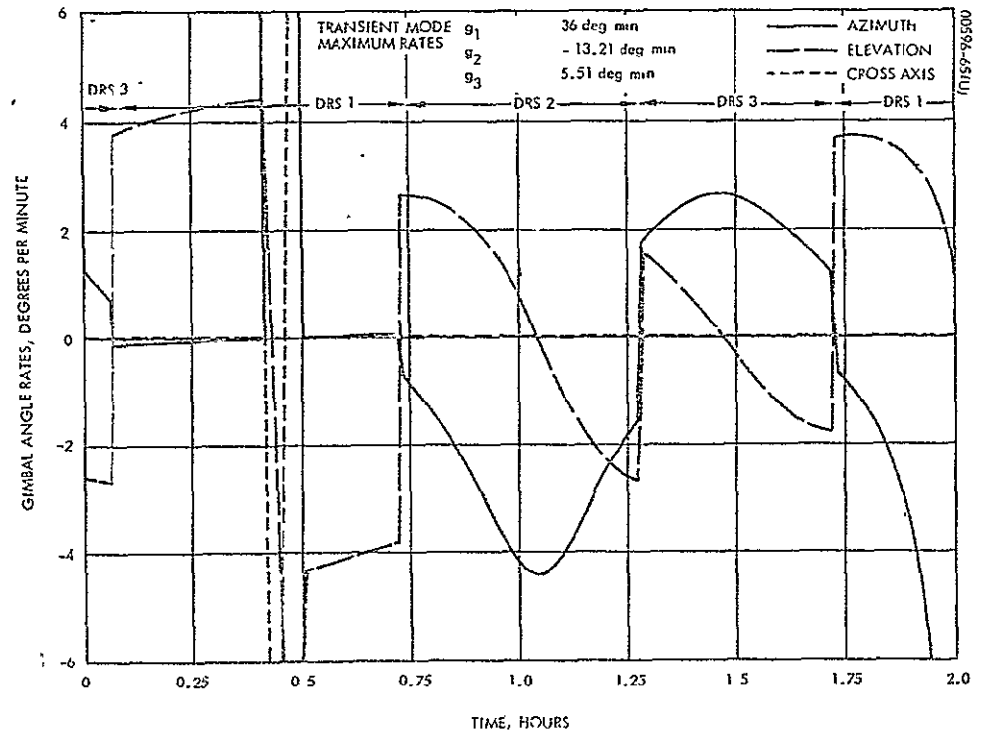

Figure 6-33. Gimbal Angle Rate Time History - Baseline Three-Gimbal System

7. LINK ANALYSIS AND DESIGN TRADES

7.1 INTRODUCTION

Throughout the study, link calculations were performed to update the Space Station communication system design in view of changing constraints and requirements. The final link power budgets are given in Appendix A as supportive material for the system design in Part I.

Subsection 7.2 reviews conventional linear link analysis and gives a sample calculation. Subsection 7.3 outlines an analysis approach for a composite PSK link through a hard-limiting repeater when it is used in frequency division multiple access. Subsection 7.4 summarizes the conclusions reached as a result of the various link analyses performed in support of the Space Station communications system design.

7.2 LINEAR LINK DESIGN

Introduction

The equations employed in the linear link analyses are given below. The performance data required to evaluate these equations can be found elsewhere:

1) For geometrical data, see Subsection 6.2.

2) For achievable TWTA powers, see Subsection 10.2.

3) For achievable system temperatures, see Subsection 10.3.

4) For results on convolutional coding, see Reference 7-1.

Range Equation

Consider a space-to-space communications link. The received carrier-to-noise density ratio can be written as

$$\frac{C}{N_o} = \frac{P_t G_t G_r}{L_t L_s N_o}$$

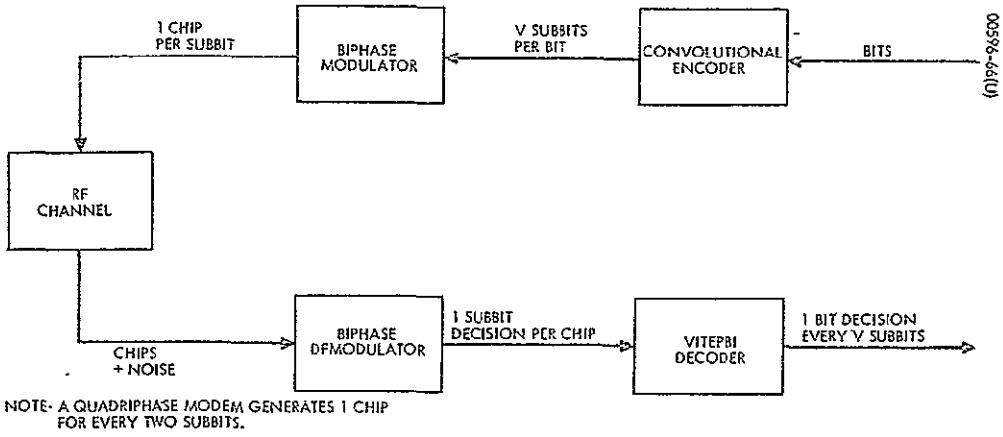

Figure 7-1. Definition of Bit, Subbit, and Chip

where

$\frac{P_t G_t}{L_t}$ = the effective radiated power,

L_s = the space loss = $\frac{16\pi^2 R^2}{\lambda^2}$

G_r = the receive antenna gain,

and

N_o = the receive system temperature.

Also, $N_o = kT_s$, where k = Boltzmann's constant and $T_s = T_{antenna} + 290° (L_r - 1) + T_{receiver}$.

C/N_o Required for Biphase PSK

The performance of digital links is described in terms of the bit rate, R_B, and the bit error probability, P_B. Modulation theory determines the required bit energy-to-noise density, E_B/N_o, for a given P_B. For example, if biphase PSK is coherently detected, an E_B/N_o = 9.6 dB at the demodulator results in a $P_B = 10^{-5}$ in the output data stream.

Given C/N_o and R_B, the E_B/N_o at the demodulator is simply $\frac{C/R_B}{N_o}$.

C/N_o Required for Convolutional Coded Links

Simulations of convolutional encoder/decoder performance determine the required received E_B/N_o for a given P_B. These results can therefore be applied directly to link design as shown above for uncoded PSK. It should be noted, however, that a code of rate = 1/V generates V-subbits for every information bit. Therefore, the biphase modulator operates at a clock rate of VR_B since one biphase chip represents one subbit. (See Figure 7-1.) The link summaries are given in terms of the RF chip rates and the required E_{CHIP}/N_o. This clarifies the RF structure of the data links and identifies the SNR seen by the phase tracking loop and the subbit time synchronizer.

Representative Calculation

Table 7-1 shows a representative calculation for a convolutional coded biphase PSK link. The first portion of link summary determines

the signal power received at the ALS. Given the ALS receive system noise temperature, the received C/N_o is then calculated. The chip rate in the channel is 2 x 57.6 chips/second, since a V = 2 code is used. Therefore, the received E_C/N_o is $C/R_{CHIP}/N_o$ = 50.6 dB·Hz. The 2 dB "degradation in the detector" includes the effects of intersymbol interference, carrier phase tracking error, and chip synchronization error. A 1.0 dB margin is allocated to the detection process independent of the 1.9 dB margin in the RF system. Since a rate 1/2 code is used, the bit energy available to the Viterbi decoder is two times the received chip energy. This is indicated as a factor of E_{BIT}/E_{CHIP} = 3.0 dB. The E_B/N_o received by the decoder is then 5.2 dB. Simulations at MSC have shown that at this E_B/N_o, the Viterbi decoder outputs on the average only one erroreous bit decision in every 10^5 bits (Reference 7-1).

7.3 DESIGN OF A COMPOSITE PSK LINK THROUGH A HARD-LIMITING REPEATER

Although a communications satellite is conceptually simply a "repeater," the characteristics of typical relay satellite designs should be considered in a composite link design. The use of a hard-limiting repeater precludes the use of the conventional linear link design techniques described above. The analysis approach below could be used in the preliminary design of a composite PSK link through a hard-limiting repeater.

Typical Repeater Designs

The DRS repeater may be used by several low altitude vehicles on a random basis. Assuming that a frequency translation design is used, the repeater bandwidth can be used by multiple users with orthogonal signals. Orthogonal signaling schemes can be achieved by access in time or frequency division or by the use of pseudo-random codes. Frequency division multiple access (FDMA) has been the most widely used approach and will be assumed in this study.

The signals and noise entering a typical repeater are sometimes simply translated and linearly amplified. However, if the input signal levels can vary significantly, the input may be limited or automatic gain control may be employed. Furthermore, the output power amplifier of a communications satellite is often driven to saturation because of the resultant increased efficiency. The limited input and saturated output amplifier repeater is often called simply a "hard-limiting repeater."

Intermodulation Noise in a Hard-Limiting Repeater

Although a link through a linear repeater can be analyzed largely on the basis of retransmitted noise and downlink noise, the hard-limiting repeater produces a nonlinear distortion of the signal and an intermodulation "noise" when multiple users are present. Intermodulation noise (IM) in FDMA systems sets an upper bound on the quality of the relayed data

TABLE 7-1. ALS DATA LINK SPACE STATION TO ALS (f_c = 2100 - 2300 MHz)*

PERFORMANCE SUMMARY		
Bit rate		57.6 kilobits/sec
Bit error rate		10^{-5}
Range		303 n. mi.
Channel Coding	**at Baseband**	**at RF**
Encoding	(2, 5) Convolutional Code	Biphase PSK
Decoding	Viterbi decoder (q = 8)	Coherent integrate and dump

LINK SUMMARY	
Transmitter power (including output circuit losses)	20.4 dBw
Line losses	-1.0 dB
Transmit antenna gain	-3.0 dB
Free space loss	-154.2 dB
Ellipticity loss	-1.0 dB
Receive antenna gain	-3.0 dB
Link margin	-1.9 dB
Power received at ALS	C = -143.7 dBw
Noise power density (T_s = 800°K)	N_o = 199.5 dBw/Hz
	C/N_o = 55.8 dB·Hz
Chip rate (115.2 x 10^3/sec)	50.6 dB·Hz
Received E_c/N_o	5.2 dB
Degradation in detector	-2.0 dB
Detector margin	-1.0 dB
E_{BIT}/E_{CHIP}	+3.0 dB
E_B/N_o to Viterbi decoder	5.2 dB

* ...requires 244 KHz within this band

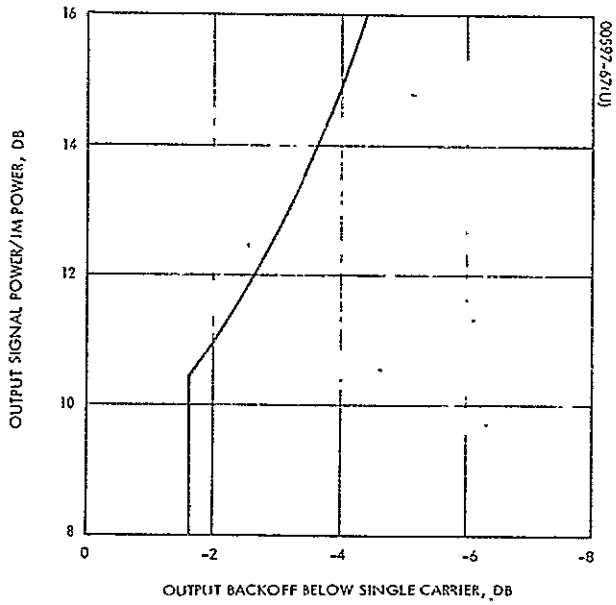

Figure 7-2. Output Backoff Versus Average Signal to Average Distortion Power

independent of thermal noise considerations. Studies have shown that the output signal to IM noise power ratio approaches about 10 dB as the number of equal-power and equally-spaced FDMA users grows very large (and is at least six) (References 7-2 and 7-3). Figure 7-2 shows how this signal to IM ratio varies with the amplifier (TWT) backoff below the saturated (single carrier) case. Given the maximum signal to IM ratio, the maximum attainable E_B/N_o in a PSK channel can also be calculated. If the IM noise is spread in the $2R_B$ bandwidth of a PSK signal of bit rate R_B, then the

$$\frac{E_B}{N_o} = \left(\frac{S}{N}\right) \frac{T_B}{\frac{1}{2R_B}} \qquad \text{where } T_B = \frac{1}{R_B}$$

and with $\left(\frac{S}{N}\right) = 10$,

$$\frac{E_B}{N_o} = (10) \times 2 \rightarrow 13 \text{ dB.}$$

Design of the Composite Link

The design of the "composite" data link should consider (as a minimum) uplink noise, IM noise, power sharing, TWT backoff, and downlink noise. A rule-of-thumb analysis which includes all these factors is given below. The resulting equation (at the bottom of page 7-13) was used to obtain Figure 7-3. The curves illustrate the penalties which IM noise imposes on the design of PSK links to and from the satellite. The links must be of very high quality if very low bit error rates are to be obtained; very little noise in addition to the IM noise can be tolerated. Note that in the case of $(E_B/N_o)_{UP} = 13.0$ dB, the downlink must be essentially noiseless to obtain a $P_B < 10^{-5}$. In order to obtain an improvement in P_B from 10^{-3} to 10^{-5} with $(E_B/N_o)_{UP} = 13.0$ dB, the downlink quality must improve by 11 dB.

Use of Coding Techniques

The use of error correcting codes on the DRS link permits a reduction in SNR to the point where IM noise in the repeater is not a major factor. Rate 1/2 convolutional codes can be considered for this application, but research should be done on their performance in an IM noise environment. The K = 5, V = 2 code with Viterbi decoding requires an E_B/N_o of only about 5.2 dB at a 10^{-5} BER. Since two biphase PSK channel symbols (chips) are used for each information bit, the $E_{CHIP}/N_o = (5.2 - 3.0) = 2.2$ dB. If 2dB is allowed for degradation in the detector and about 3 dB

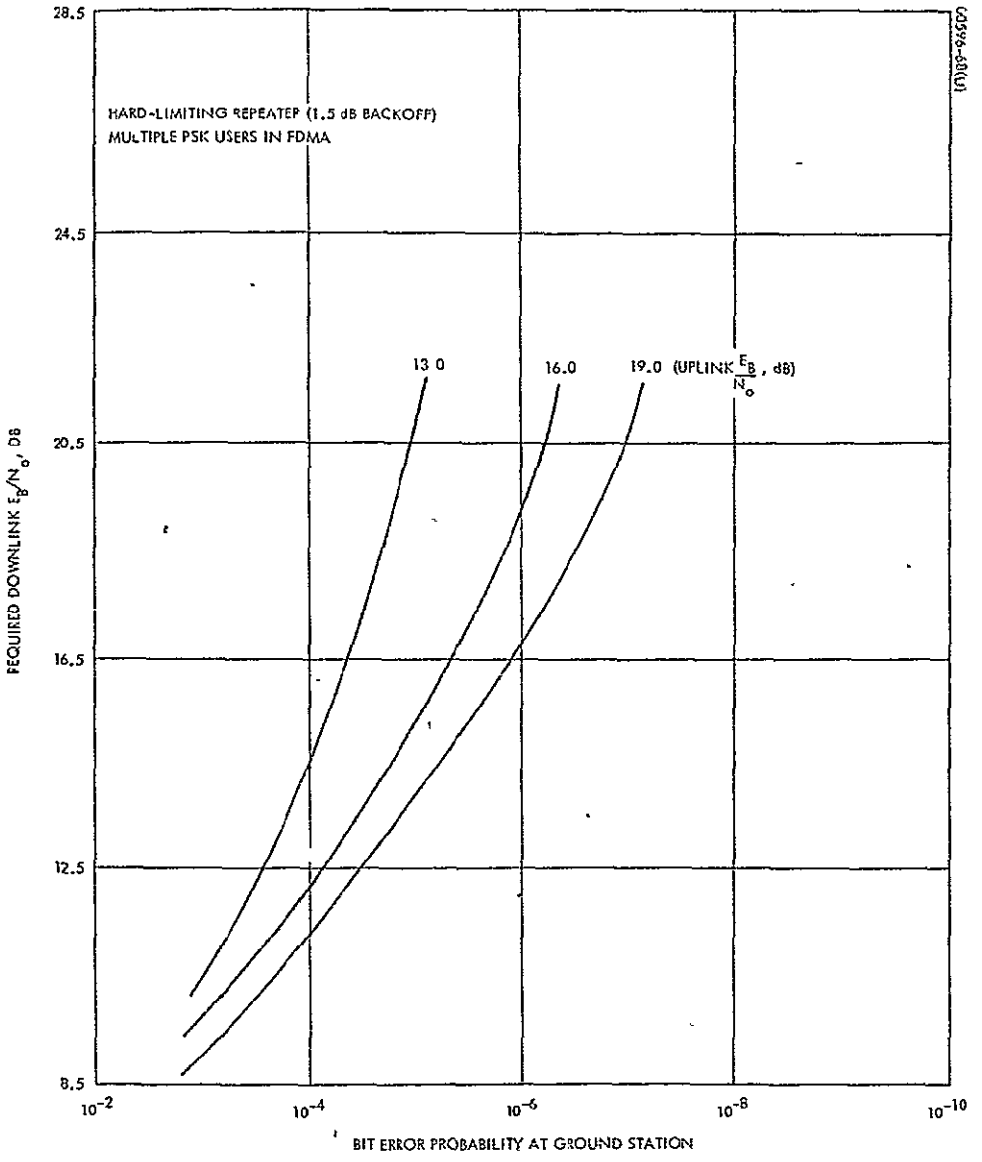

Figure 7-3. Composite Link Bit Error Performance

for a link margin, the RF system must deliver $E_C/N_o \approx 7$ dB to the PSK integrate and dump. At $E_C/N_o = 6.8$, the corresponding chip error rate is 10^{-3}. From Figure 7-3, it is seen that this sort of performance is easily achievable in a relay system utilizing a hard-limiting repeater. (Recall that each RF chip corresponds to a bit in a conventional PSK system. Therefore, in Figure 7-3, read "bit error probability" as "chip error probability.")

Figure 7-4 shows the various tradeoffs in designing a relay system which will achieve a chip error rate of 10^{-3} (or a bit error rate of 10^{-5} when using convolutional codes and allowing reasonable margins). The ordinate of this curve is actually the required downlink E_C/N_o minus the TWT backoff. This gives a "cost function" which takes into account the reduced IM and reduced power when a TWT is "backed-off." The ordinate can be interpreted as far more than just DRS antenna gain. The relative link performance required can be achieved by varying the DRS or ground station antenna, the receiver system temperature, the weather losses (by varying the frequency), or by choosing a TWT of different saturated-single-carrier rating. The curves indicate that with a high quality uplink, the IM is tolerable and to minimize the requirements on the downlink system, the TWT should not be backed-off. When the uplink is severely constrained and say $(E_C/N_o)_{UP} < 8.5$ dB, the downlink system becomes severely burdened when the TWT is driven to saturation. It appears that choosing an $(E_C/N_o)_{UP} = 10.0$ dB would be a reasonable choice for the Space Station $\rightleftharpoons$ data relay link. This does put a severe burden on the downlink when using a hard-limiting repeater. The required DRS antenna gain is also shown to change very little as the TWT is backed-off into the linear region. This permits more flexible repeater operation.

Composite Link Equation for Multiple Biphase PSK Signals Through a Hard-Limting Repeater

Let the total available RF power of the relay satellite be fixed at bC, where

C = single carrier TWT power

b = backoff.

This power will be shared by the signals and noise inputted to the repeater.

η = fraction of output constituting relay noise

δ_i = fraction of output diverted to the i^{th} signal

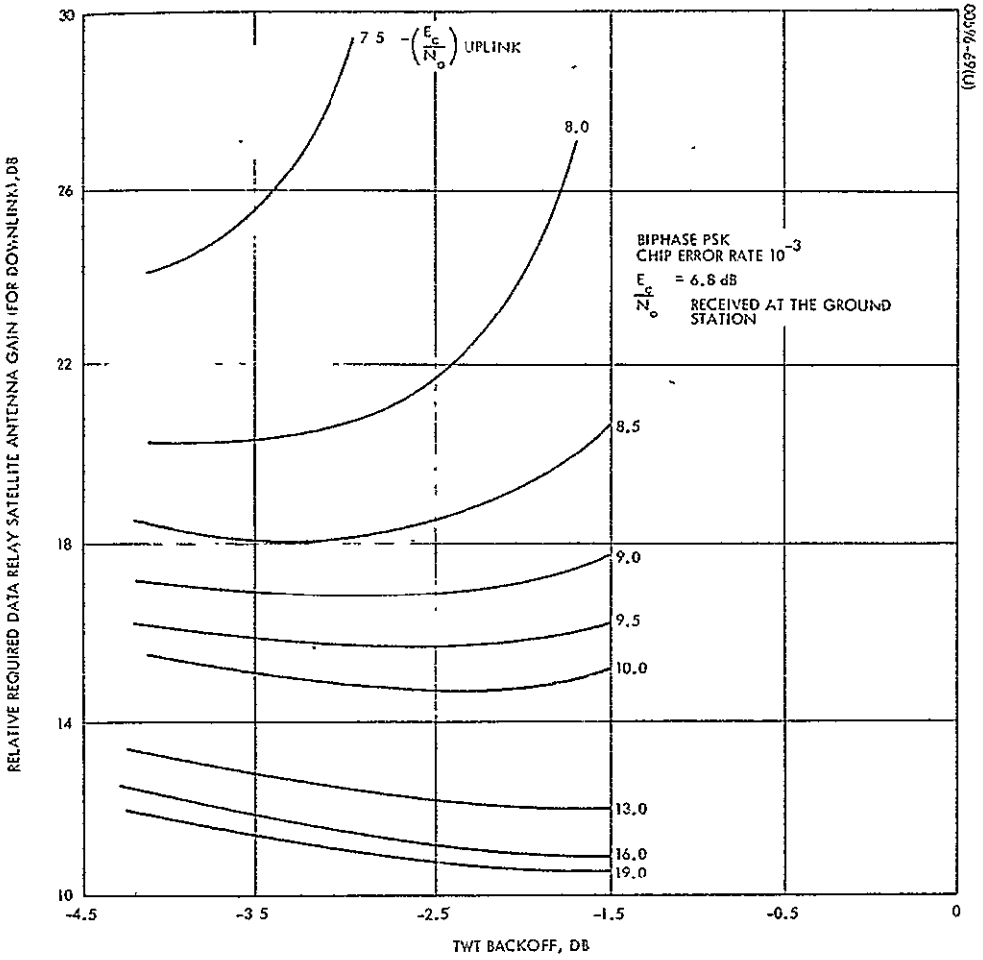

Figure 7-4. Downlink Capacity Versus TWT Operating Point

and

$$\left(\eta + \sum_{i=1}^{n} \delta_i\right) = 1.$$

By definition, output power $= \left(\eta + \sum_{i=1}^{n} \delta_i\right) bC.$

Relayed Noise Power

The noise input to the TWT is due to thermal noise, IM noise, and various cross-terms (which we neglect here as second order effects).

$$\text{noise in} = \text{thermal noise power + IM noise power}$$

$$= N_o B + \alpha (n P_i)$$

where

N_o = density of thermal noise

B = repeater bandwidth

P_i = power in i^{th} signal.

nP_i = total input signal power resulting from n signals.

$\alpha(nP_i)$ = level of noise generated by intermodulation of the n equal power equally-spaced signals (We assume it is approximately uniform across the band).

$$\therefore \eta = \frac{\text{noise in}}{\text{noise in + signal in}}$$

$$= \frac{(N_o B + \alpha n P)}{(N_o B + \alpha n P) + (nP)}$$

and the relayed noise power

$$(N)_R = \eta bC.$$

Relayed Power per User

$$\delta = \frac{\text{signal in}}{\text{noise in} + \text{signal in}}$$

$$= \frac{P}{(N_o B + \alpha\, nP) + (nP)}$$

$$(P)_R = \delta\, bC.$$

N_o at Ground Station

$$(N)_{ground} = K(N)_{relayed} + (N)_{downlink}$$

K = Sum of all system gains and losses.

If we assume the repeater bandwidth is just wide enough to pass the spectra of the n PSK signals each of data rate R, its bandwidth is n(2R).

Therefore,

$$(N_o)_G = K\left[\frac{(N)_R}{2nR}\right] + (N_o)_D$$

Energy at Ground Station Per User

$$(E)_G = K\left[\frac{\delta bC}{R}\right]$$

at Ground Station Per User

$$\left(\frac{E}{N_o}\right)_G = \frac{\delta \frac{KbC}{R}}{\eta \frac{KbC}{2nR} + (N_o)_D}$$

but $\frac{1}{n} \frac{KbC}{R} \frac{1}{(N_o)_D} = \frac{E}{N_o}$ in the downlink per user

$$\left(\frac{E}{N_o}\right)_G = \frac{\delta n \left(\frac{E}{N_o}\right)_{Down}}{\frac{\eta}{2}\left(\frac{E}{N_o}\right)_{Down} + 1}$$

Now, rewriting the expressions for η and δ using $P = ER$, $B = n(2R)$, and $\left(\frac{E}{N_o}\right)_{UP} = \frac{P/R}{N_o}$, we have

$$\eta = \frac{2 + \alpha\left(\frac{E}{N_o}\right)_{UP}}{2 + \alpha\left(\frac{E}{N_o}\right)_{UP} + \left(\frac{E}{N_o}\right)_{UP}}$$

and

$$\delta = \frac{\frac{1}{n}\left(\frac{E}{N_o}\right)_{UP}}{2 + \alpha\left(\frac{E}{N_o}\right)_{UP} + \left(\frac{E}{N_o}\right)_{UP}}$$

Therefore,

$$\left(\frac{E}{N_o}\right)_G = \frac{2 \cdot \left[\frac{\left(\frac{E}{N_o}\right)_{UP}}{2 + \left(\frac{E}{N_o}\right)_{UP}(1+\alpha)}\right]\left(\frac{E}{N_o}\right)_{Down}}{\left[\frac{2 + \alpha\left(\frac{E}{N_o}\right)_{UP}}{2 + \left(\frac{E}{N_o}\right)_{UP}(1+\alpha)}\right]\left(\frac{E}{N_o}\right)_{Down} + 2}$$

It must be remembered that a definite relationship exists between α and $N_{o_{Down}}$, since both are a function of the TWT backoff. Reference 7-1 gives the expression

$$\alpha = .19\,(b^{1.8})$$

for $-1.5 > b > -3.75$ dB.

7.4 DESIGN TRADES

All links except the emergency voice link are convolutional coded digital systems. This approach is the most efficient transmission scheme which could be implemented in the early 1970's. Frequency modulation is employed in the emergency voice system for simplicity.

All the digital links use biphase PSK modulation except the EM_1 system. This modulation (with "integrate and dump" detection) is the optimum technique among the class of bistate modulations. Biphase PSK is also very easily implemented. To conserve bandwidth at S-band, the EM_1 links use quadriphase modulation. This scheme can be analyzed (and implemented) as the union of two biphase systems in phase quadrature. The RF bandwidth it requires is 1/2 that of a comparable biphase system, but its E_B/N_o requirement is theoretically the same.

The ALS data links and the EM_1 links employ S-band frequencies because of NASA's allocations at those frequencies and because of the availability of space-qualified hardware. It was concluded that frequencies above S-band were desirable for the 20 megabits/sec DRS data link. A higher frequency band would provide greater available bandwidth and would give a relative link improvement, assuming fixed apertures at the Station and at the DRS. Frequencies at K-band (13.7 to 15.4 GHz) were chosen because this frequency is currently within the state-of-the-art of microwave technology. At frequencies above K-band, the beamwidths developed by antenna apertures of typical size (3 to 4 feet in diameter) become so narrow that pointing problems become severe. Because the emergency voice system requires only 200 kHz, a VHF frequency band was chosen. This permits full communications service with relatively low power levels and omnidirectional antennas. The power levels required would be about 250 times greater if S-band were used.

Since all the links are full-duplex, the communications terminals in the remote vehicles (either the ALS, EM_1, or DRS) are approximately equivalent to the corresponding terminal on the Station itself. The characteristics assumed for these remote terminals are commensurate with their missions. The ALS uses only flush-mounted omni antennas for communication with the Station, because it must re-enter the earth's atmosphere.

Retractable high gain antennas would add significant complexity. The EM_1 does utilize a high gain antenna. This vehicle is only used in a space environment and furthermore, its principal mission is to collect data and return it to the Space Station. The DRS is assumed to have earth coverage antennas at VHF and K-band and one or more high gain antennas at K-band. Its transmitted power per carrier has been assumed to be modest (5 watts at 14 GHz and 18 watts at 140 MHz), since it may serve many users.

7.5 REFERENCES

7-1 "Program Definition for Computer Simulation of the Viterbi Decoding Algorithm," Lockheed Electronics Company, under Contract NAS 9-5191 to the Manned Spacecraft Center, 1 May 1970.

7-2 "A Study of Channelized Repeaters for Tactical Satellite Communications," (Classified Confidential) Hughes Aircraft Co, IR and D Program, 9 December 1968.

7-3 "Applied Research Study on Satellite Communications, Report No. 5," Contract No. 00442(5), ITT Federal Laboratories, for the U. S. Army Satellite Communications Agency, 30 June 1966.

8. ANTENNA ACQUISITION AND TRACKING STUDIES

8.1 INTRODUCTION

Analysis early in the study indicated that DRS data link constraints would require the use of a high gain antenna on the Space Station. A study was begun which examined problems of initial antenna pointing, antenna acquisition, and antenna tracking.

Consideration was given first to the programmed tracking concept outlined in Subsection 8.2, in which slewing, acquisition, and tracking become essentially the same operation. It was determined that computer control of the antenna was indeed feasible for the Space Station mission. This approach was not chosen for the baseline design because of its open-loop nature and because it requires a continuous interface with either a computer or a mass storage device. The programmed tracking study did indicate that the Space Station K-band antenna could be initially pointed toward the DRS within its 3-dB beamwidth.

Antenna beam broadening was not given extensive consideration simply because the DRS is normally expected to be found within the beamwidth required for communication. Beam broadening requires additional RF complexity. Acquisition by scanning entails only additional use of the slew or manual positioning mode. Scanning can sometimes cause excessive gimbal wear, but it should be required very seldom during the Space Station mission. Subsection 8.3 provides a statistical model of antenna acquisition by scanning. The analysis develops expressions for the probability of acquisition and false acquisition given the basic system parameters. It also develops estimates of the mean time to acquisition.

Subsection 8.4 gives the basic expressions for the theoretical performance of various autotrack techniques. A comparison of the techniques is also made assuming similar system parameters.

The Space Station high gain antenna design is an outgrowth of the various studies. The antenna is initially pointed toward the DRS on the basis of computer-generated pointing commands. If the DRS beacon signal is not present within the beamwidth, communication control generates a scan pattern using the slew mode. If the DRS signal is still not located,

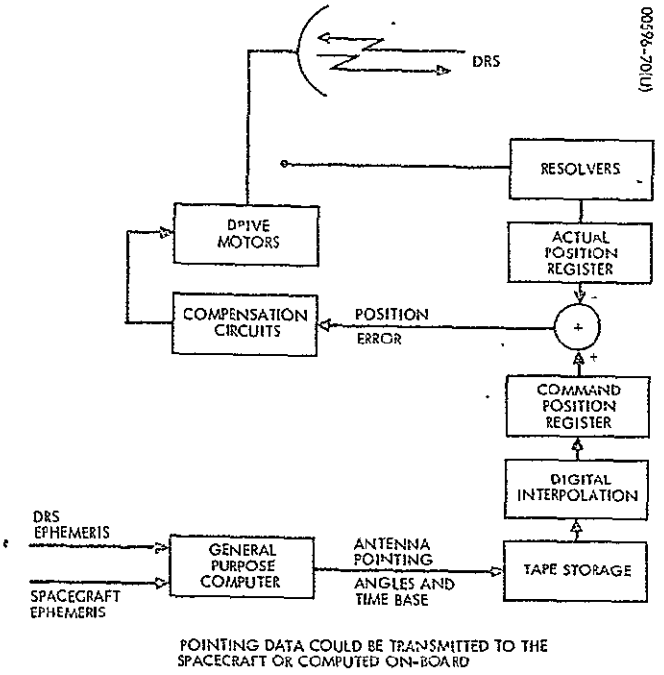

Figure 8-1. Programmed Tracking Concept

a new position estimate is taken from the computer data and another sequence is begun. If acquisition is not attained after several attempts, the operator is alerted. Antenna tracking is accomplished by the use of time-shared monopulse. Its theoretical performance is at least equal to other schemes and it has been used successfully in many hardware designs.

8.2 PROGRAMMED TRACKING CONCEPT

Although monopulse techniques have been used for many years, open-loop, programmed tracking provides an attractive alternative. This approach has been used at ground stations when ephemeris data permits the target vehicle track to be accurately predicted.

The suggested programmed tracking concept is diagrammed in Figure 8-1. Note that while the tracking is open-loop, the antenna positioning is closed-loop, since the actual position of the antenna is monitored by the angle resolvers. The computer interface required by the programmed tracking approach appears to be a negative factor. However, computer generated pointing commands will be a necessity for initial antenna pointing in any mission utilizing a DRSS, and even when a monopulse technique is used for tracking, a computer interface will probably be required for acquisition. The general purpose computer itself need not be located on-board the spacecraft when used to generate either initial pointing or tracking commands. Programmed tracking does require a continuous interface with either the computer or some mass storage device.

The success of an open-loop design requires that all possible error sources can be determined and that their total effect is less than the required error tolerance. Table 8-1 gives a pointing error budget for the Space Station antenna pointing problem. Assuming that the structural deflection is negligible, the pointing error is acceptable even without use of inputs from the spacecraft attitude control system.

Table 8-2 summarizes the advantages and disadvantages of programmed tracking. The references referred to document contain problems that have been encountered with the Apollo monopulse systems.

8.3 ANTENNA ACQUISITION BY SCANNING

The Scanning Problem

To establish the communication link between a spacecraft employing a high gain antenna and a DRS, some method must be used to grossly point the antenna toward the DRS. This section treats the method of link acquisition called scanning, in which the antenna system then searches that angular region of space in which the DRS is expected. When a thresholding device indicates the presence of the DRS signal, the antenna system switches to the autotrack mode and discontinues scanning.

TABLE 8-1. POINTING ERROR BUDGET

	Initial Acquisition, degrees	Extensive Calibration, degrees
Station attitude stability*	0.25	0.25
Station structural deflection	← Unknown →	
Alignment of boom on station	0.05	(N)
Boom deflection	0.02	(N)
Orthogonality of axes	0.02	(N)
Antenna boresight collimation	0.05	(N)
Antenna boresight deflection	0.02	(N)
Antenna positioner accuracy	0.006	0.006
Antenna gimbal encoder accuracy	0.003	0.003
Dynamic overshoot	0.01	0.01
Accuracy of ephemeris and local clock	0.006	0.006
Computational step size	0.005	0.005
Maximum sum error	0.440	0.280
Expected RSS error	0.263	0.251

(N) - Negligible

*This error dominates. It can be tracked out given the actual spacecraft attitude.

TABLE 8-2. ADVANTAGES AND DISADVANTAGES OF PROGRAMMED TRACKING CONCEPT

Advantages

- Pointing is maintained under low signal-to-noise conditions or even during signal drop-out.
- Tracking performance is unimpaired by the presence of low frequency amplitude modulation on the communications signal. (In Apollo, an incidental amplitude modulation on the uplink signal has caused the appearance of an unwanted signal within the tracking system bandwidth.)(Reference 8-1).
- Tracking performance is unimpaired by the presence of multi-path signals. (In testing, it was noted that in the wide-beam mode, the CSM antenna may falsely acquire a signal reflected from the spacecraft surface) (Reference 8-2).
- The approach is easily adapted to anticipate shadowing by the vehicle itself or DRS occultation by the earth.
- Corrections for axes misalignments, calibratable structure flexures, or encoder errors may be conveniently introduced.
- The programmed tracking approach greatly simplifies the antenna feed design and eliminates the usual error signal processing electronics.
- The use of digital techniques greatly reduces the system's sensitivity to component drift.

Disadvantages

- The technique -- like all open-loop designs -- is not adaptable to systems in which all contingencies cannot be anticipated in advance. An error source which goes unrecognized during the design phase could prevent proper system operation.
- A near-real time interface is required with a computer or a mass storage device.
- To achieve the required tracking accuracy an interface may be required with the spacecraft attitude control system. This is especially true when the vehicle (such as the ALS) is capable of extensive maneuvering.

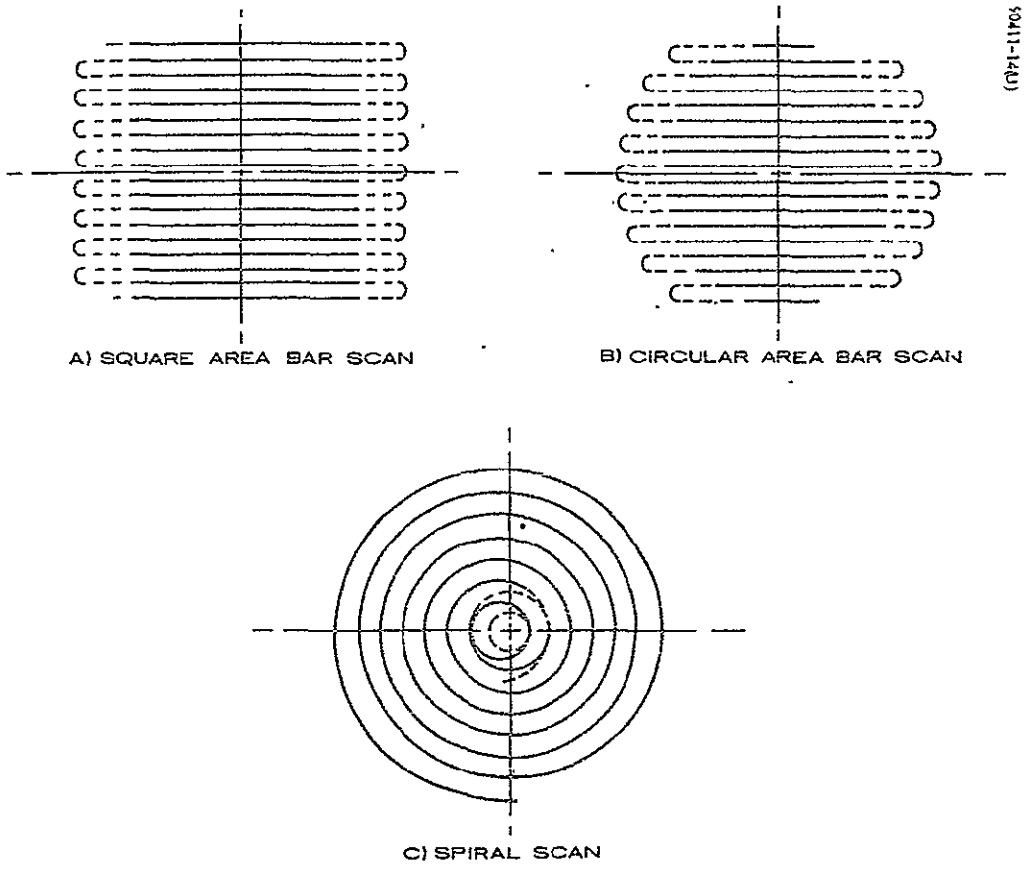

Figure 8-2. Scan Patterns

If $\psi < 10$ degrees and $\theta < 20$ degrees,

$$k \approx \frac{4\psi^2}{\theta^2} \quad (8\text{-}4)$$

An approximation relating antenna 3 dB beamwidth and gain, valid for beamwidths less than 10 degrees, is given by

$$\theta^2 = \frac{2.7 \times 10^4}{G} \text{ (degrees)}^2 \quad (8\text{-}5)$$

Substituting equation 8-5 into 8-4

$$k \approx (1.48 \times 10^{-4})\ G\psi^2 \ (\psi \text{ in degrees}) \quad (8\text{-}6)$$

If $k \leq 1$, then $A \leq a$, i.e., the antenna view area is as large or larger than the search area, so no scanning is required.

If T_s is the total allowable search time, the view period T_k, for a given angular position in the search area is given by

$$T_k = T_s/k \quad (8\text{-}7)$$

Detector Operations

The basic detector assumed in the analysis below is the square law device. Both linear and square law devices have been analyzed by Marcum (Reference 8-3) and shown to have nearly identical detection characteristics. The detector, itself, is preceded by a bandpass filter and followed by a sampler. The sampler is, in turn, followed by an adder which sums the last m outputs from the sampler. A threshold switch is used to indicate a signal detection when the adder output voltage exceeds a bias level, b. This combination of functions is shown in Figure 8-4.

If T_K denotes the time that a DRS is within the receiving pattern of the antenna and t_s is the time between samples, then m is given by T_K/t_s. The samples may be considered independent if $t_s \geq 1/B$, where B is the input filter bandwidth. For acquisition, the bandwidth must be large enough

to accommodate the effects of doppler shift and oscillator variation on the transmitted signal. The maximum doppler shift is given by

$$(\Delta f_D)_{max} = \frac{V_S + V_D \cos i}{C} f \qquad (8\text{-}8)$$

where C is the speed of light, V_S and V_D are the velocities of the station and DRS, i is the orbit inclination, and f is the nominal transmission frequency. For a Space Station altitude of 200 n. mi. and an inclination of 55 degrees,

$$(\Delta f_D)_{max} = (3 \times 10^{-5}) f \qquad (8\text{-}9)$$

Oscillator stability generally results in an order of magnitude less variation. Assuming a stability of one part in 10^{-6},

$$(\Delta f)_{max} = (3.1 \times 10^{-5}) f \qquad (8\text{-}10)$$

The bandwidth must be twice this value, i.e.,

$$B = (6.2 \times 10^{-5}) f \qquad (8\text{-}11)$$

and so

$$m \leq (6.2 \times 10^{-5}) f T_K \qquad (8\text{-}12)$$

The noise will be assumed to be white gaussian noise due to thermal motion of electrons in the receiver. The average noise power, N, is given by

$$N = K T B \qquad (8\text{-}13)$$

where K is Boltzmann's constant and T is the effective noise temperature (°K).

Probability of Error

When no signal is received, the noise alone may cause the adder output to exceed the threshold bias level. The output of the detector will then have a probability density of:

$$p(v) = \begin{cases} \frac{1}{N} \exp\left(-\frac{v}{N}\right) & v \geq 0 \\ 0 & v < 0 \end{cases} \tag{8-14}$$

where:

N = average IF noise power

v = detector output voltage

This density is derived in Reference 8-4, pages 253 - 254.

Normalizing the noise power

$$p(y) = \begin{cases} e^{-y} & y \geq 0 \\ 0 & y < 0 \end{cases} \tag{8-15}$$

where $y = v/N$ is the normalized detector output. The characteristic function of this density is given by

$$C(p) = \frac{1}{p+1} \tag{8-16}$$

The characteristic function of the sum of m independent samples is

$$C_m(p) = \left[C(p)\right]^m = \left[\frac{1}{p+1}\right]^m \tag{8-17}$$

Taking the inverse transform, the density function for the normalized adder output voltage is given by

$$P_m(y) = \begin{cases} \dfrac{y^{m-1} e^{-y}}{(m-1)!} & y \geq 0 \\ 0 & y < 0 \end{cases} \tag{8-18}$$

The probability of error, P_e, is the probability that the adder output due to noise alone will exceed the threshold level, b. The normalized threshold level is denoted by b_n, where

$$b_n = b/N \tag{8-19}$$

Then

$$P_e = \int_{b_n}^{\infty} p_m(y)\, dy \tag{8-20}$$

In Reference 8-5, b_n is computed as a function of P_e and m.

Probability of Detection

Using characteristic functions as above, it can be shown (see Reference 8-3) that the probability density of the adder output with signal plus noise at the input is given by

$$q_m(v) = \begin{cases} \left(\dfrac{v}{mR}\right)^{\frac{m-1}{2}} e^{-(v+mR)} I_{m-1}\left(2\sqrt{mRv}\right) & v \geq 0 \\ 0 & v < 0 \end{cases} \tag{8-21}$$

where R is the signal-to-noise power ratio and I_{m-1} is the modified Bessel function of the first kind and of order m - 1.

Then the probability of detection, P_d, is given by

$$P_d = \int_{b_n}^{\infty} q_m(v)\, dv \tag{8-22}$$

This integral may be expressed as

$$P_d = 1 - T_{\sqrt{b_n}}\,(2m - 1,\ m - 1,\ \sqrt{mR}) \tag{8-23}$$

where

b_n = b/N = normalized bias level

b = threshold bias level

N = rms noise power

R = signal-to-noise power ratio

T = incomplete Toronto function (see Reference 8-3)

P_e is the probability that at a given time the detector will indicate a detection when the DRS signal is not present. P_d is the probability that a detection will be indicated when the DRS signal is present.

Probability of False Alarm

A false alarm occurs when the detector registers a signal detection and there is no signal present at the time. This happens if the output of the adder exceeds the threshold bias level due to noise alone. The probability of false alarm is given by

$$P_{fa} = 1 - (1 - P_e)^{k-1} \tag{8-24}$$

If G, ψ^2 and P_{fa} are fixed, then P_e is determined by Equations 8-24 and 8-6, which in turn determines b_n by using Equation 8-20.

Note the following relationships and conditions:

$$\left.\begin{aligned} P_e &= P_{fa} \qquad k < 2 \\ P_e &\approx \frac{P_{fa}}{k-1} \quad , \; k \geq 2, \; P_e k \ll 1 \end{aligned}\right\} \tag{8-25}$$

It may be noted from Equation 24 that $P_e \leq P_{fa}$. Thus, if $kP_{fa} \ll 1$ then $kP_e \ll 1$, and so

$$P_e \approx \frac{P_{fa}}{k-1} \qquad k \geq 2 \tag{8-26}$$

Probability of Acquisition

The probability that the DRS signal will be properly detected during the scanning process is given by:

$$P_{acq} = P_A \sum_{n=1}^{k} P_n P_d (1 - P_e)^{n-1} \tag{8-27}$$

where P_A is the probability that the DRS lies in the search area and P_n is the probability that the DRS lies in n^{th} angular position of the search area. The above summation expression is the sum of probabilities that an error was not made in the previous (n - 1) positions and that a correct decision is made in n^{th} position times the probability that the DRS is in the n^{th} position.

A useful and simplifying assumption is that $P_n = 1/k$. This assumption is not generally correct, but is sufficiently accurate to allow a good estimate of the probability of acquisition. Using it allows Equation 8-27 to be further reduced

$$P_{acq} = \frac{P_A P_d}{kP_e} \left[1 - (1 - P_e)^k\right] \tag{8-28}$$

If P_e is small $\ll 1$, then

$$\left[1 - (1 - P_e)^k\right] \approx k P_e - \frac{k(k-1)}{2} P_e^2 \qquad (8\text{-}29)$$

Thus for $P_e \ll 1$,

$$P_{acq} = P_A P_d \left[1 - \left(\frac{k-1}{2}\right) P_e\right] \qquad (8\text{-}30)$$

and if $kP_e \ll 1$,

$$P_{acq} \approx P_A P_d \qquad (8\text{-}31)$$

It should be noted that if $k \leq 1$, then

$$P_{fa} = P_e$$

and

$$P_{acq} = P_A P_d$$

where A is now the area defined by the antenna beamwidth which is larger than the required search area. Figures 8-5, 8-6, and 8-7 show P_{acq}/P_A as a function of P_d with P_e and k as parameters. The first two indicate the validity of Equation 8-31 for $kP_e \ll 1$.

Parametric Results

From Equation 8-20, b_n is a function of P_e and m, and from Equation 8-23, P_d is a function of b_n, m, and the signal-to-noise power ratio, R. Thus, P_d is a function of P_e, m, and R or inversely R is a function of P_d, P_e, and m.

If it is assumed that $kP_e \ll 1$ (i.e., $kP_e < 0.1$), then from Equation 8-31, $P_{acq} = P_A P_d$. If A is taken to be the area defined by letting ψ

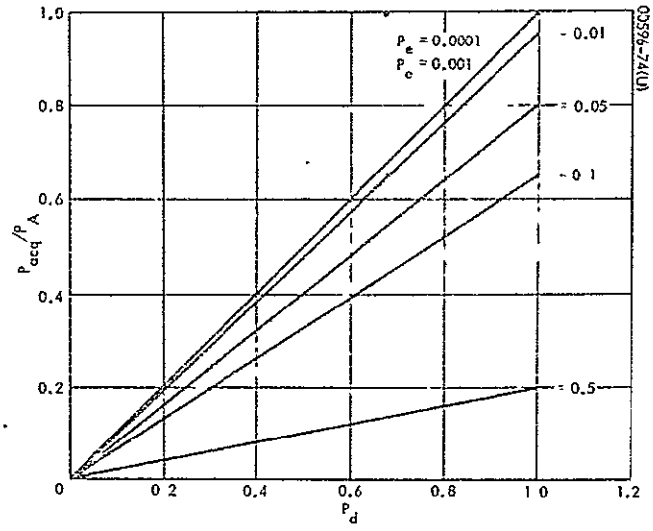

Figure 8-5. Probability of Acquisition When k = 10

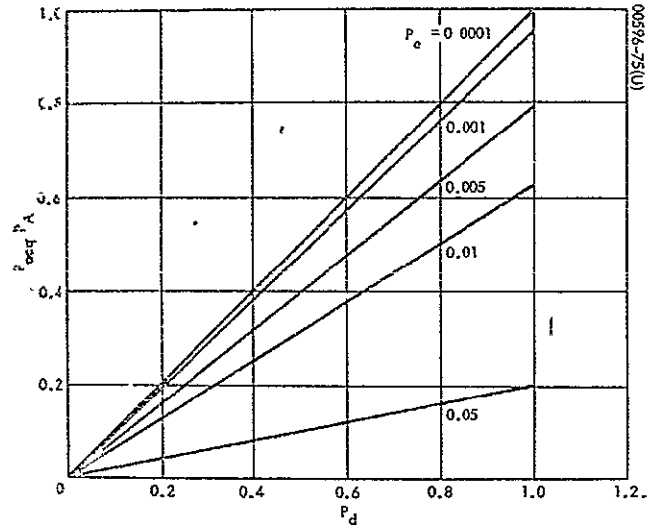

Figure 8-6. Probability of Acquisition When k = 100

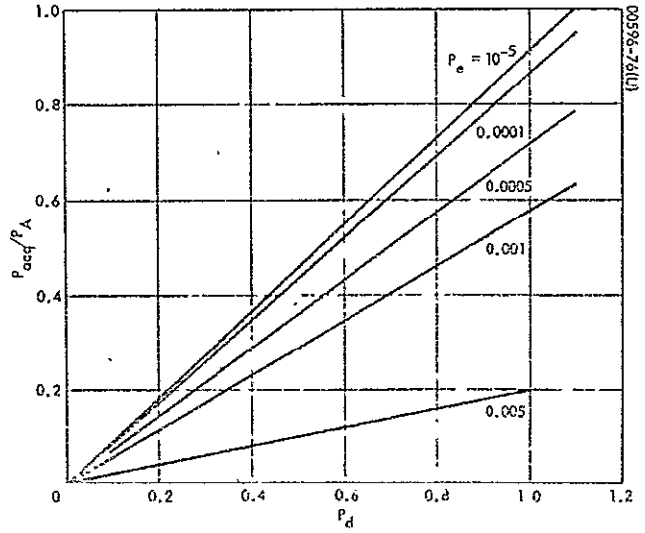

Figure 8-7. Probability of Acquisition When k = 1000

in Equation 8-1 equal the 3σ value of antenna boresight deviation from the nominal position, then

$$P_A = 0.9974 \tag{8-32}$$

and

$$P_d = P_{acq}/0.9974 \tag{8-33}$$

And then R is a function of P_{acq}, P_e and m. The value of m will probably depend more on hardware implementation considerations than on the theoretical limitations of Equation 8-23.

For instance, it is expected that 25 dB $\leq$ G $\leq$ 60 dB and $0 \leq \psi \leq 3°$ (for the Space Station mission) thus, from Equation 8-6, $k \leq 1.33 \times 10^3$. It was shown above that due to doppler shift and oscillator uncertainty, $B \geq (6.2 \times 10^{-5})f$. Furthermore, it is expected that $T_s > 30$ seconds. Thus, for f = 2 GHz, $BT_s \geq 3.72 \times 10^6$. Then, from Equation 8-23, m $\geq$ 21,000. It is not expected that the detector could add this many samples.

In Reference 8-5, b_n is tabulated as a function of m and P_e for values of m between 1 and 150 and P_e between 10^{-1} and 10^{-12}. In Reference 8-5, P_d is plotted as function of b_n, m, and mR for m = 1, 3, 10, 30, 100, 300, 1000 and 3000.

From Equation 8-33, the following list is valid:

P_{acq}	P_d
0.90	0.9023
0.95	0.9525
0.99	0.9926
0.995	0.9976

Combining this list with the data from the above mentioned References, the required signal-to-noise ratio is listed in Table 8-3 as a function of P_{acq}, P_e and m. For P_{acq} = 0.99, curves of R versus m with P_e as a parameter is shown in Figure 8-8.

Using Equations 8-6 and 8-25, the signal-to-noise ratio may be determined as a function of $G\psi^2$ with m, P_{acq}, P_{fa} as parameters. Using the data of Table 8-3, curves of R versus $G\psi^2$ with m as a parameter were plotted for P_{acq} = 0.99 and $P_{fa} = 10^{-5}$. These curves are shown in Figure 8-9.

Figure 8-8. Required Signal-to-Noise Ratio Versus Number of Detector Samples

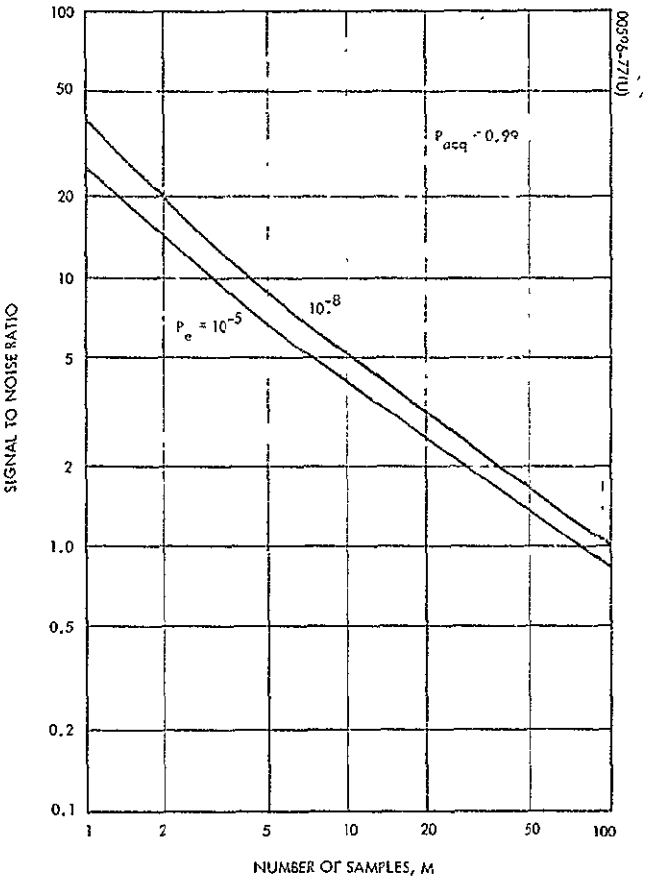

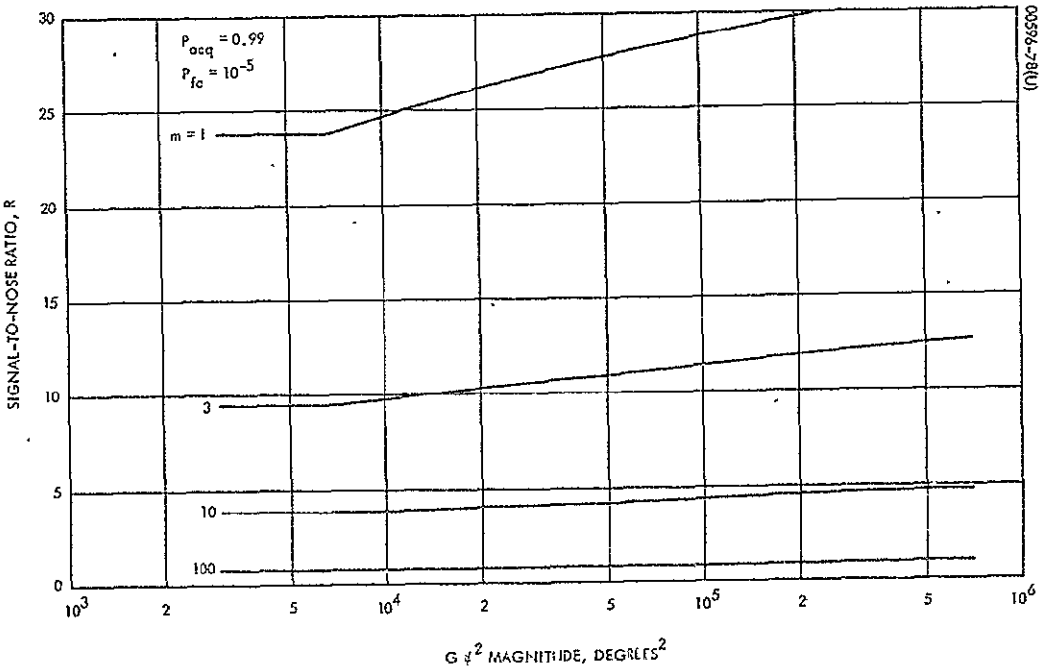

Figure 8-9. Required Signal-to-Noise Ratio Versus $G\psi^2$

TABLE 8-3. SIGNAL-TO-NOISE POWER RATIO

P_e	m	b_n	P_{acq} = 0.90 P_d = 0.9023	0.95 0.9525	0.99 0.9926	0.995 0.9976
10^{-5}	1	11.51	18.0	20.5	25.3	27.7
	3	16.55	7.3	8.17	10.0	11.2
	10	29.52	3.0	3.20	4.0	4.30
	30	59.29	1.38	1.57	1.88	2.0
	100	148.5	0.68	0.74	0.86	0.94
10^{-6}	1	13.82	21.2	23.5	28.5	32.0
	3	19.13	8.5	9.5	11.4	12.5
	10	32.71	3.3	3.2	4.4	4.8
	30	63.55	1.59	1.74	2.02	2.22
	100	154.9	0.74	0.84	0.94	1.01
10^{-7}	1	16.12	23.5	25.8	31.7	35.2
	3	21.67	9.53	10.5	12.7	13.8
	10	35.79	3.70	4.0	4.8	5.2
	30	67.60	1.75	1.88	2.22	2.37
	100	160.9	0.81	0.87	1.01	1.08
10^{-8}	1	18.42	26.5	29.4	36.0	39.0
	3	24.18	10.5	11.4	13.6	15.0
	10	39.80	4.0	4.3	5.2	5.7
	30	71.48	1.87	2.03	2.32	2.53
	100	166.6	0.87	0.95	1.08	1.16

Conclusions on Detection

It has been shown that the number of samples used in the detector's adder has a dramatic influence on the required signal-to-noise ratio, whereas the effect of the gain-search area product (proportional to $G\psi^2$) is much less. In Figure 8-9, where $P_{fa} = 10^{-5}$, the change due to the maximum variation of $G\psi^2$ causes the signal-to-noise ratio to change by a maximum factor of 1.44 or approximately 1.6 dB, when m = 1. The change due to $G\psi^2$ is much less when m > 1.

The change due to a variation of m is much larger; in Figure 8-9, for $G\psi^2 = 10^5$, increasing m from 1 to 3 reduces the required SNR from 29 (14.6 dB) to 11.5 (10.6 dB). If m is further increased to 10, the required SNR is reduced to 4.5 or 6.55 dB.

Thus, the number of samples added in the detector prior to the threshold switch is the major factor in determining the required signal-to-noise ratio for given probabilities of acquisition and false alarm.

Acquisition Time

It has been shown above that the parameters of interest are related by

$$m \leq \frac{T_s B}{k} \tag{8-34}$$

where $k = 4\psi^2/\theta^2$, the number of view areas contained in the search area.

For a reasonable relationship between search area and antenna beamwidth, $k \leq 100$. Then, if P_e is limited to a maximum of 10^{-7}, the probability of false acquisition will be less than $(k - 1) P_e = 10^{-5}$. Referring to Figure 8-8, if a probability of acquisition of 0.99 is desired with a signal-to-noise ratio of 2(3 dB), then $m \geq 40$. The IF bandwidth should be as small as is compatible with the expected doppler shift and oscillator instability. This requirement is shown to place a lower limit of $(6.2 \times 10^{-5})f$ on the IF bandwidth, B, where f is the transmission frequency.

Substituting the above numerical quantities into Equation 8-34:

$$T_s \geq (2.58 \times 10^6) \frac{\psi^2}{\theta^2 f} \text{ seconds} \tag{8-35}$$

This inequality seems to indicate that the search time may be decreased by increasing the transmission frequency, f. This, of course, is not necessarily true because the resultant larger IF bandwidth will reduce the

signal-to-noise ratio. The same effect is possible by increasing the bandwidth at any frequency, f. Inequality (Equation 8-35) relates the search time to the other parameters for the minimum IF bandwidth. Independent link analysis will insure the required signal-to-noise ratio, taking into account antenna sizes and transmitter power.

Figure 3-10 is a result of using Equation 8-35 for transmission frequencies of 2.2 GHz and 14 GHz. From this figure, it may be seen that for small values of ψ/θ, the search time may be quite small; thus, the actual search time may be determined by mechanical considerations rather than by the operation of the signal detector.

Figures 8-11 and 8-12 show the search time as a function of ψ/θ and signal-to-noise ratio (SNR) for transmission frequencies of 2.2 GHz and 14 GHz, respectively. The relationship between m and SNR of Figure 8-2 was combined with inequality (Equation 8-34) to produce these figures.

Mean Time to Acquisition

The minimum time which must be allowed to scan the search area has been discussed above. The mean time to acquisition, T_a, is related to the search time and is given by the following expression:

$$T_a = \sum_{n=1}^{k} \left[P_n P_d n\tau + P_n P_e (n\tau + T_L + T_a) \right] \qquad (8\text{-}36)$$

where

P_n = probability of target lying in the n^{th} antenna view area within the search area

P_D = probability of detection when target is within the antenna view

P_e = probability of error when the target is within the antenna view

T_L = time lost due to an error

$\tau = T_s/k$

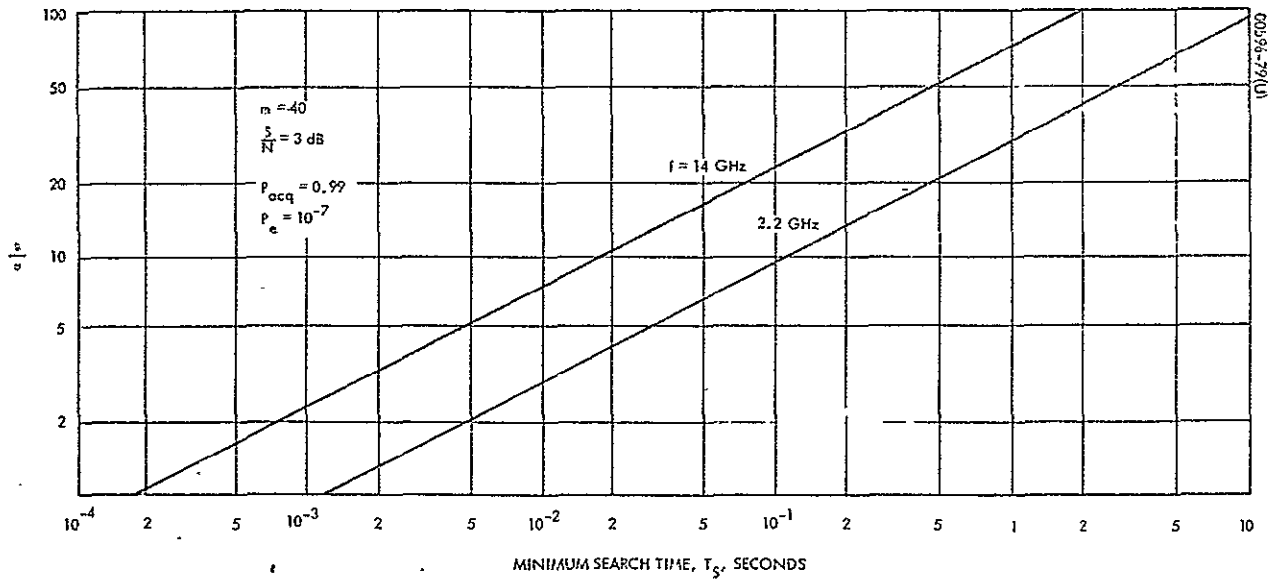

Figure 8-10. Minimum Search Time Versus ψ/θ

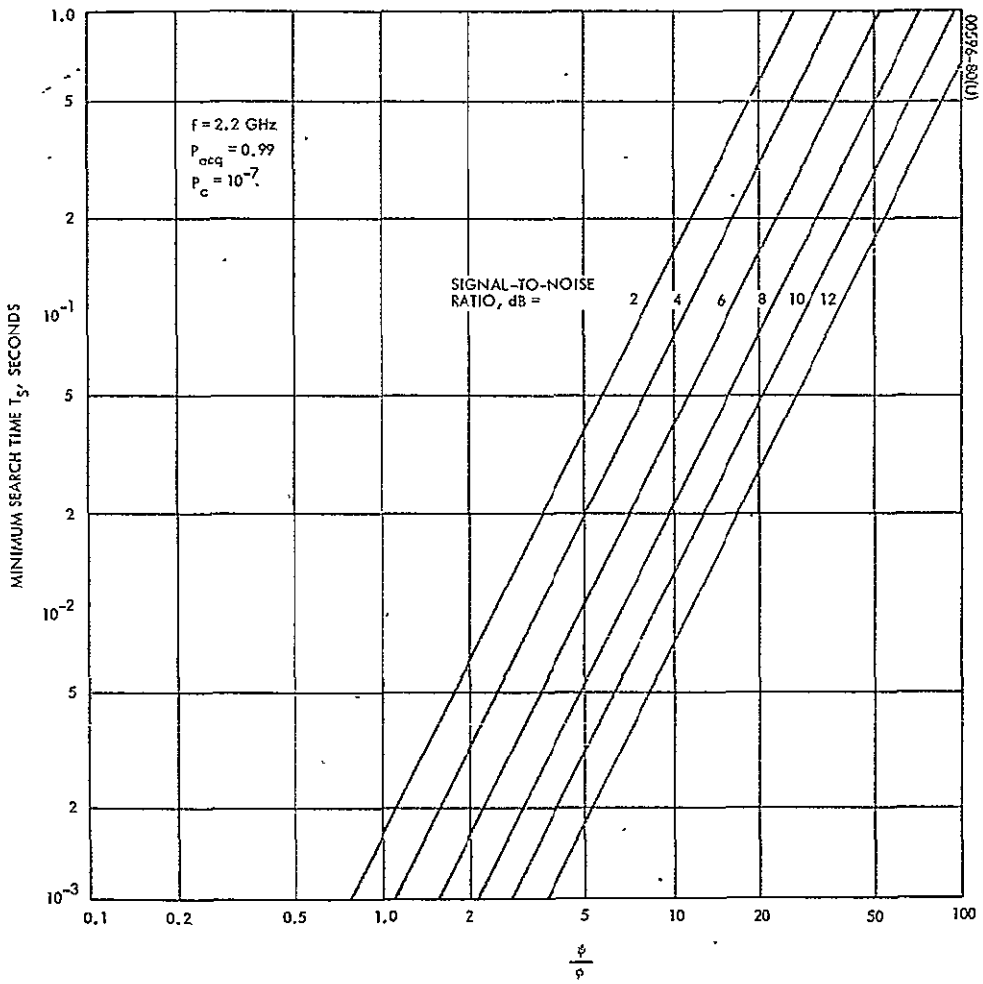

Figure 8-11. Minimum Search Time Versus ψ/θ at S-Band

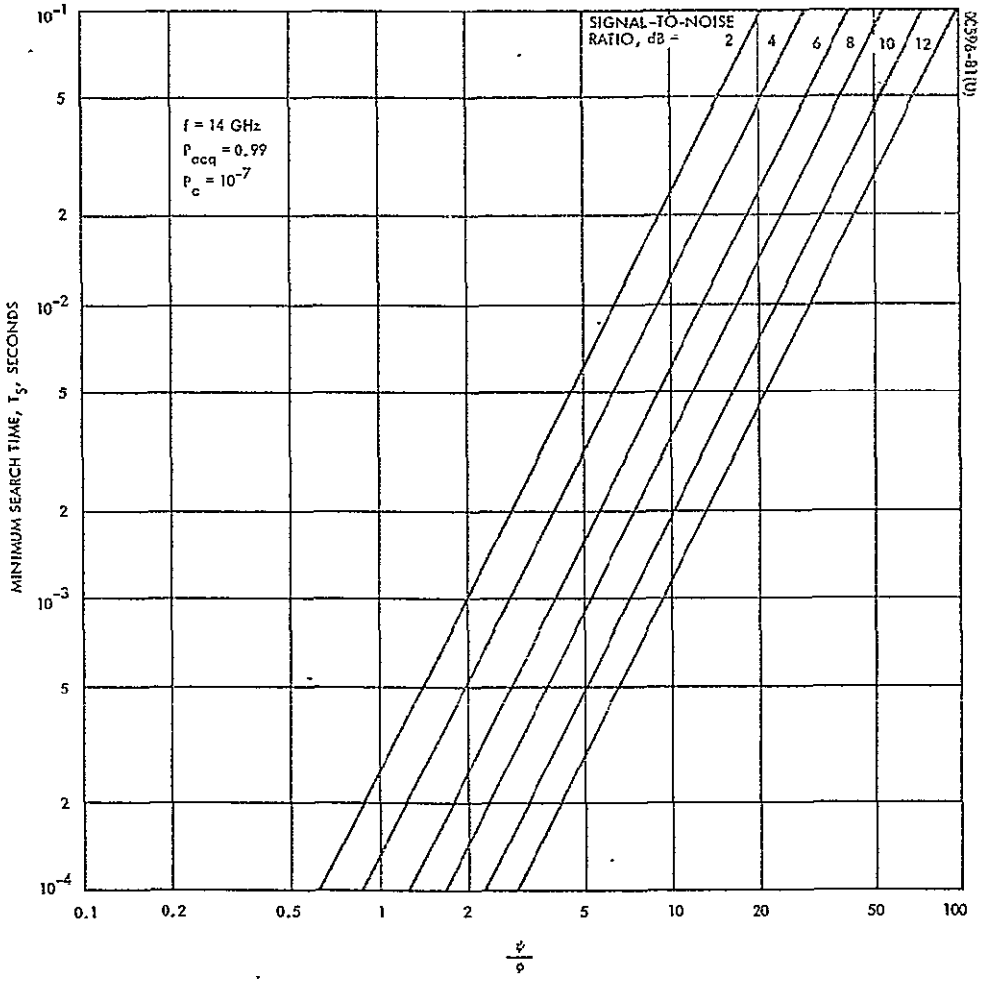

Figure 8-12. Minimum Search Time Versus ψ/θ at K-Band

If it is assumed that the target may lie at any point within the search area with equal probability, then Equation 8-36 reduces to

$$T_a = \left(\frac{1}{1 - P_e}\right)\left[\frac{T_s}{2}(P_d + P_e)\left(1 + \frac{1}{k}\right) + P_e T_L\right] \qquad (8\text{-}37)$$

for

$$k = \frac{4\psi^2}{\theta^2} \geq 1 \qquad (8\text{-}37)$$

The uniform probability assumption is not correct but in many cases leads to results very nearly the same as with a more accurate and more complex probability distribution.

If $P_e \leq 10^{-6}$, as will usually be the case, then Equation 8-37 becomes

$$\frac{T_a}{T_s} \approx \frac{P_d}{2}\left(1 + \frac{\theta^2}{4\psi^2}\right) + P_e \frac{T_L}{T_s} \quad \left(\frac{\psi}{\theta} \geq \frac{1}{2}\right) \qquad (8\text{-}38)$$

And if $T_L/T_s \leq 100$, then

$$\frac{T_a}{T_s} \approx \frac{P_d}{2}\left(1 + \frac{\theta^2}{4\psi^2}\right) \qquad (8\text{-}39)$$

Figure 8-13 shows $T_a/P_d T_s$ as a function of ψ/θ.

Example

Let ψ be the 3σ deviation of the boresight from the nominal. Then, as shown previously, for $P_e \ll 1$

$$P_d = P_{acq}/0.9974 \qquad (8\text{-}40)$$

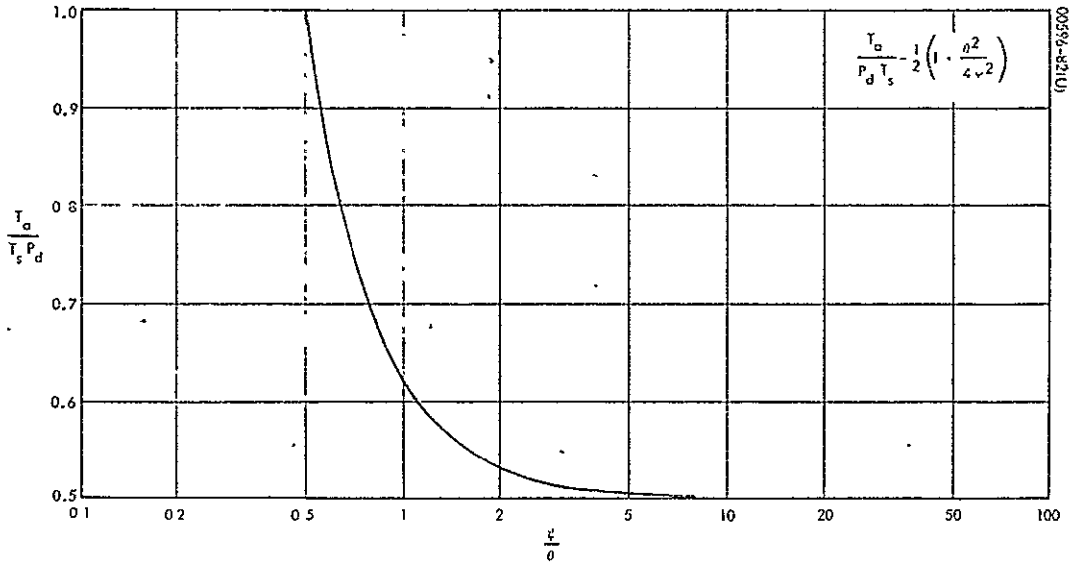

Figure 8-13. T_a/T_sP_d Versus ψ/θ

where P_{acq} is the probability of acquisition. And let the following system parameters be given:

$$P_{acq} = 0.99$$

$$\psi = 3 \text{ degrees}$$

$$\theta = 1 \text{ degree}$$

$$P_e = 10^{-7}$$

$$m = 40$$

Then $P_d = 0.9926$, $\psi/\theta = 3$, and there are

$$k = \left(4\frac{\psi}{\theta}\right)^2 = 36$$

antenna view areas in the search area. From Figure 8-10, the total search time which must be allowed is 1.7 ms for f = 14 GHz and 11 ms for f = 2.2 GHz. From Figure 8-11, $T_a/T_s P_d = 0.514$, and so $T_a \approx 0.866$ ms for f = 14 GHz, and $T_a = 5.61$ ms for f = 2.2 GHz.

8.4 THEORETICAL COMPARISON OF AUTOTRACK SYSTEMS

This section compares the theoretical tracking accuracy due to thermal noise of three types of autotrack systems: 1) true monopulse, 2) conical scan, and 3) time-shared monopulse.

The derivation of the tracking accuracy for the true monopulse systems has been presented in various references, one of which is Reference 8-6. In this reference, the rms tracking error for a single axis has been derived for both correlation detection and coherent detection of the error signals. These equations are shown below

True Monopulse -- Correlation Detection

$$\theta_{rms} = \frac{\sqrt{\frac{B_N}{B_{IF}}\left[1 + \left(\frac{S_i}{N_i}\right)\right]}}{k_m\left(\frac{S_i}{N_i}\right)} \qquad (8\text{-}41)$$

True Monopulse -- Coherent Detection

$$\theta_{rms} = \frac{1}{k_m} \sqrt{\frac{\frac{B_N}{B_{IF}}}{\left(\frac{S_i}{N_i}\right)}} \tag{8-42}$$

where

θ_{rms} = rms tracking error along single axis in fractional beamwidths

$2B_N$ = two-sided servo noise bandwidth

B_{IF} = IF bandwidth

$\frac{S_i}{N_i}$ = Sum channel IF signal-to-noise ratio at the receiver input

k_m = error slope factor of the monopulse difference pattern normalized to the antenna beamwidth

The derivation of the tracking accuracy for the conical scan system has also been presented in various references, including References 8-6 and 8-7. Here the tracking error is shown to be,

Conical Scan – Square-Law Detection

$$\theta_{rms} = \frac{\sqrt{\frac{B_N}{B_{IF}} \left[1 + 2\left(\frac{S_i}{N_i}\right)\right]}}{k_{cs}\left(\frac{S_i}{N_i}\right)}$$

Conical Scan -- Coherent Detection

$$\theta_{rms} = \frac{1}{k_{cs}} \sqrt{\frac{\frac{B_N}{B_{IF}}}{\left(\frac{S_i}{N_i}\right)}} \tag{8-44}$$

where all parameters are defined as before except

k_{cs} = error slope factor of the conical scan system normalized to the antenna beamwidth.

The theoretical tracking accuracy for the time-shared monopulse system has been derived in Reference 8-8. The implementation of the system is also described in this reference. The equation for the tracking accuracy is given below.

Time-Shared Monopulse -- Square-Law Detection

$$\theta_{rms} = \frac{1}{k_m\left(\frac{S_i}{N_i}\right)} \sqrt{\frac{\frac{B_N}{B_{IF}}\left[1 + 2k_1\left(\frac{S_i}{N_i}\right)\right]}{k_1 k_2}} \tag{8-45}$$

where all parameters are defined as before except

k_1 = loss of sum channel signal power due to coupler (throughput loss)

k_2 = loss of error signal power due to coupler (coupler loss)

In order to compare the systems on a comparable basis, the following assumptions were made:

1) No line losses between antenna output and receiver input.

2) IF bandwidth/servo noise bandwidth = 10^6.

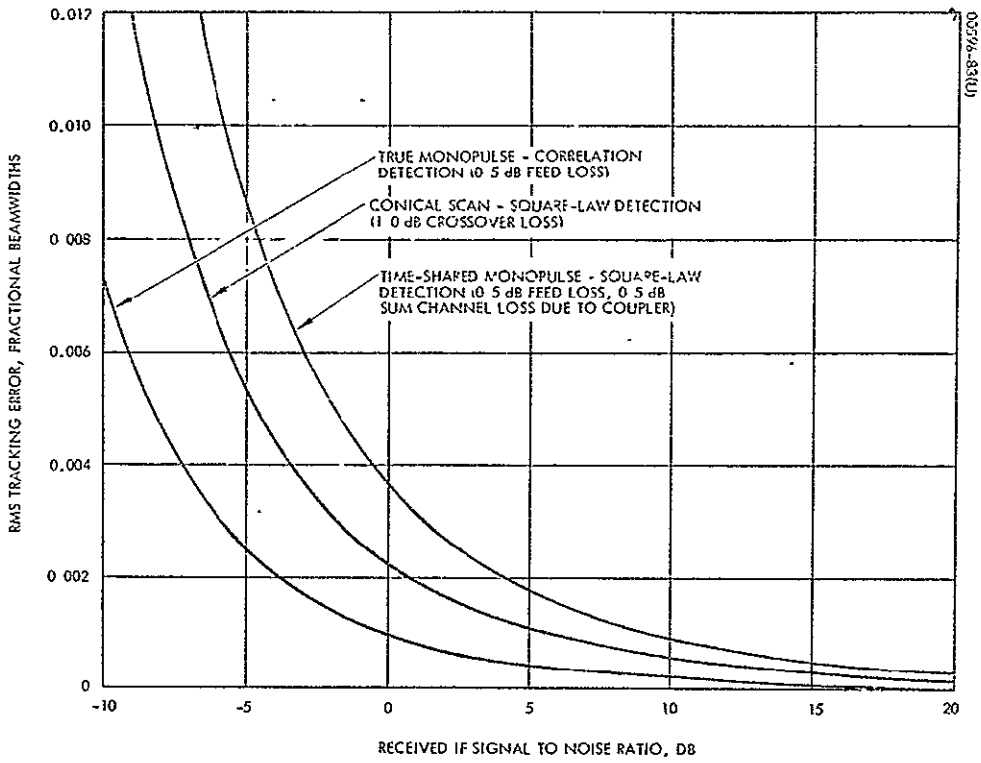

Figure 8-14. RMS Tracking Error Due to Thermal Noise

3) True monopulse system incurs 0.5 dB loss of signal power due to the use of multiple feeds.

4) Conical scan system operates with 1.0 dB crossover loss.

5) Time-shared monopulse incurs 0.5 dB loss of signal power due to multiple feeds and another 0.5 dB loss due to coupler.

6) The error slope factor for the monopulse feeds, k_m, is assumed to be 1.57/beamwidth error. This is based on the discussion in Reference 8-9, pp. 272-275.

7) The error slope factor for the conical scan system, k_{cs}, is assumed to be 0.8/beamwidth error. This is based on the discussion in Reference 8-9, pp. 269, for a 1.0 dB crossover loss.

The tracking accuracy due to thermal noise for the three systems is shown in Figure 8-14. The curve for the true monopulse system is based on correlation detection, and the curves for the conical scan and time-shared monopulse are based on square-law detection. The abscissa of Figure 8-14 is based on the IF signal-to-noise ratio before reduction of the signal power by assumptions 3), 4), and 5) above.

It can be seen from Figure 8-14 that for the parameters chosen, the conical scan system provides 4 to 6 dB poorer performance than the true monopulse, and the time-shared monopulse provides from 6 to 10 dB poorer performance. It is of interest to note that if the coupler loss were 3 dB for the time-shared monopulse, i.e., $k_1 = k_2 = 1/2$, the rms tracking error for the time-shared system with square-law detection would be exactly twice as great as for the true monopulse system with correlation detection.

8.5 REFERENCES

8-1 "Tracking Effect due to IAM on the Uplink Mode Containing both S-Band Subcarriers," TRW Systems Group, under Contract NAS 9-4810, to the Manned Spacecraft Center, 19 March 1968.

8-2 "An Investigation of the Multipath Problems Associated with the Apollo CSM and LM S-Band High-Gain Communication Antenna Tracking Systems," TRW Systems Group, under Contract NAS 9-8166 to the Manned Spacecraft Center, 16 December 1968.

8-3 J. I. Marcum, "A Statistical Theory of Target Detection by Pulsed Radar," with mathematical index, RAND Research Memo RM-754, 1 December 1947.

8-4 W. B. Davenport and W. L. Root, Random Signals and Noise, McGraw-Hill, 1958.

8-5 J. Pachares, "A Table of Bias Levels Useful in Radar Detection Problems," IRE Trans. on Information Theory, IT-4, No. 1 (1958) pp. 38-45.

8-6 J. M. Stephenson, et al: "Design Criteria for a Large Multi-Purpose Tracking Antenna," ASTIA Document No. AD 267147, January 1961.

8-7 G. M. Pelchat, "The Effects of Receiver and Antenna Noise on the Performance of a Conical-Scan Tracking System," The Microwave Journal, February 1965, pp. 37-40, 61.

8-8 E. T. Hazelton, "Thermal Noise Errors in Time-Shared Monopulse," Hughes IDC No. 2794/61, 22 January 1970.

8-9 D. K. Barton, Radar System Analysis, Prentice-Hall, Inc., Englewood Cliffs, New Jersey, Chapter 9, 1964.

9. MODEM AND TIME DIVISION MULTIPLEX STUDIES

9.1 INTRODUCTION

Figure 9-1 shows the conceptual arrangement of a digital communications system for the transmission of several analog signals. The source encoder/decoder devices accomplish the mapping of the data source signal from the analog domain to the digital domain and then back into the analog. The digital portion of the channel coding device generates one or more subbits for every information bit. These subbits are represented in the RF communications channel by the analog modulator. Its output symbols are called chips.

After consultation with the Manned Spacecraft Center (MSC), the selected channel encoding utilizes biphase or quadriphase PSK in conjunction with convolutional coding. The performance of a representative biphase demodulator is discussed in Section 9.2. This device recovers both subbit timing and a coherent carrier reference from the PSK signal itself. The performance of various convolutional codes with Viterbi decoding has been documented by MSC and has not been part of this study. The physical characteristics of Viterbi decoders were investigated and are summarized in Section 10.4. Section 9.3 summarizes the design study of the Space Station time division multiplex (TDM) system. The statistical analysis of the frame sync technique is given special emphasis. The source encoding problem was not addressed during the study. The physical characteristics of a particular source encoder/decoder suggested by MSC were estimated. These results appear in Section 10.4.

9.2 DEMODULATION OF CONVOLUTIONAL CODED BIPHASE PSK SIGNALS

This section considers the technique shown in Figure 9-2 for the demodulation of convolutional coded biphase PSK signals.

Subbit Synchronizer

The subbit time synchronizer phase detects the data, locates the subbit transition times, and outputs a sampling time signal to the integrate and dump circuit. A synchronizer has been built at the Jet Propulsion

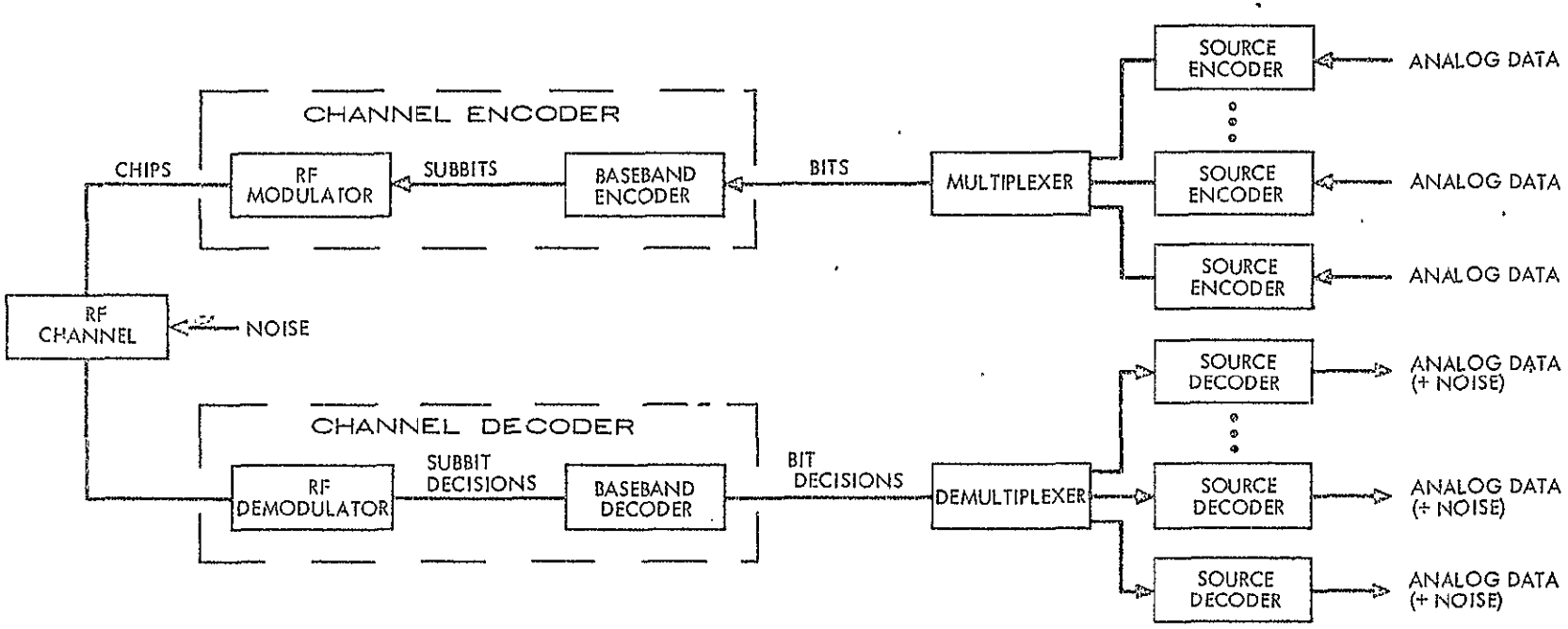

REPRESENTATIVE DESIGNS

SOURCE ENCODER/DECODER: DELTA MODULATION (VOICE)

RF CODING: BIPHASE PSK WITH COHERENT DETECTION

BASEBAND CODING: CONVOLUTIONAL CODING WITH VITERBI DECODING

Figure 9-1. Conceptual Arrangement of Digital Communications System

Laboratory (JPL) which provides negligible system degradation down to $E_{subbit}/No = -5.0$ dB at data rates up to 250 kHz (Reference 9-1). The design's performance is attributable to the use of a digital loop filter and a specially designed phase detector. Although implementation of these techniques may not be possible at 40 MHz rates because of the limitations imposed by circuit speeds, it will be assumed here that subbit timing is perfect. (Subbit timing information can also be recovered at baseband — after the coherent reference is reinserted and before the integrate and dump.)

Squaring Loop

The carrier phase tracking loop design is shown in Figure 9-3. This "squaring loop" takes the modulated carrier and recovers the original carrier. (It has been shown that this sort of system design is more efficient in terms of total power than that in which a separate reference signal is used (Reference 9-2). Another loop design might be used, but the squaring loop is representative of the possible configurations.) Now, an expression for the overall system error should include the effects of both the PLL and the integrate and dump. It has been shown that the probability of a detection error for PSK given a phase error, ϕ, is

$$P\,(\text{Error}/\phi) = \frac{1}{\sqrt{2\pi}} \int_t^\infty \exp\left[\frac{-x^2}{2}\right] dx$$

$$\text{where } t = \sqrt{\frac{2\,E_s}{N_o}}\,\cos\phi$$

$$\therefore P\,(\text{Error}/\phi) = \text{Erfc}\left[\sqrt{\frac{2\,E_s}{N_o}}\,\cos\phi\right]$$

Viterbi (Reference 9-3) has shown that for a first order PLL the steady-state phase error (mod 2π) probability density is given by

$$P(\phi) = \frac{\exp\,(\alpha\,\cos\phi)}{2\pi\,I_o(\alpha)}\,,\quad |\phi| \le \pi$$

where α is the SNR in the loop noise bandwidth and I_o is the imaginary Bessel function of order zero. Lindsay has shown experimentally (Reference 9-4) that this form is also approximately correct for the second order

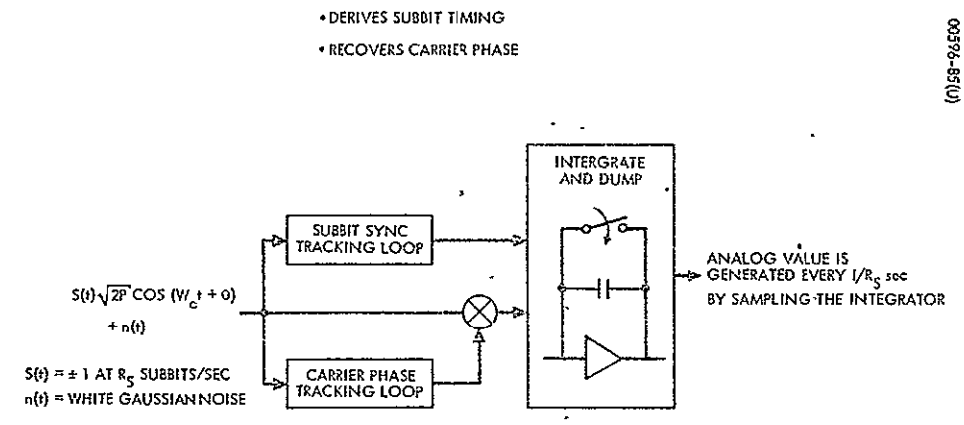

Figure 9-2. Demodulator for Biphase PSK

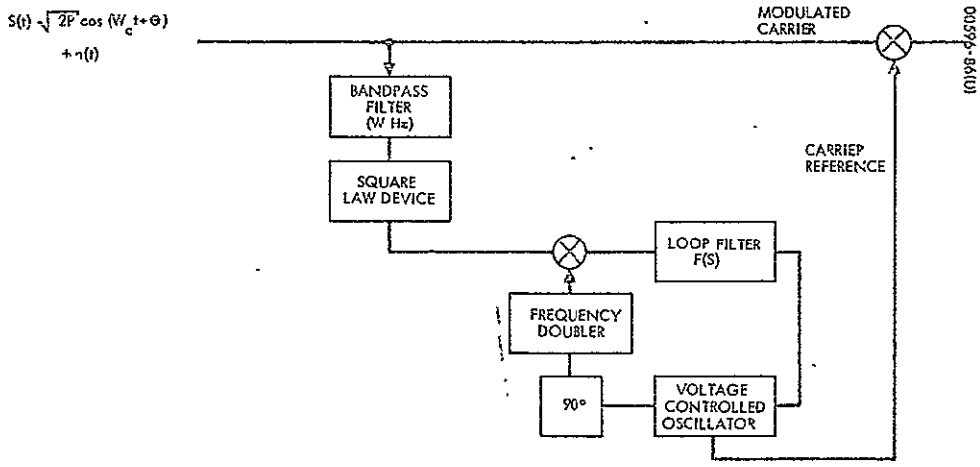

Figure 9-3. Carrier Phase Tracking Loop (Squaring Loop)

loop when α is large enough to be of practical interest. The overall P_s'' (the subbit error probability) can now be written:

$$P_s = P(\text{Error}/\phi)\ P(\phi)$$

$$= \frac{1}{\pi} \int_o^{\pi} \frac{\exp(\alpha \cos\phi)}{I_o(\alpha)} \operatorname{Erfc}\left(\sqrt{\frac{2E_s}{N_o}} \cos\phi\right) d\phi$$

this expression has been evaluated numerically by both Lindsay and Viterbi. We shall first determine the range of α and E_s/N_o which are of interest. Next, for a loop giving good tracking, the acquisition characteristics will be investigated.

Bandpass Filter and Squarer

To determine the loop parameters which will give good tracking, the effects of the filter and square law device must be evaluated.

The received signal plus noise "seen" by the filter is

$$y(t) = x(t) + n(t)$$

where

$$x(t) = \sqrt{2P} \sin\left(\omega_c t + \phi + s(t)\frac{\pi}{2}\right) = s(t)\sqrt{2P}\cos(\omega_c t + \phi)$$

$s(t) = \pm 1$ (the random data)

P = carrier power

ϕ = phase random process

$n(t)$ = white Gaussian noise of one-sided density N_o

The bandpass filter is matched to the spectrum of the signal — which is roughly $2R_s$ MHz wide where R_s is the subbit rate. The total carrier frequency uncertainties are given approximately by Table 9-1, assuming no programmed Doppler offset. Since they are an order of magnitude less than $2R_2$, a sharp cutoff filter of width $W \cong 2R_s$ will pass the signal without significant distortion.

TABLE 9-1. TOTAL CARRIER FREQUENCY UNCERTAINTY

	MHz
fc = 2.2 GHz	
Doppler shift	0.112
Oscillator shift	0.004
Total	0.116
fc = 14 GHz	
Doppler shift	0.714
Oscillator shift	0.028
Total	0.742

Now, since the noise bandwidth B_L of the PLL following the squarer need not even be as large as the frequency uncertainty which must be "tracked out," it holds that $W \gg B_L$. The signal X noise and noise X noise terms out of the square law device can then be approximated as Gaussian noise with a new density

$$N_o' = 4 N_o \frac{P}{2} + N_o^2 W$$

This assumption is used by Viterbi (Reference 9-3, p. 291), and by Lindsay (Reference 9-5), and was examined in detail by Marcum (Reference 9-6). The signal term out of the square law device is of the form

$$[s(t)]^2 \; (2P) \left[\frac{\cos 2(\omega_c t + \theta) + 1}{2}\right]$$

and $\therefore [1]\ (P)\ [\cos (2\omega_c t + 2\phi)]$ after filtering. The squaring operation maps the $s(t) = \pm 1$ modulation into $(\pm 1)^2 = 1$. (Note that the carrier phase reference may be in error by 180 degrees. The subbit characters may become "inverted". They can be re-inverted by examining the frame sync word.)

Phase Locked Loop

The baseband PLL model used by Viterbi to derive the phase error probability density (given above) is shown in Figure 9-4. It can be applied to the system of interest if we replace our VCO and doubler with a single VCO which generates twice the first VCO's frequency (for the same input voltage). From the linear theory, the phase error variance of the reference at $2\omega_c$ is

$$\sigma_{2\phi}^2 = \frac{N_o' B_L}{P^{2/2}}$$

where $N_o' B_L$ is the noise power and $P^{2/2}$ is the carrier power. However, since the loop output is taken to be at ω_c the phase error variance is $1/4\ \sigma_{2\phi}^2$ or

$$\sigma_\phi^2 = \frac{N_o' B_L}{2P^2} \equiv \frac{1}{\alpha}$$

$$\therefore \frac{1}{\alpha} = \frac{N_o B_L}{P}\left(1 + \frac{N_o W}{2P}\right).$$

Since

$$P_s = E_s R_s$$

$$\frac{1}{\alpha} = \frac{N_o B_L}{E_s R_s}\left(1 + \frac{N_o W}{E_s\ 2R_s}\right)$$

Constraints on B_L for near theoretical P_B

In the expression for P_s given above

$$P_s = \frac{1}{\pi}\int_o^{\pi} \frac{\exp(\alpha \cos\phi)}{I_o(\alpha)}\ \text{Erfc}\sqrt{\frac{2E_s}{N_o}}\cos\phi)\ d\phi$$

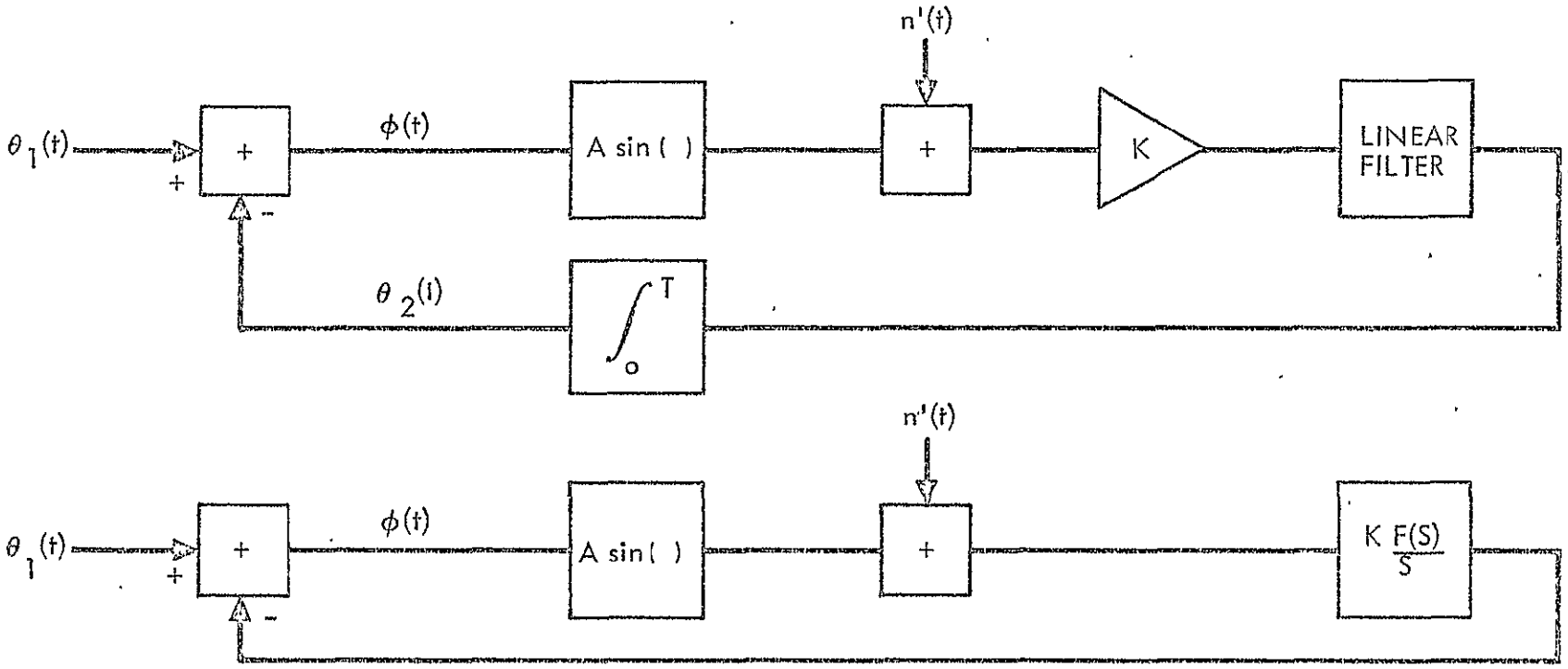

00596-87(U)

Figure 9-4. PLL Baseband Model

the error probability is a function of α and E_s/N_o. Lindsay's integration of the expression is graphed as a function of E_s/N_o with $\delta = \alpha/(E_s/N_o)$ as a parameter.

The upper set of curves in Figure 9-5 give Lindsay's results. The two sets taken together can be used to determine the P_s degradation due to imperfect tracking. The curves also show the required E_b/N_o increase needed to meet a specified P_B given constant δ. Figure 9-6 illustrates the use of Figure 9-5. (We assume here that the analog signal which constitutes the integrator's level at the sampling time has the same characteristics whenever the P_s is the same. Actually, a hard-decision on which subbit was sent is never made.)

Now it is desirable to make α (and δ) as large as possible so that the P_B degradation is negligible. This does not require increased power but only a decrease in B_L.

$$\frac{1}{\alpha} = \frac{1}{\delta}\frac{N_o}{E_s} = \frac{N_o}{E_s}\frac{B_L}{R_s}\left(1 + \frac{N_o}{E_s}\right)$$

$$B_L = \frac{R_s}{\delta}\frac{\frac{E_s}{N_o}}{\left(1 + \frac{E_s}{N_o}\right)}$$

This curve is plotted in Figure 9-7. Note that for $\delta \approx 10$ (0.4 dB degradation) the $B_L \approx 2$ MHz. It seems likely that $\delta = 100$ represents less than 0.1 dB degradation. At $\delta \approx 100$ the $B_L \approx 0.2$ MHz.

Loop Acquisition Performance

Now consider the acquisition properties of a PLL with $0.2 \text{ MHz} \leq B_L \leq 2.0$ MHz. (Since the available literature deals with this problem only for the noiseless case, it can be assumed that the results below are an upper limit on the performance.) When operating linearly with an input signal of voltage A and loop gain K, a second order PLL has a closed loop function

$$H(S) = \frac{AK\,(S + a)}{S^2 + AKS + AKa}$$

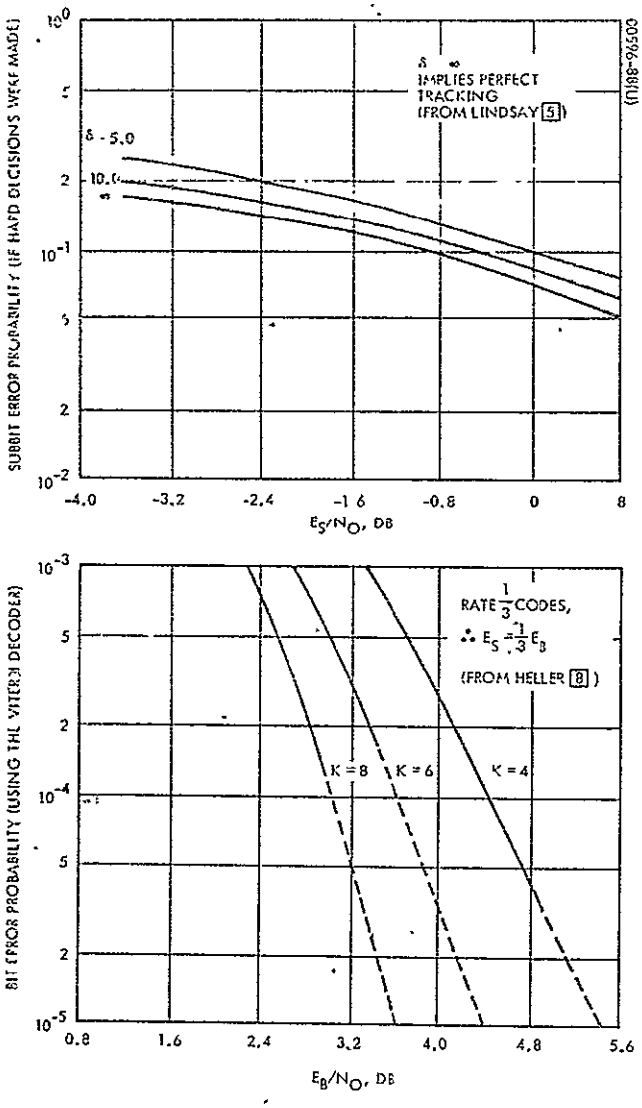

Figure 9-5. Comparison of Bit Error Probability and Subbit Error Probability

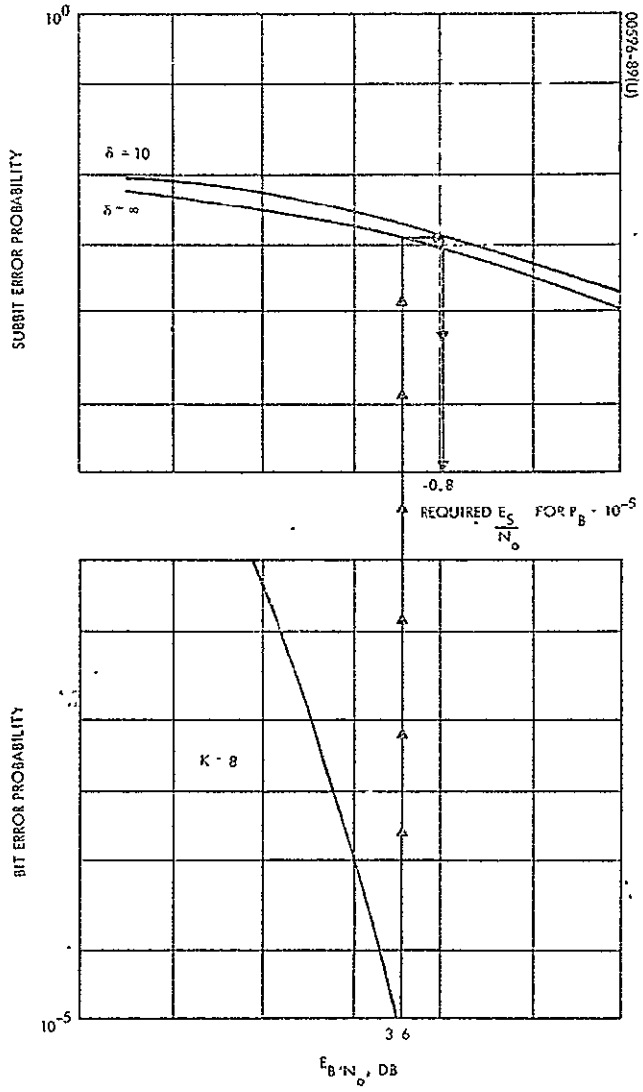

Figure 9-6. Use of Figure 9-5

The two parameters A and K can be written in terms of the damping coefficient δ and natural frequency ω_n.

$$\delta = \frac{1}{2\sqrt{a/AK}} , \qquad \omega_n^2 = aAK$$

Also,

$$B_L \equiv \frac{1}{2\pi} \int_0^\infty |H(i\omega)|^2 \, d\omega$$

and

$$B_L = \frac{AK + a}{4} \text{ for the H(S) above.}$$

It is common practice to fix one of the two loop parameters to give a "good" transient response. With $\delta = 1/\sqrt{2}$ the PLL is said to have a good balance between stability and speed of response. This leaves one parameter undetermined; this parameter is B_L through its relationship to ω_n.

$$\zeta = \frac{1}{2\sqrt{a/AK}} , \qquad \text{but} \quad = \frac{1}{\sqrt{2}}$$

$$\therefore a/AK = 1/2$$

$$B_L = \frac{AK + a}{4} = \frac{3}{8} AK .$$

$$\omega_n^2 = aAK = \frac{1}{2}(AK)^2 = \frac{32}{9} B_L^2$$

Although the second-order loop can theoretically "track-out" any constant frequency off-set (doppler shift), the pull-in range is usually limited to several times B_L. When the off-set is within this range, the time to pull-in is given by Gardner (Reference 9-7) as

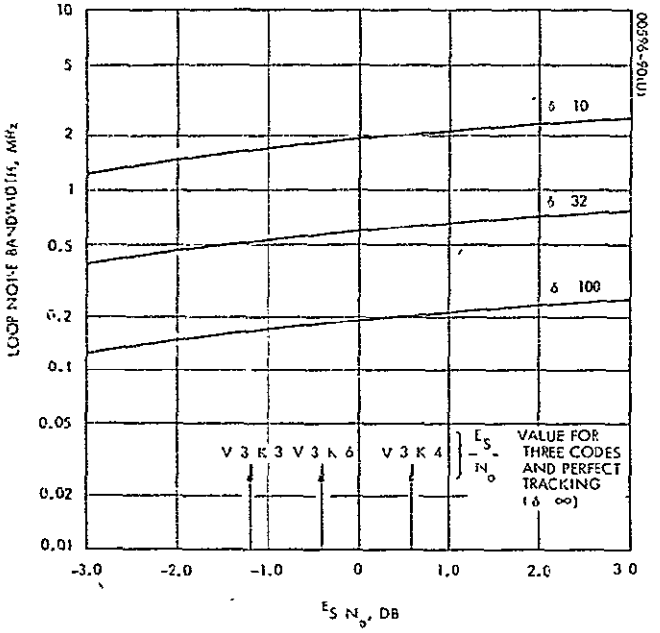

Figure 9-7. Loop Noise Bandwidth (BL) Versus E_S/N_O For Given δ

δ is proportional to loop SNR

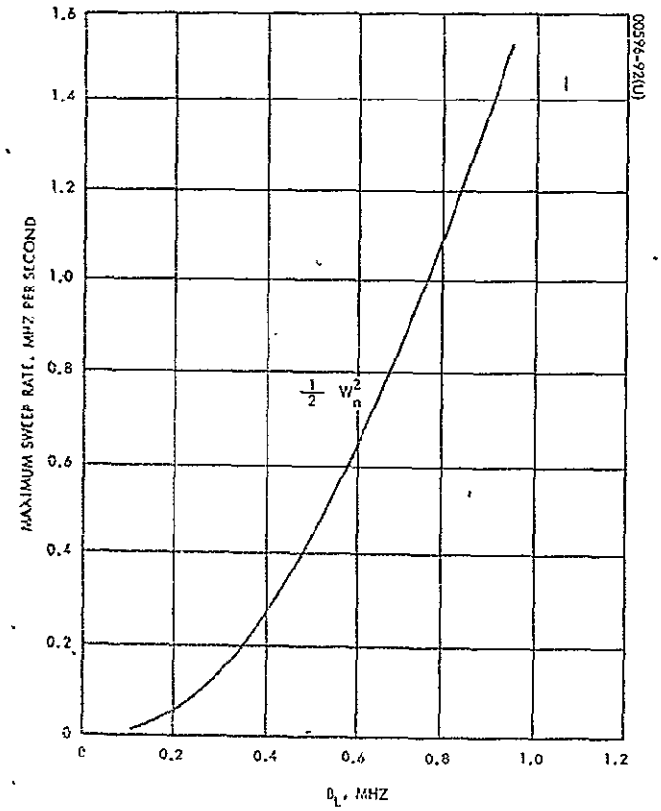

Figure 9-9. Maximum Sweep Rate Versus Loop Noise Bandwidth (BL) (Without Noise)

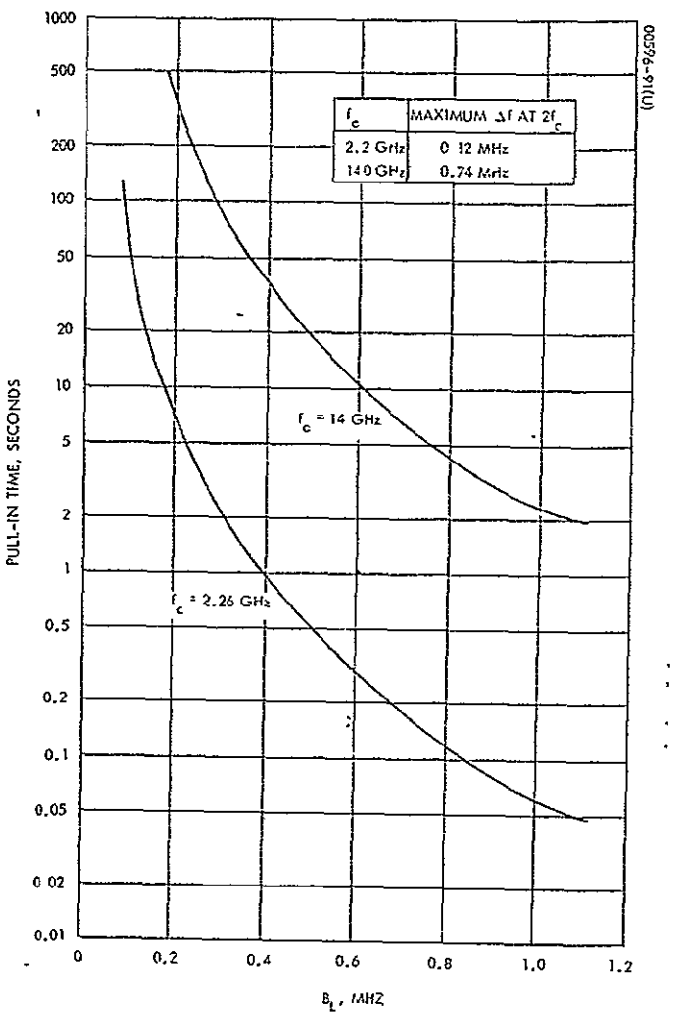

Figure 9-8. Loop Pull-In Time Versus Loop Bandwidth For Expected Frequency Offsets (Without Noise)

$$T_P \cong \frac{4.2\,(\Delta f)^2}{B_L^3} \text{ sec for } \zeta = \frac{1}{\sqrt{2}}$$

The second-order loop cannot perfectly track a frequency ramp (doppler rate). The steady-state error is given by

$$\text{Phase error} = \frac{\Delta\dot{\omega}}{\omega_n^2}$$

$$= \frac{9}{32B_L^2}\,(\Delta\dot{\omega})$$

The PLL cannot attain or maintain lock if the $\Delta\dot{\omega}$ is much greater than $1/2\,\omega_n^2$. This characteristic determines the rate at which a VCO can be swept in order to enhance loop acquisition.

Figures 9-8 and 9-9 are plots of the above equations. At f_c = 14 GHz, the time to lock becomes greater than 10 seconds when $B_L < 0.6$. If it is determined that B_L must be less than about 0.6 MHz, sweeping of the VCO should be considered. At f_c = 2.2 GHz, the acquisition time will be only a few seconds for any B_L of interest. Since the doppler rate is very small, the steady state error is negligible (that is, the principal contribution to tracking error is the channel noise). If VCO sweeping is desired at f_c = 14 GHz, the permissible rate is 0.05 MHz/sec at B_L = 0.2 MHz. The entire uncertainty of 1.48 MHz can be swept in 30 seconds.

Conclusions

A squaring loop can provide a near-perfect carrier reference in a high rate convolutional coded biphase PSK system in which the data is directly modulated on the carrier (such as the Station/DRS data link). A second order loop with $B_L \cong 1$ MHz gives less than 0.4 dB degradation in the station/DRS data. Such a loop can also acquire and track the maximum frequency offset within a 3-second lockup time. Since the carrier component tracked by the PLL is very "clean," false lock is not considered a difficulty.

The use of programmed doppler offset during acquisition would permit the loop bandwidth to be reduced by an order of magnitude. This would greatly improve the loop's tracking capability.

9.3 DESIGN STUDY OF THE SPACE STATION TDM SYSTEM

The structure of the Space Station Data Relay Link TDM System is determined to a very large extent by the format of the main data frame. The various factors influencing the TDM frame design are listed in Table 9-2 and are discussed in the following paragraphs. The design resulting from this study is detailed in the discussion of the baseband subsystem.

System Constraints

At this early period in the design of Space Station's communications system, it is desirable to maintain a high degree of simplicity and symmetry within the system structure. This yields a system which can be readily modified at the detail level during future design iterations and still retain the desired system characteristics. The future need for asymmetry or special services should receive special scrutiny in order that a "patch-work" design does not result. To assist configuration management, and simplify the interfaces, the data rates at interface points with other systems have been set at the IRIG standard of 75×2^N bits/sec, where $N = 0, 1, 2, \ldots,$. Table 9-3 shows the rates to which the communications system is constrained.

TABLE 9-2. FACTORS INFLUENCING THE TDM FRAME DESIGN

Consider overall system problems.

- Maintain system symmetry and simplicity
- Maintain standard interfaces
- Design for high information content by minimizing the percentage of bits used for sync and control

Provide required information capacity

- Consider the error quality which the various data types require
- Consider the need for estimates of the channel quality for the various data types
- Minimize buffer complexity

Provide control words for system flexibility

Provide a frame synchronization word

- Consider both scan and maintenance mode requirements
- Consider channel noise, internal noise, and expected data drop-out times

TABLE 9-3. STANDARD BIT RATES (75×2^N)

N	Bits/Sec	Kilobits/Sec	Megabits/Sec
0	75		
1	150		
2	300		
3	600		
4		1.2	
5		2.4	
6		4.8	
7		9.6	
8		19.2	
9		38.4	
10		76.8	
11		153.6	
12		307.2	
13		614.4	
14			1.2288
15			2.4576
16			4.9152
17			9.8304
18			19.6608
19			39.3216
20			78.6432

In formatting the TDM frame, the number of bits devoted to the sync word and control functions should always be minimized to use the RF link efficiently. Since the link performance can rarely be designed (or even measured) to better than 0.1 dB (or 1.023 numeric), any loss in information capacity due to framing and control bits can be ignored if these bits constitute only about 2.3 percent of the data stream.

Data Requirements

Representative data types and their nominal rates are listed in Table 9-4. It is apparent that except for the delta modulated voice, these nominal rates are not commensurate with the standard rates.

No requirements have been placed on the need to monitor the quality (bit error rate) of the relay link. It will be assumed that link quality measurements are an ancillary function of the frame sync word recognizer.

The multiplexing of the various data types of Table 9-4 involves the buffering and interleaving of several high rate data streams. The complexity of these buffers increases with the ratio of the input/output rates and the number of bits within the buffer at any one time. As the frame rate is increased, fewer bits are required per frame, and the buffer size is reduced. However, as the number of information bits per frame is made small, the framing bits may become an unacceptably large portion of the data stream. For a preliminary design, let the bits constituting the "overhead" be fixed at around 2 percent of the total bits per frame. The buffering required will be assumed to be acceptable.

TABLE 9-4. REPRESENTATIVE DATA SERVICE REQUIREMENTS FOR RELAY LINK (FULL-DUPLEX)

Type	Nominal Rate	Bit Error Requirements*
12 voice channels (delta modulation)	19.2 kilobits/sec (per channel)	10^{-3}
Digital television	12.0 megabits/sec	10^{-4}
Experiments data	3.0 megabits/sec**	10^{-4}

*Modem bit error rate has been fixed at 10^{-5}.

**Simultaneous with 12.0 megabits/sec TV.

Control Requirements

Table 9-4 summarizes the data services of the RF communication system. It is assumed that it is necessary also to provide bits which indicate which of the data channels is indeed active. (When a channel is inactive, bits from a pseudo-random generator will be inserted into the data stream.) The signaling function for the voice circuits is assumed to be performed in-band. Bits should be provided to indicate whether a high rate channel is devoted to television, is assigned to experiments data, or is not being used at all. These three states require that at least two bits be appended to the data per channel. Although these bits themselves may not be used to reconfigure the TDM system receiving the data, they do provide a positive indication of the data present in the channel at any given time.

Synchronization Word Constraints

In a TDM system, the various data types arrive at the demultiplexer in time sequence. In order to separate the TDM frame into the appropriate channels, the demultiplexer must recognize when a new frame begins. This can be accomplished by prefixing a frame synchronization word to each frame. The frame time synchronizer that uses the sync word operates in two modes: A scan (or acquisition) mode and a maintenance (or tracking) mode. A typical synchronizer and its analysis is presented below. (The final design arrived at is very similar.)

Scanning

During scanning, the "recognizer" correlates each successive n data bits with an n-bit frame sync word reference. When the recognizer is examining random ones and zeros, the correlation will be near zero. When both framing bits and information bits are present, the use of a proper sync code will result in a negative correlation with the reference word. (This is the "overlap" region. Note that to the recognizer, all bits which are not framing bits are "information" bits.) If the sync word itself is correlated with the reference word, the correlation will be at a maximum. Since channel errors may corrupt the received word, there is always a possibility that even when the sync word is actually encountered, the measured correlation may not reach the theoretical maximum.

While scanning, there is a certain probability that n successive random data bits will occur in the frame sync word pattern. This probability can be bounded above (see Reference 9-9) when it is assumed that:

1) The true sync word has just been missed.

2) The sync word is a random bit pattern (not an optimum sync pattern).

Figure 9-10. Average Number of Frames in Scanning Mode Versus Sync Word Length, Given R = r/r + m (M Versus m, Given R)

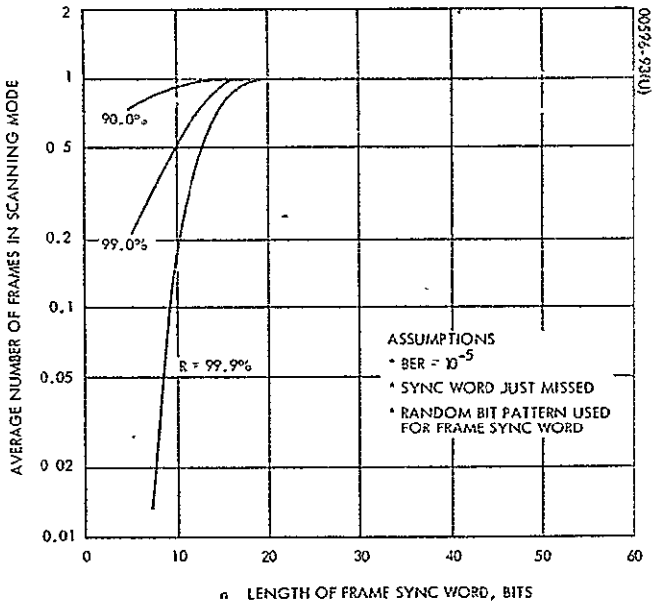

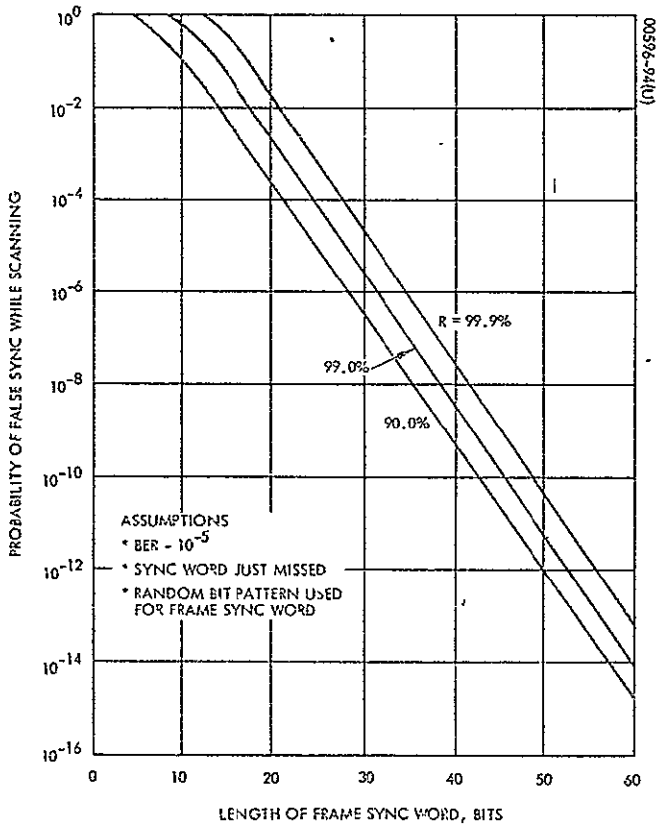

Figure 9-11. Probability of False Sync While Scanning Versus Frame Sync Word Length, Given R = r/r + m (P_{tfs} Versus m, Given R)

the probability of false sync on the first frame is

$$P_{fs} = 1 - (1 - P_i)^{r+n-1}$$

where

n = number of bits in sync word

$r+n$ = total frame length

$P_i = \left(\frac{1}{2}\right)^n$ since each bit has a probability of 1/2 of occurring as the correct framing bit.

Now, on the average, M frames will actually be scanned, where

$$M = \frac{1}{P_{fs} + P_c (1 - P_{fs})} \left[\frac{1 - (1 - P_i)^{r+n}}{P_i (r+n)} \right]$$

$$P_c = 1 - (1 - P_e)^n$$

P_e = bit error probability

and we assume no errors are permitted in word recognition. Figure 9-10 plots M versus n given $R = \frac{r}{r+n}$. Once scanning is completed, the probability that the established sync is false is given by

$$P_{tfs} = \frac{P_{fs}}{P_{fs} + P_c (1 - P_{fs})}$$

In Figure 9-11, the probability $P_{tfs} < 10^{-3}$ for R = 99 percent and any n. (This means that the system will attain true sync within only a very few frames.) When a false sync condition is discovered, the system returns to the scan mode and again searches for true sync. The average number of frames examined before false sync is rejected is given by

$$J = \frac{1}{1 - P_i'}$$

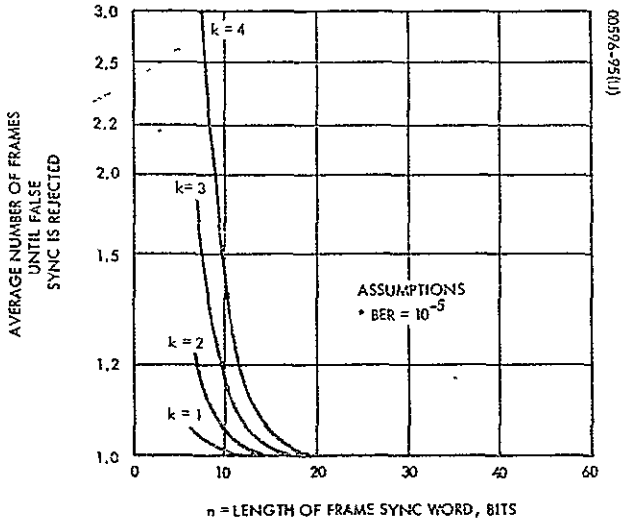

Figure 9-12. Frames Until False Sync is Rejected Versus Sync Word Length, Given Number of Errors Permitted (J Versus m, Given k)

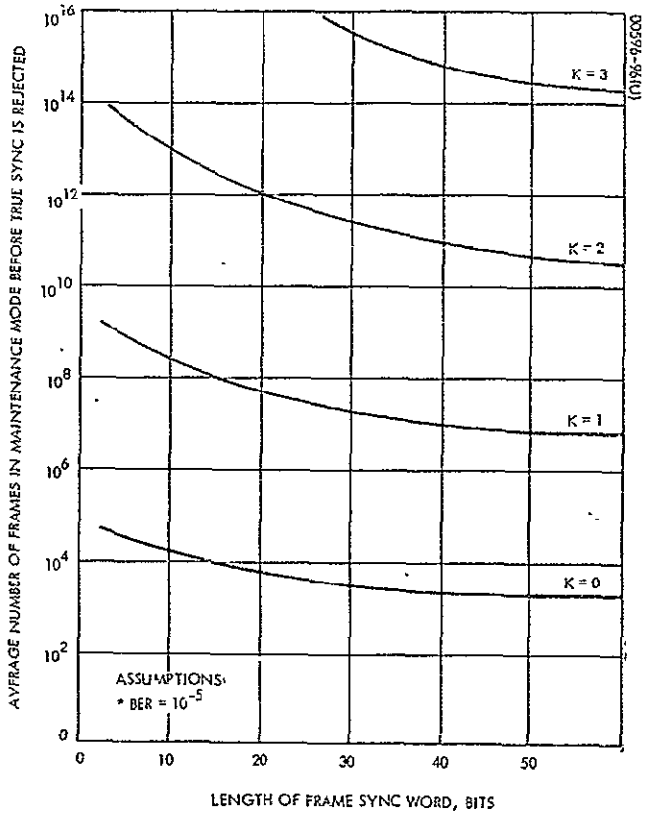

Figure 9-13. Maintenance Mode Rejection Versus Word Length Given That k Errors are Permitted (K Versus m, Given k)

where

$$P_i' = \frac{1}{2^n} \sum_{j=0}^{k} \binom{n}{j}$$

and k = the number of errors permitted in the pattern. The quantity J is plotted as a function of n in Figure 9-12.

The Maintenance Mode

When a frame synchronization system concludes that it has found the beginning of the frame, it passes from the scan to the maintenance mode. In the latter mode, the system "threshold" is reduced by permitting one or more errors in the sync pattern so that occasional channel noise will not disrupt synchronization. The system also sets a "clock" so that it only examines the n bits which arrive at the predicted beginning of a new frame. Figure 9-13 shows the average number of frames which will pass through a system before sync is rejected due to channel noise. Although it appears that one should lower the threshold significantly, i.e., increase the number of permitted errors, it should be remembered that this increases the number of frames required to reject a false sync condition.

EMI Considerations

The above analysis on synchronization performance assumes that the only perturbing influence is channel noise. Problems of internal electromagnetic interference and data drop-out are also quite important. The design suggested in the next section considers the effects of the Space Station power system in terms of transients, noise at the power distribution frequency, and noise due to ac ripple terms. It is undesirable that only occasional short data drop-outs or error bursts due to power transients should cause the frame synchronizer to return to the scan mode and cause further data loss. A design should be considered which "fly-wheels" through the expected power transient times. The frame period should not be synchronous with the period of expected EMI. The interference could cause frequent loss of sync (if it occurred during the sync word) while the data would be unaffected. Conversely, the data could be degraded periodically without the sync word recognizer giving any indication of data quality degradation.

Selection of the TDM Frame Time

Figure 9-14 summarizes some of the considerations involved in selecting a TDM frame time. The curves are plots of the frame period versus n given $R = \frac{r}{r + n}$. Since r includes information at 19.66 megabits/sec and a fixed number (64) of format bits, the frame period is given by

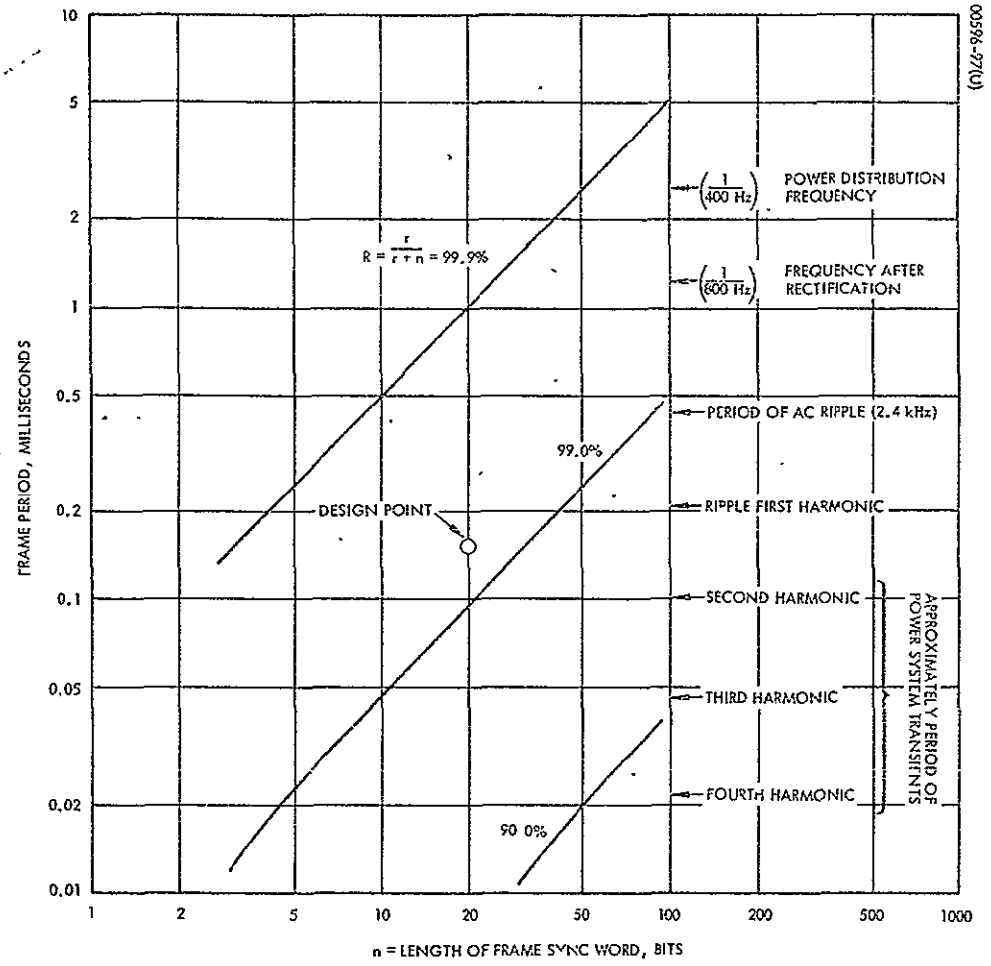

Figure 9-14. Constraints on Main Frame Period

$$P = (r - 64) \frac{1}{19.66 \times 10^6 \text{ bits/sec}}$$

$$= \left(n \frac{R}{1 - R} - 64\right) \times (0.051 \times 10^{-6} \text{ seconds}).$$

The power system constraints on the design are shown along the right hand side. The dc regulator frequency is in the range of 1 to 10 KHz. As a rule-of-thumb, the period of the switching transients will last between 0.01 and 0.10 ms. The primary power is distributed as three-phase, 400 Hz ac; single-phase, full wave rectification may cause EMI at 800 Hz. Three-phase ac ripple on the dc supply will be seen at 2.4 kHz and its harmonics. From Figure 9-14, it appears reasonable to choose a frame sync time of 0.15 ms, and a sync word length of 20. The information percentage is high and the system should be relatively immune to EMI.

The synchronization scheme chosen for the Space Station TDM system is a simple extension of the typical approach discussed above. During scan, two successive pattern recognitions (with no errors) must occur before sync is established. During the maintenance mode, sync is not assumed lost unless at least two errors are discovered in two successive pattern examinations. At the frame rate selected above, this approach permits loss of one frame during power transients without a return to the scan mode.

9.4 REFERENCES

9-1. W. J. Hurd and J. O. Anderson, "Digital Transition Tracking Symbol Synchronizer for Low SNR Coded Systems," IEEE Trans. on Com. Tech., Vol. 18, No. 2, April 1970, pp 141-147.

9-2. J. J. Stiffler, "On the Allocation of Power in Synchronous Binary PSK Communication Systems," Proc. 1964, Nat'l Telemetering Conf., June 2-4.

9-3. A. J. Viterbi, Principles of Coherent Communication, McGraw-Hill Book Co., New York, 1966.

9-4. W. C. Lindsay, "A Theory for the Design of One-Way and Two-Way Phase-Coherent Communication Systems," TR 32-986, Jet Propulsion Laboratory, Pasadena, California, July 15, 1969.

9-5. W. C. Lindsay, "Phase-Shift-Keyed Signal Detection with Noisy Reference Signals," IEEE Trans. on A and ES, Vol. 2, No. 4, July 1966, pp 393-401.

9-6. J. I. Marcum, "Statistical Theory of Target Detection by Pulse Radar," IRE Trans. on I. T., p 174, April 1960.

F. Gardner, Phaselock Techniques, John Wiley and Sons, New York, 1966.

A. Heller, "Sequential Decoding: Improved Performance of Constraint Length Convolutional Codes," JPL Space Programs Summary 37-56, Vol. III, pp 82-83.

L. B. Milstein, "Summary of Frame Synchronization Techniques, HAC IDC 2292/655, March 10, 1969.

10. EQUIPMENT SURVEYS

10.1 INTRODUCTION

To determine the level of current technology, several equipment surveys were performed during the study. The communications system design described in Part I utilizes this state of the art technology. Section 10.2 summarizes the power output and power efficiencies achievable in current traveling-wave tube amplifiers (TWTA). TWTA physical characteristics are also included. Section 10.3 gives noise temperature data for two types of microwave preamplifiers. System temperature estimates are given, assuming two types of background noise. Section 10.4 gives physical data on hardware for source encoding and digital channel encoding. These designs do not require the development of digital devices beyond the current state of the art.

10.2 TWTA'S FOR SPACE APPLICATION (2 TO 15 GHZ)

For medium power space applications above S-band, the TWT remains the most desirable transmitting device. A survey of available TWTA's is summarized below.

Output Power, Gain and Efficiency

Currently available continuous wave spaceborne TWTA's typically generate 10 watts RF with a 45 dB gain and 33 percent efficiency. As Figure 10-1 shows, the characteristics of a given unit can be modified by increasing the beam voltage, but increased output power is achieved at the expense of decreased gain.

Bandwidth, Gain Flatness

Bandwidths of 10 percent or more are attainable depending upon the gain-flatness specification. For example, at S-band carrier frequencies, TWTs make an RF bandwidth of greater than 200 MHz a possibility. The wideband nature of these devices is also a liability in that they require RF filters.

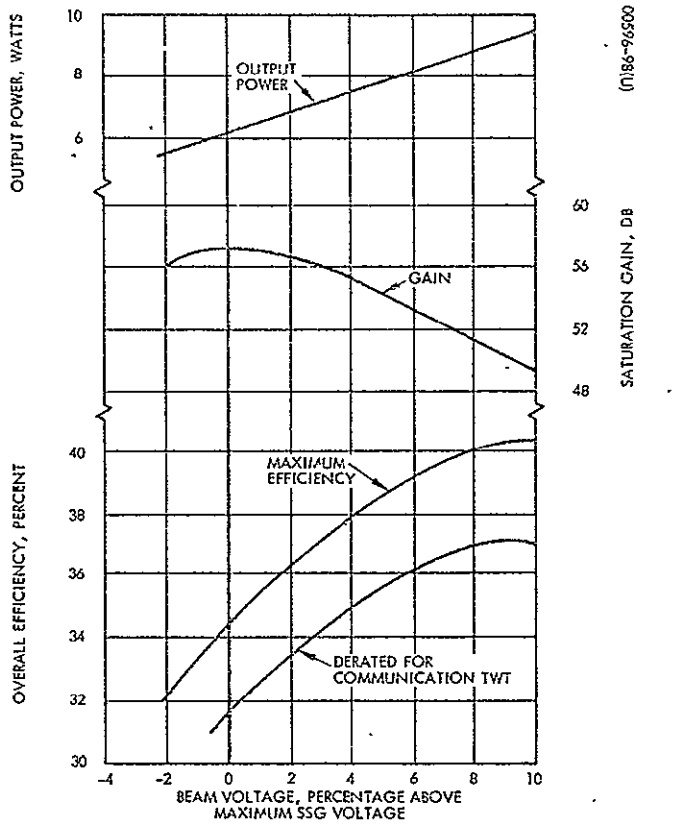

Figure 10-1. Power, Gain, and Efficiency Versus Beam Voltage For Intelsat IV Type Output TWT

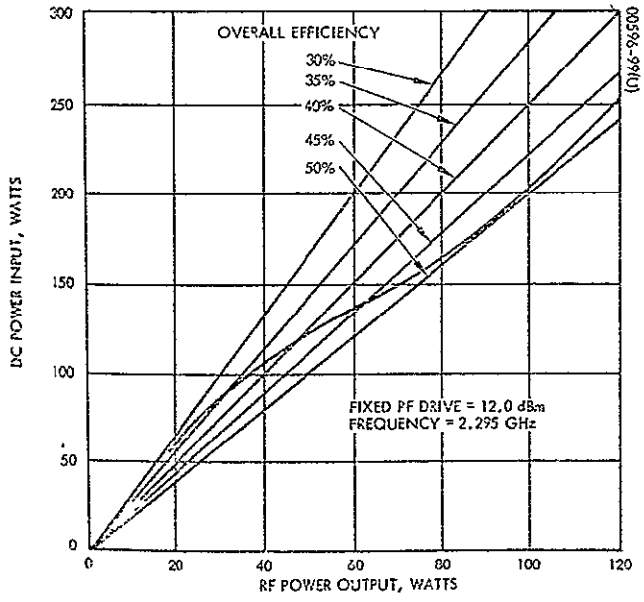

Figure 10-2. Variable Power Operation of the WJ-395

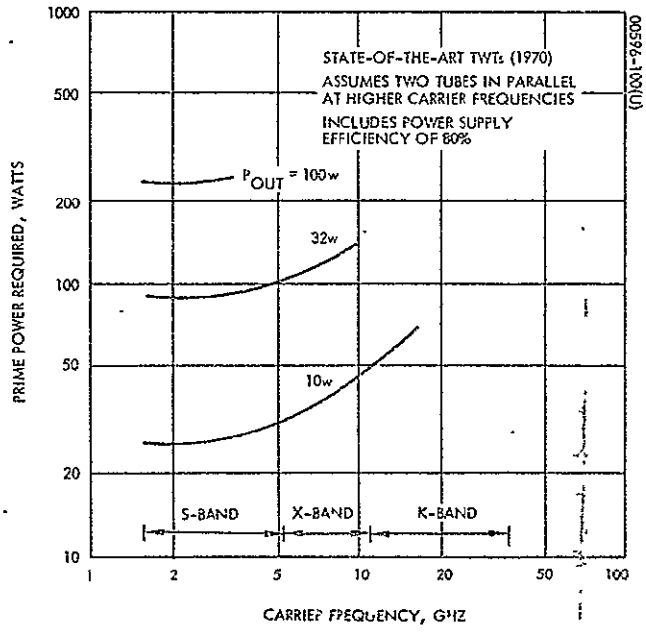

Figure 10-3. TWT Transmitter Efficiency and Power Output Versus Frequency

Size, Weight, and Prime Power

The TWT units themselves typically weigh 18 ounces, and occupy a space 2 by 2 by 10 inches. Each tube, however, must be accompanied by a power supply which delivers up to 5,000 volts dc. These units are typically 80 to 85 percent efficient, weight 3 pounds, and occupy a space 4 by 6 by 2 inches. Their weight and size increase with the power level handled, the voltage required (which generally increases with frequency and efficiency), and the number of telemetry points taken within the unit.

Reliability

TWTA's have demonstrated excellent reliability in both actual space missions and laboratory life tests. The failure of a spacecraft communication system has yet to be traced directly to a Hughes tube. Life tests of space-qualified TWTs have yet to produce a failure. After more than 8 years, Syncom 2.5 watt L-band tubes are still operating at the Hughes Electron Dynamics Division lifetest facility. Their only degradation appears to be a 0.1 dB drop in power level every 3 years.

Available TWTs

Table 10-1 is a partial list of the units now available from Hughes and is representative of the current technology. The list is ordered according to frequency, but as the missions of the tubes indicate, this is also the approximate order of tube development. The movement to higher frequencies has prompted TWT development. Up through 10 GHz, TWTs are available which provide 20 watts output with 33 percent efficiency. Although tubes at higher frequencies have been operated in space, their output levels and efficiencies are notably lower. At 14 GHz, the only Hughes TWT which has been flown delivers 1 watt with an efficiency of 20 percent.

Of the tubes developed by the many other companies in the TWT field, two tubes built by Watkins-Johnson for JPL should be singled out. (Reference 10-1) The tubes are shown in Table 10-2 to have been designed for high output levels and high efficiencies (at the expense of bandwidth and gain). Furthermore, their output levels can be adjusted over a 10 dB range by simply programming the power supply voltages. Figure 10-2 shows how the efficiency of the 100 watt varies with output power and can be used to determine the true prime power savings when operating at reduced output levels. Although these tube designs have some remaining problems, (Reference 10-2) they may be very useful for Space Station S-band applications.

The current state of the art in TWTs in terms of efficiency and power output is summarized in Figure 10-3 as a function of frequency. It can be assumed that this technology will be improved significantly in the next several years due to research and development for commercial and military applications.

TABLE 10-1. MEDIUM POWER CW TRAVELING-WAVE TUBES
(PARTIAL LIST OF HUGHES TWT'S)

Band	Tube No.	Frequency Range, (GHz)	Power Out, watts	Approximate* Prime Power, watts	Overall Tube Efficiency, percent	Saturated Gain, db	Status	Mission
S	314H	1.5- 2.5	2.5	16.	20	33	Operational	Syncom
	214H	2.5- 2.4	8.0	30	33	27	Operational	Pioneer
	394H	1.8- 2.6	20.0	76	33	26	Operational (a)	Apollo
C	235H	3.0- 5.0	10.0	37	34	43	Operational	Intelsat III
	261H	3.0- 5.0	6.0	24	31	50	Operational	Intelsat IV
X	240H	7.0- 7.7	20.0	76	33	43	Operational (b)	TACSAT
	219H	7.5- 9.0	20.0	72	35	30	Operational	---
K	837H	10.0-15.5	1.0	6	20	45	Operational	---
	274H	10.0-15.5	5.0	30	20	46	Experimental	---
	818H	12.5-15.0	18.0	107	21	45	Operational (c)	Lab TWTA
	267H	17.5-21.5	4.0	31	16	50	Developmental	Comsat Corp.
	268H	18.0-22.0	2.0	17	15	42	Developmental	ATS F and G
	254H	27.0-33.0	2.0	23	11	42	Developmental	ATS F and G

*Prime power estimate assumes 80 percent efficient power supply.

(a) Also delivers 5 watts RF with 25 percent efficiency.

(b) Two tubes are used in parallel to deliver 40 watts.

(c) Although now used in a laboratory amplifier, this unit could be space-qualified.

TABLE 10-2. WATKINS-JOHNSON S-BAND
50 AND 100 WATT TWT'S

Tube	Frequency, GHz	Power Out watts	*Approximate Prime Power, watts	Overall Tube Efficiency, percent	Saturated Gain, dB
WJ-448	2.3	50	105	43	30
WJ-395	2.3	103	263	45	38

*Prime power estimate assumes 80 percent efficient power supply

10.3 MICROWAVE PREAMPLIFIERS

The noise temperature ranges of various state of the art low noise microwave amplifiers are shown in Figure 10-4. Figure 10-5 shows the system temperature of a receiver with a "worst case" tunnel diode preamplifier and galactic background noise. Figure 10-6 shows the system temperature when a TDA is used and a 290°K earth is "seen" by the receive antenna (as in the case of a DRS).

10.4 VITERBI DECODERS AND ZOP DATA COMPRESSORS

Introduction

The digital units which are discussed in this section are located within the overall communication system as described in Section 9.1. Since the Space Station links have been specified as full-duplex, their counterparts will also be required at the remote communications terminal.

Compressor (Source Encoder)

Table 10-3 shows the weight and power required for the data compressor. The zero order predictor algorithm was assumed. This technique has been found to have a good balance between performance and equipment complexity (Reference 10-3). The algorithm compares a "new" sample value with a prediction (which is the value of the last nonredundant sample). If the difference between the new sample and the prediction is within some tolerance, the sample is deleted from the data stream. If the new sample is not redundant, it is "tagged" and sent to the buffer for transmission.

Encoder (Digital Channel Encoder)

The encoder schematic for a convolutional code of rate $1/V$ and constraint length K is shown in Figure 10-7. When implemented, such a device

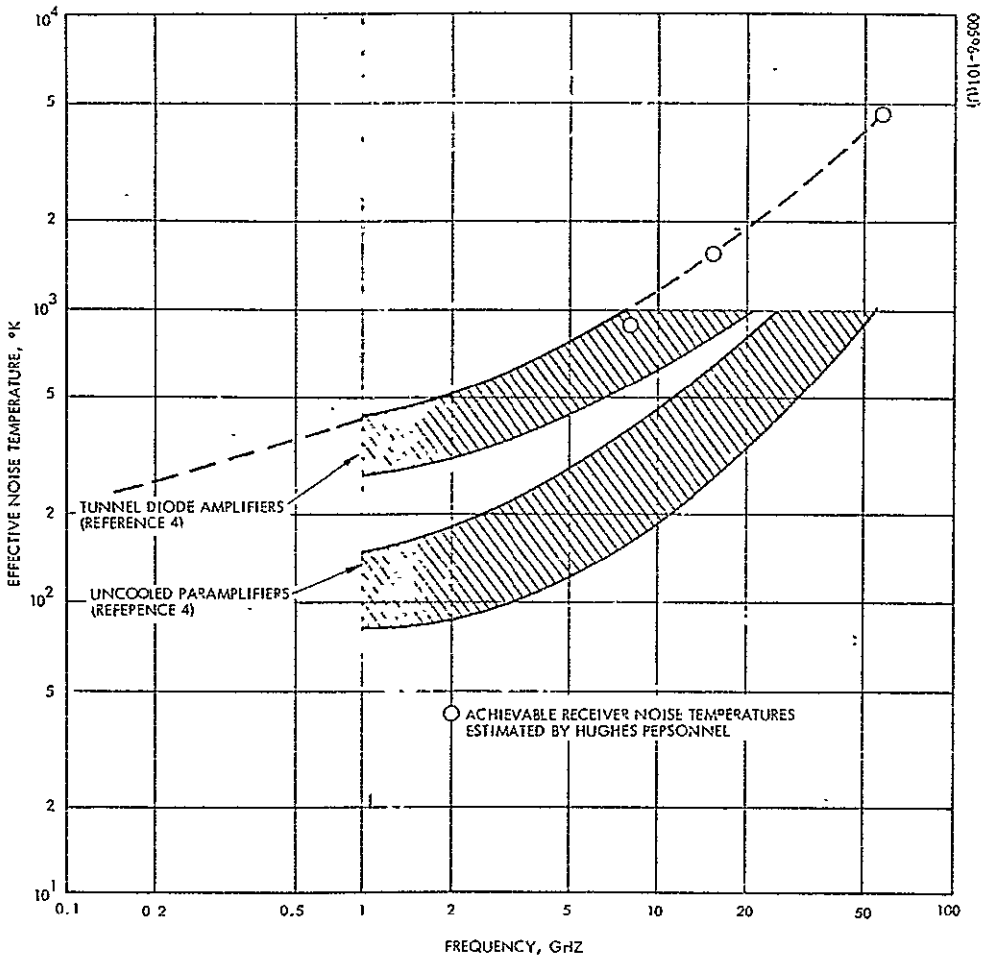

Figure 10-4. Receiver System Noise Temperature Versus Frequency

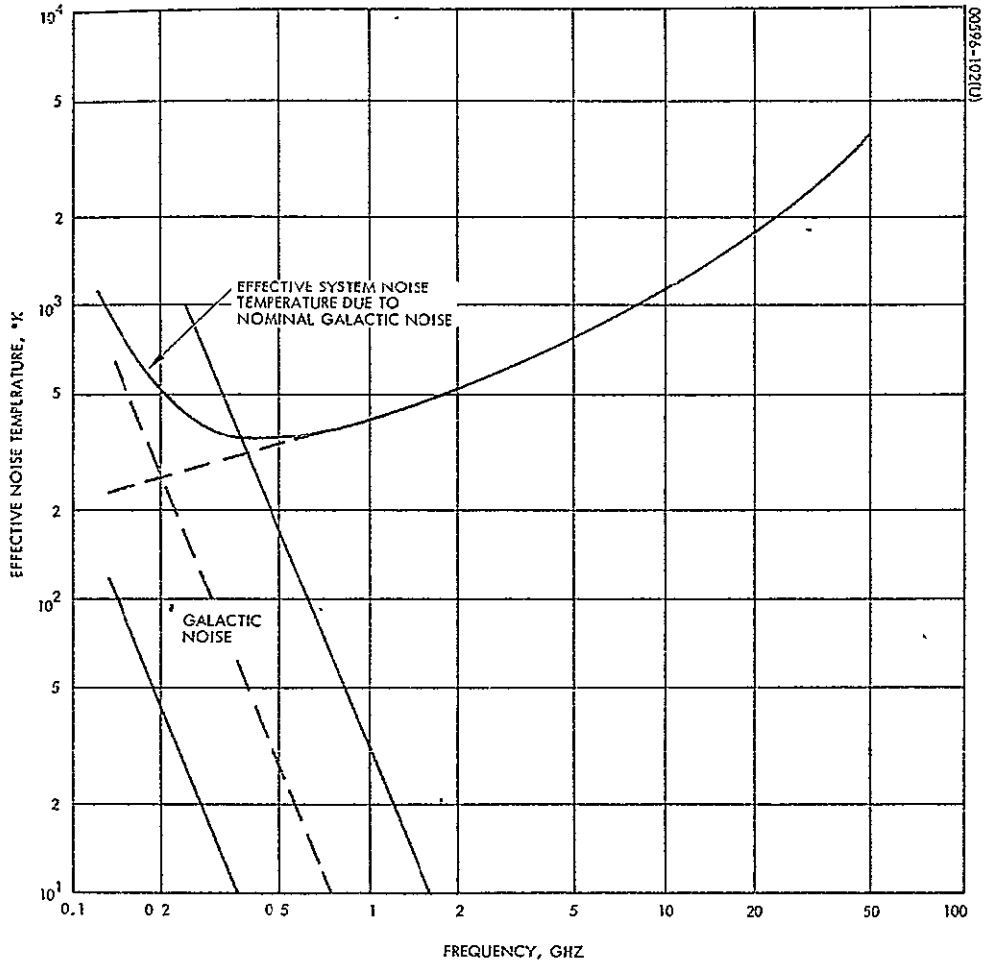

Figure 10-5. Effective System Noise Temperature Versus Frequency (Data Relay to Space Station Link)

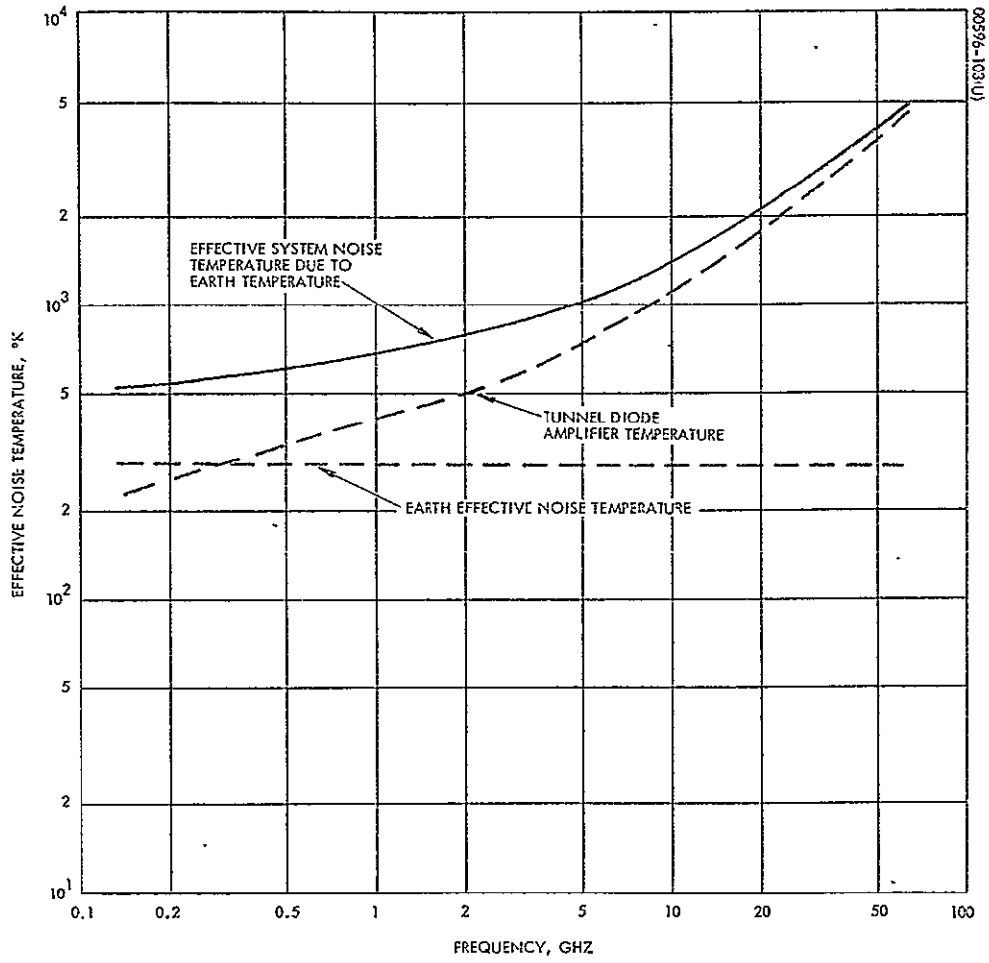

Figure 10-6. Effective System Noise Temperature Versus Frequency (Space Station to Data Relay Link)

TABLE 10-3. ZOP DATA COMPRESSOR
PHYSICAL CHARACTERISTICS

Bit Rate (Before 4:1 Compression)	Weight, pounds	Power, watts
50 kilobits/sec	7.9	11.4
3 megabits/sec	7.9	11.4
50 megabits/sec	12.0	45.0

Includes power supply (for each) and supply efficiency.

requires negligible weight and power compared to the rest of the system. It would probably be advantageous to integrate the encoder with other digital units and save packaging weight and volume. (The simplicity of the encoder makes coding especially attractive for deep space missions where a decoder is needed only at the ground terminal).

Decoder (Digital Channel Decoder)

Table 10-4 shows the physical characteristics of Viterbi decoders for three bit rates and two codes. The highest bit rate of 12 megabits/sec corresponds to a 4:1 compression of commercial quality digital television. The codes assumed were suggested by MSC. Note that for rates above several hundred kilobits/sec, a parallel implementation is required. For low rates, a serial design permits using fewer packages with corresponding weight savings. Now, since the number of operations required by the Viterbi algorithm grows exponently with K, the parts count and power consumption also grows rapidly with increasing K. Operation at higher data rates with the same code also requires greater power. (The ultimate decoding speed is dependent on the speed of the available logic. The Linkabit Corporation now has a 40 megabits/sec system operational with K = 4, V = 2.) (Reference 10-4).

Expander (Source Decoder)

Table 10-5 shows the weight and power required for the data expander. This device takes the data format generated by a zero order predictor and outputs a conventional PCM data stream.

Conclusions

The data compression and coding system discussed (4:1 compression of 50 megabits/sec data and K = 8, V = 3 code) requires hardware which weighs approximately 50 pounds and consumes 210 watts.

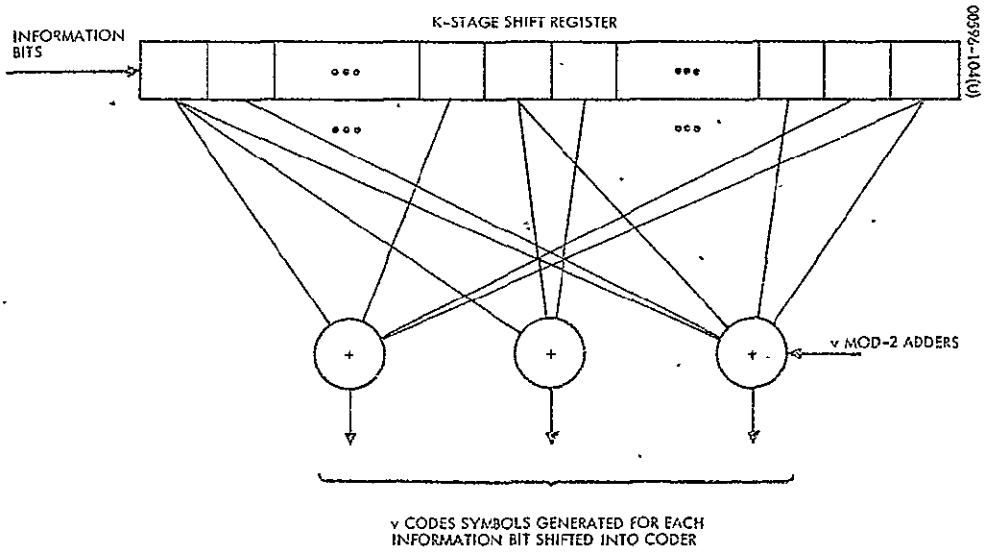

Figure 10-7. Binary Convlutional Codes

TABLE 10-4. DECODER PHYSICAL CHARACTERISTICS

Bit Rate = 50 Kilobits/sec (Serial Decoder)		
Code:	K = 6, V = 3	K = 8, V = 3
Weight, pounds:	6.0	8.0
Power, watts:	17.0	30.0
Volume, cubic inches:	80.0	110.0
Bit Rate = 0.7 Megabits/sec (Parallel Decoder)		
Code:	K = 6, V = 3	K = 8, V = 3
Weight, pounds:	10.0	35.0
Power, watts:	30.0	100.0
Volume, cubic inches:	210.0	720.0
Bit Rate = 12.5 Megabits/sec (Parallel Decoder)		
Code:	K = 6, V = 3	K = 8, V = 3
Weight, pounds:	10.0	35.0
Power, watts:	40.0	150.0
Volume, cubic inches:	210.0	720.0

Includes power supply (for each) and supply efficiency. Assumes available high speed units.

TABLE 10-5. ZOP DATA EXPANDER PHYSICAL CHARACTERISTICS

Bit Rate (After 1:4 Expansion)	Weight, pounds	Power, watts
50 kilobits/sec	2.5	1.7
3 megabits/sec	2.5	1.7
50 megabits/sec	5.6	15.5

Includes power supply (for each) and supply efficiency.

For future tradeoff analyses, it should be noted that data compression is especially desirable, since it lowers the data rate requirement of both the encoder/decoder and the channel. The weight of the decoder is roughly independent of the data rate for megabit rates, but the power it requires increases with increasing data rates. The decoder weight increases greatly with increasing constraint length. While the K = 8 code requires a decoder which weighs over three times the decoder for K = 6, the link performance is improved by only about 0.8 dB (based on the results due to Heller (Reference 10-5)).

10.5 REFERENCES

10-1. E. R. Dornseif and L. A. Roberts, "Modern Traveling-Wave Tubes for Space Application," Microwave Journal, Vol. 12, No. 4, April 1969, pp. 55-59.

10-2. Robert S. Hughes, "Spacecraft S-Band 10-100 W RF Power Amplifier Tubes," paper No. 70-506, AIAA 3rd Communications Satellite Systems Conference, Los Angeles, California, April 6 - 8, 1970.

10-3. "Potenial Applications of Digital Techniques to Apollo Unified S-Band Communication System," Martin Marietta Corporation, Denver Division, February 1970, under Contract NAS 9-9852.

10-4. Private Communication with R. Martin of Linkabit Corporation, July 21, 1970.

10-5. J. A. Heller, "Sequential Decoding: Improved Performance of Short Constraint Length Convolutional Codes," JPL Space Programs Summary 37-56, Vol. III, pp 82-83.

APPENDIX A. LINK POWER BUDGETS

The following tables present the final power budget summaries for the baseline design of Part I. The link analysis approach used is discussed in detail in Section 7.2.

TABLE A-1. TRACKING BEACON, DATA RELAY SATELLITE TO STATION (f_c = 14.26 GHz)

PERFORMANCE SUMMARY

Bit rate	150 bits/sec
Bit error rate	10^{-3}
3σ tracking error	0.16 degrees

Channel coding	at Baseband	at RF
Encoding	PN code of length 10	Biphase PSK
Decoding	Ref. PN generator	Coherent integrate and dump

LINK SUMMARY

Radiated power	-16.5 dBw
Transmit antenna gain (beam edge)	+15.0 dB
Free space loss (23,800 n.mi.)	-208.5 dB
Ellipticity loss	-1.0 dB
Receive antenna gain (4 foot diameter)	+41.7 dB
Receive pointing error loss (±0.25 degrees)	-0.5 dB
Link margin	-1.3 dB
Received power at Station	C = -171.1 dBw
Noise power density (T_s = 391°K)	N_o = -202.7 dBw/Hz
	C/N_o = 31.6 dB·Hz
Chip rate (1500/sec)**	-31.8 dB·Hz
Degradation in detector	-2.0 dB
Detector margin	-1.0 dB
E_{BIT}/E_{CHIP}	+10.0 dB
E_{BIT}/N_o	+6.8 dB
SNR in 3kHz IF*	-3.2 dB

System temperature calculation, °K

Antenna temperature	= 75.4
(L-1) 290°, L = 0.5 dB	= 35.4
Normalized preamp temperature	= 280.0
System temperature	= 390.8

*Determines tracking performance
**A PN code of length 10 is transmitted every bit time.

TABLE A-2. TRACKING BEACON, STATION TO DATA RELAY SATELLITE (f_c = 15.35 GHz)

PERFORMANCE SUMMARY

Bit rate	150 bits/sec
Bit error rate	10^{-3}

Channel Coding	at Baseband	at RF
Encoding	PN code of length 10	Biphase PSK
Decoding	Ref. PN generator	Coherent integrate and dump

LINK SUMMARY

Transmitter power (including output circuit losses)	-10.6 dBw
Line losses	-1.4 dB
Transmit antenna gain (4 foot diameter)	+42.3 dB
Transmit pointing error loss (±0.25 degrees)	-0.5 dB
Free space loss (23,800 n.mi.)	-209.1 dB
Ellipticity loss	-1.0 dB
Receive antenna gain (beam edge)	+15.0 dB
Link margin	-0.9 dB
Received power at DRS	C = -166.2 dBw
Noise power density (T_s = 1200°K)	N_o = -197.8 dB/HZ
	C/N_o = 31.6 dB·Hz
Chip rate (1500/sec)	-31.8 dB·Hz
Degradation in detector	-2.0 dB
Detector margin	-1.0 dB
E_{BIT}/E_{CHIP}	+10.0 dB
E_{BIT}/N_o	+6.8 dB

TABLE A-3. DRS DATA LINK, DATA RELAY SATELLITE TO STATION
(f_c = 13.70 - 14.20 GHz)§

PERFORMANCE SUMMARY		
Bit rate		20.2 megabits/sec
Bit error rate		10^{-5}
Channel Coding	at Baseband	at RF
Encoding	(2, 5) convolutional code	Biphase PSK
Decoding	Viterbi decoder (q = 8)	Filter and sample

LINK SUMMARY	
Radiated Power per carrier	+7.0 dBw
Transmit antenna gain	+41.9 dB
Transmit pointing error loss (±0.25 degrees)	-0.5 dB
Free space loss (23,800 n.mi.)	-208.3 dB
Ellipticity loss	-1.0 dB
Receive pointing error loss (±0.25 degrees)	-0.5 dB
Receive antenna gain (4 foot diameter)	+41.9 dB
Link margin	-1.5 dB
Received power at station	C = -121.0 dBw
Noise power density (T = 390.8°K)*	N_o = -202.7 dBw/Hz
	C/N_o = 81.7 dB·Hz
Chip rate (40.4×10^6/sec)	76.0 dB·Hz
E_c/N_o in downlink to station	+5.7 dB
Degradation due to uplink**	-0.5 dB
Detector degradation	-2.0 dB
Detector margin	-1.0 dB
E_{BIT}/E_{CHIP}	+3.0 dB
E_{BIT}/N_o to Viterbi decoder at station	+5.2 dB

§Bandwidth of 80 MHz is required within 500 MHz band

*See Table A-1

**Assumes a linear repeater with $(E_c/N_o)_{up} \geq 15.0$ dB

TABLE A-4. DRS DATA LINK, STATION TO DATA RELAY SATELLITE (f_c = 14.85 - 15.35 GHz)§

PERFORMANCE SUMMARY		
Bit rate		20.2 megabits/sec
Bit error rate		10^{-5}
Channel Coding	at Baseband	at RF
Encoding	(2, 5) convolutional code	Biphase PSK
Decoding	Viterbi decoder (q = 8)	Filter and Sample

LINK SUMMARY	
Transmitter power (including output circuit losses)	+16.4 dBw
Line losses	-1.4 dB
Transmit antenna gain (4 foot diameter)	42.5 dB
Transmit pointing error loss (±0.25 degrees)	-0.5 dB
Free space loss (23,800 n.mi.)	-208.9 dB
Ellipticity loss	-1.0 dB
Receive pointing error loss (±0.25 degree)	-0.5 dB
Receive antenna gain	+42.5 dB
Link margin	-3.0 dB
Power received at DRS	C = -113.9 dBw
Noise power density T_s = (1200°K)	N_o = -197.8 dBw/Hz
	C/N_o = 83.9 dB
Chip rate (40.4×10^6/sec)	76.0 dB·Hz
E_c/N_o in uplink to DRS	7.9 dB
Degradation due to downlink**	2.7 dB
Detector degradation	-2.0 dB
Detector margin	-1.0 dB
E_{BIT}/E_{CHIP}	+3.0 dB
E_{BIT}/N_o to Viterbi decoder at ground	+5.2 dB

§Bandwidth of 80 MHz required within 500 MHz band

**Assumes a linear repeater with $(E_c/N_o)_{down} \geq 8.6$ dB

TABLE A-5. EMERGENCY VOICE LINK, STATION TO DATA RELAY SATELLITE (f_c = 149.22 - 149.32)§

PERFORMANCE SUMMARY		
Voice bandwidth		3 kHz
Output SNR		32.6 dB
Channel Coding	**at Baseband**	**at RF**
Encoding	Pre-emphasis	FM
Decoding	De-emphasis	Threshold extension demodulator

LINK SUMMARY	
Transmitter power (including output circuit losses)	19.0 dBw
Line losses	-0.9 dB
Transmit antenna gain	-3.0 dB
Free space loss (23,800 n.mi.)	-168.9 dB
Ellipticity loss	-1.0 dB
Receive antenna gain (beam edge)	+15.0 dB
Link margin	-1.0 dB
Power received at DRS	C = -140.8 dB
Noise power density (T_s = 800°K)	N_o = -199.5 dBw/Hz
	C/N_o = +58.7 dB·Hz
Receive bandwidth (36 kHz + 7 kHz doppler)	-46.3 dB·Hz
Received C/N at DRS	12.4 dB
Degradation due to downlink*	-5.4 dB
Demodulator margin	-1.0 dB
C/N to threshold extension demodulator	+6.0 dB

§Two 50 kHz channels available for uplink

*Assumes a linear repeater and (C/N) down ≥ 8.5 dB

TABLE A-6. EMERGENCY VOICE LINK, DATA RELAY SATELLITE TO STATION (f_c = 135.60 - 135.70 MHz)§

PERFORMANCE SUMMARY		
Voice bandwidth		3 kHz
Output SNR		32.6 dB
Channel Coding	at Baseband	at RF
Encoding	Pre-emphasis	FM
Decoding	De-emphasis	Threshold extension demodulator

LINK SUMMARY	
Radiated power (per carrier)	+12.7 dBw
Transmit antenna gain (beam edge)	+15.0 dB
Free space loss (23,800 n.mi.)	-168.0 dB
Ellipticity loss	-1.0 dB
Receive antenna gain	-3.0 dB
Link margin	-1.0 dB
Power received at Station	C = -145.3 dBw
Noise power density (T_s = 723°K)	N_o = 200.0 dBw/Hz
	C/N_o = 54.7 dB·Hz
Receive bandwidth (36 kHz + 7 kHz doppler)	-46.3 dB·Hz
C/N in downlink to station	+8.4 dB
Degradation due to uplink*	-1.4 dB
Demodulator margin	-1.0 dB
C/N to threshold extension demodulator	+6.0 dB

System temperature calculation, °K

Antenna temperature	= 250
(L-1) 290°, L = 1.5 dB	= 119
Normalized preamp temperature	= 354
System temperature	= 723

§Two 50 kHz channels available for downlink

*Assumes a linear repeater and (C/N) up ≥ 12.6 dB

TABLE A-7. EMERGENCY VOICE LINK, SPACE STATION TO ALS (f_c = 135.60 to 135.70 MHz or 149.22 to 149.32 MHz)[§]

PERFORMANCE SUMMARY		
Voice bandwidth		3 kHz
Output SNR		32.6 dB
Range		3000 n.mi.
Channel Coding	at Baseband	at RF
Encoding	Pre-emphasis	FM
Decoding	De-emphasis	Threshold extension demodulator

LINK SUMMARY	
Transmitter power (including output circuit losses)	19.0 dBw
Line losses	-0.9 dB
Transmit antenna gain	-3.0 dB
Free space loss (3000 n.mi.)	-150.3 dB
Ellipticity loss	-1.0 dB
Receive antenna gain	-3.0 dB
Link margin	-7.0 dB
Power received at ALS	C = -146.2 dBw
Noise power density (T_s = 800°K)	N_o = -199.5 dBw/Hz
	C/N_o = 53.3 dB Hz
Receive bandwidth (43 kHz)	-46.3 dB Hz
Received C/N at ALS	7.0 dB
Demodulator margin	-1.0 dB
C/N to threshold extension demodulator	+6.0 dB

[§]Both the Station and the ALS can either transmit or receive within these bands. Each band containing two 50 kHz channels.

TABLE A-8. EMERGENCY VOICE LINK, ALS TO SPACE STATION* (f_c = 135.60 - 135.70 MHz or 149.22 - 149.32 MHZ)§

PERFORMANCE SUMMARY

Voice bandwidth	3 kHz
Output SNR	32.6 dB
Range	3000 n.mi.

Channel Coding	at Baseband	at RF
Encoding	Pre-emphasis	FM
Decoding	De-emphasis	Threshold Extension Demodulator

LINK SUMMARY

Radiated power (per carrier)	20.1 dBw
Transmit antenna gain	-3.0 dB
Free space loss	-150.3 dB
Ellipticity loss	-1.0 dB
Receive antenna gain	-3.0 dB
Link margin	-9.5 dB
Power received at Station	C = -146.7 dBw
Noise power density (T_s = 723°K)	N_o = -200.0 dBw/Hz
	C/N_o = 53.3 dB·Hz
Receive bandwidth (43 kHz)	-46.3 dB·Hz
Received C/N at Station	7.0 dB
Demodulator margin	-1.0 dB
C/N to threshold extension demodulator	+6.0 dB

*Both the Station and the ALS can either transmit or receive within these bands. Each band contains two 50 kHz channels.

TABLE A-9. ALS DATA LINK, SPACE STATION TO ALS
(f_c = 2100 - 2300 MHz)§

PERFORMANCE SUMMARY		
Bit rate		57.6 kilobits/sec
Bit error rate		10^{-5}
Range		303 n.mi.
Channel Coding	at Baseband	at RF
Encoding	(2, 5) convolutional code	Biphase PSK
Decoding	Viterbi decoder (q = 8)	Coherent integrate and dump

LINK SUMMARY	
Transmitter power (including output circuit losses)	20.4 dBw
Line losses	-1.0 dB
Transmit antenna gain	-3.0 dB
Free space loss	-154.2 dB
Ellipticity loss	-1.0 dB
Receive antenna gain	-3.0 dB
Link margin	-1.9 dB
Power received at ALS	C = -143.7 dBw
Noise power density (T_s = 800°K)	N_o = -199.5 dBw/Hz
	C/N_o = 55.8 dB·Hz
Chip rate (115.2×10^3/sec)	50.6 dB·Hz
Received E_c/N_o	5.2 dB
Degradation in detector	-2.0 dB
Detector margin	-1.0 dB
E_{BIT}/E_{CHIP}	+3.0 dB
E_B/N_o to Viterbi decoder	5.2 dB

§Link requires 244 kHz within this band.

TABLE A-10. ALS DATA LINK, ALS TO SPACE STATION
(f_c = 2100 - 2300 MHz)[9]

PERFORMANCE SUMMARY

Bit rate	57.6 kilobits/sec
Bit error rate	10^{-5}
Range	303 n.mi.

Channel Coding	at Baseband	at RF
Encoding	(2, 5 convolutional code	Biphase PSK
Decoding	Viterbi decoder (q = 8)	Coherent integrate and dump

LINK SUMMARY

Radiated power (per carrier)	18.4 dBw
Transmit antenna gain	-3.0 dB
Free space loss	-154.2 dB
Ellipticity loss	-1.0 dB
Receive antenna gain	-3.0 dB
Link margin	-3.6 dB
Power received at station	C = -146.4 dBw
Noise power density (T_s = 437.8°K)	N_o = -202.2 dBw/Hz
	C/N_o = 55.8 dB·Hz
Chip rate (115.2×10^3/sec)	50.6 dB·Hz
Received E_c/N_o	5.2 dB
Degradation in detector	-2.0 dB
Detector margin	-1.0 dB
E_{BIT}/E_{CHIP}	+3.0 dB
E_B/N_o to Viterbi decoder	5.2 dB

System temperature calculation, °K

Antenna temperature	= 200.0
(L-1) 290°, L - 1.3 dB,	= 102.0
Normalized preamp temperature	= 135.8
System temperature	= 437.8

[9] Requires 244 kHz within this band.

TABLE A-11. EXPERIMENT MODULE DATA LINK, STATION TO EM_1 (f_c = 2100 - 2300 MHz)[¶]

PERFORMANCE SUMMARY

Bit rate	7.38 megabits/sec
Bit error rate	10^{-5}
Range	450 n.mi.

Channel Coding	at Baseband	at RF
Encoding	(5, 2) convolutional code	Quadriphase PSK
Decoding	Viterbi decoder (q = 8)	Coherent integrate and dump

LINK SUMMARY

Transmitter power (including output circuit losses)	20.4 dBw
Line losses	-1.0 dB
Transmit antenna gain	-3.0 dB
Free space loss	-157.9 dB
Ellipticity loss	-1.0 dB
Receive antenna gain	+20.0 dB
Transmit pointing error loss	-0.5 dB
Link margin	-2.3 dB
Power received at EM_1	C = -125.3 dB
Noise power density (T_s = 437.8°K)	N_o = -202.2 dBw/Hz
	C/N_o = 76.9 dB·Hz
Chip rate (7.38×10^6/sec)	-68.7 dB·Hz
Received E_c/N_o	8.2 dB
Degradation in detector	-2.0 dB
Detector margin	-1.0 dB
E_{BIT}/E_{CHIP}*	0.0 dB
E_B/N_o to Viterbi decoder	5.2 dB

[¶]Link required 15 MHz within this band.

*The V = 2 encoder generates two subbits per bit; the quadriphase modulator outputs one chip per two subbits. See Sec 7.2.

TABLE A-12. EXPERIMENT MODULE DATA LINK, EM_1 TO STATION (f_c = 2100 - 2300 MHz)[9]

PERFORMANCE SUMMARY	
Bit rate	7.38 megabits/sec
Bit error rate	10^{-5}
Range	450 n.mi.

Channel Coding	at Baseband	at RF
Encoding	(5, 2) convolutional code	Quadriphase PSK
Decoding	Viterbidecoder (q = 8)	Coherent integrate and dump

LINK SUMMARY	
Radiated power (per carrier)	19.4 dBw
Transmit antenna gain	20.0 dB
Transmit pointing error	-0.5 dB
Free space loss	-157.9 dB
Ellipticity loss	-1.0 dB
Receive antenna gain	-3.0 dB
Link margin	-2.3 dB
Power received at station	C = -125.3 dBw
Noise power density (T_s = 437.8°K)*	N_o = -202.2 dBw/Hz
	C/N_o = 76.9 dB Hz
Chip rate (7.38×10^6/sec)	-68.7 dB Hz
Received E_c/N_o	8.2 dB
Degradation in detector	-2.0 dB
Detector margin	-1.0 dB
E_{BIT}/E_{CHIP}	0.0 dB
E_B/N_o to Viterbi decoder	5.2 dB

[9] Link requires 15 MHz within this band.

*See Table A-10

APPENDIX B. ELECTRONICALLY SCANNED ARRAYS FOR COMMUNICATION DURING ARTIFICIAL-G OPERATIONS

INTRODUCTION

Space Station operation in the artificial-g mode imposes the requirement that the K-band antenna system must provide spherical coverage from a platform rotating at 4 rpm. It appears that this spherical coverage requirement can be met by the use of multiple mechanically steered antennas (as used in the baseline design). At the request of the Manned Spacecraft Center, a special study was undertaken to consider the possible use of multiple electronically steered arrays. It was concluded that the technique was indeed feasible, but that the approach requires far greater weight and volume than the mechanical system. The ESA system weighs 2563 pounds and utilizes 80 square feet of spacecraft surface to a depth of up to 2.5 feet.

The study summarized below considers problems of coverage, weight, size, power, and the state of the current technology. Recommendations for future work are also included.

SPHERICAL COVERAGE WITH ESA

To obtain spherical coverage with electronically steered arrays requires an assembly of arrays that are a compromise among many factors. The number of apertures and the orientation with respect to each other is determined principally by the design and configuration of the station structure. Consequently, it is not feasible to consider all possible configurations to obtain the configuration that is "best" in some sense. What has been done for this study was to consider that coverage which is obtained by using a number of planar arrays that would each cover a different but overlapping angular region. As the pointing direction moves from one angular region to another, the appropriate array would be switched on, all others would be off. Such an arrangement would then require only sufficient electronics for a single array, plus additional logic and control circuitry to perform the switching operation.

The determination of the number of arrays and the number of elements to perform the scanning electronically must take into account a number of factors. The number of radiating elements required depends on both the coverage region of each array and on the required array gain. To understand this dependence, consider the following argument. The beamwidth of each element in an array must be large enough to encompass the

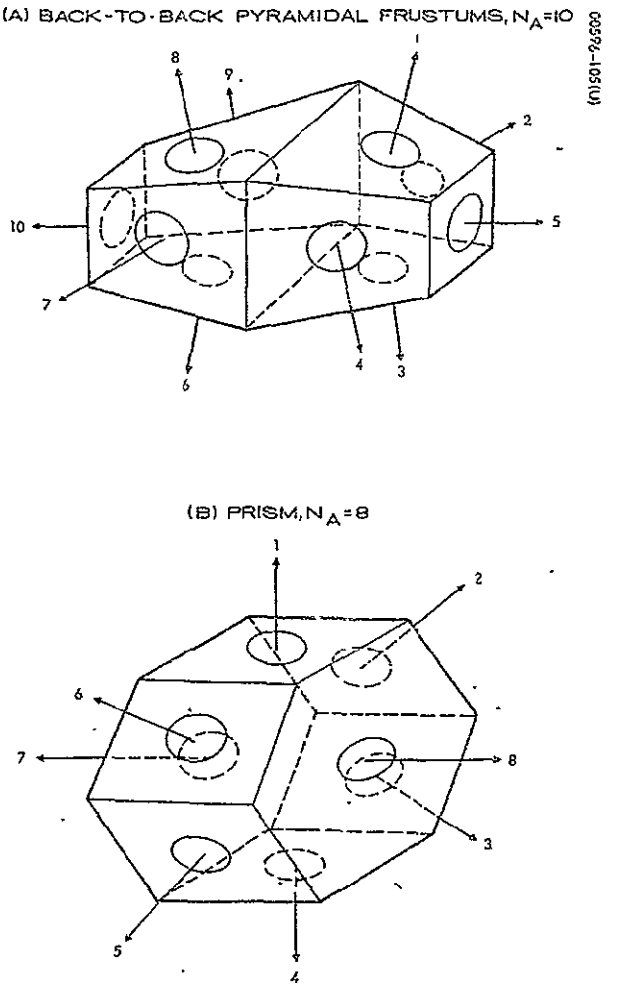

Figure B-1. Array Configurations That Provide Spherical Coverage by Means of Electronic Scanning

...verage region of that array. If the coverage region is large, then ...ent must be electrically and physically small. A large number of ...s per array is then required to obtain the desired gain. If the array ... region is small, the element beamwidth can also be small. Con... the element gain is higher and fewer elements are required. ...rays are required, however, to cover 4π sr so that the total number ...nts does not vary rapidly. There is, however, some optimum num... arrays that result in a minimum total number of elements. In addition, ... electronics is to be shared among arrays, it is desirable to attempt ...mize the number of controllable elements per array. This approach ...ly cannot be pursued to its limit, however, since there would result ...rate array for each beam pointing direction. Some compromise is ...ore required.

In a previous study related to hemispherical coverage, it was found ...tive arrays whose faces lay on the surfaces of a frustum of a pyramid ...adequate coverage. Two such configurations back-to-back — that is, ... arrays — would give spherical coverage (see Figure B-1). With this ...ngement the maximum scan angle required of an array is 47.1 degrees. ... elements in the array are assumed to have a gain beamwidth product ...bout 8,

$$G_E \beta_e^2 \approx 8, \qquad \text{(B-1)}$$

... G_E is the element gain and β_e is the 3-dB beamwidth, then the ...ment gain is

$$G_E \approx 8/\beta_e^2 = 8/(94.2/57.3)^2 = 2.96$$

$$G_E \rightarrow 4.72 \text{ dB}$$

...tion (B-1) assumes a radiation efficiency of about 80 percent. The ...er of elements in each array is then given by

$$N_E = \frac{G_A}{G_E} = G_A \frac{\beta_e^2}{8} = 0.338\, G_A \qquad \text{(B-2)}$$

... G_A is the array gain. The number of elements are listed in ... la for gains ranging from 20 dB to 49 dB. The table relates peak ... in a direction normal to the array to the total number of array ... However, if the gain is to be achieved at the extreme limit of ... region, the number of elements must be doubled, since at the ... coverage region, the array gain is down 3 dB from its value at

TABLE B-1. NUMBERS OF ELEMENTS VERSUS GAIN FOR A TEN-ARRAY CONFIGURATION (BACK-TO-BACK PYRAMIDAL FRUSTUMS)

a. Peak Array Gain G_A

dB	Numerical	N_E	$N_T = 10\ N_E$
20	100	34	340
23	200	68	680
26	400	135	1350
30	1000	338	3380
33	2000	676	6760
36	4000	1352	13520
40	10000	3380	33800
43	20000	6760	67600
46	40000	13520	135200
49	80000	27040	270400

b. Peak Array Gain G_A

dB	Numerical	N_E	$N_T = 10\ N_E$
20	100	54	540
23	200	107	1070
26	400	214	2140
30	1000	535	5350
33	2000	1070	10700
36	4000	2140	21400
40	10000	5350	53500
43	20000	10700	107000
46	40000	21400	214000
49	80000	42800	428000

An additional source of loss is present in phase scanned arrays. This loss occurs in the phase shifters and the feeding structure and may vary from 1 to 2.5 dB or more, depending on frequency. If a value of 2 dB is selected for illustrative purposes, the number of elements in each array would be given by

$$N_E = 0.535\, G_A$$

The numbers of element required with this loss is given in Table B-1b.

The half-power beamwidth versus gain of a uniformly illuminated circular array is shown in Figure B-2 for dissipative losses of 0, 1, 2 and 3 dB. The curve for 1 dB loss corresponds approximately to an element gain beamwidth product of 8 and no phase shifter loss. The curve for 3 dB loss corresponds to an element gain beamwidth product of 8, with an additional 2 dB of phase shifter loss.

In the above section, an array of ten planar arrays arranged on the faces of the two pyramidal frustums back-to-back was considered as a reasonable design approach to the problem of providing spherical coverage with a minimum number of elements. Other arrangements include N_A arrays on the faces of a prism. When $N_A < 10$, this arrangement results in smaller scan requirements than those of the pyramidal frustum configurations. For $N_A = 5$ to 10, the maximum scan angle, number of elements per array, total number of elements and element gain are listed in Table B-2.

Because mutual coupling at the aperture varies with beam scan position, an array cannot be impedance matched over the full range of coverage. The resulting reflection losses at the aperture are minimized by the selection of elements with a cos θ power pattern (120 degrees beamwidth) and the reduction of the maximum required scan angle (one-half the element beamwidth). From Table B-2, it is evident that to minimize scan loss and the number of elements and to meet a gain requirement over the range of coverage, there is some optimum value of N_A. This value most likely lies in the range 7 to 10. Probably the most important loss factor in selecting N_A is the variation in ellipticity ratio as a function of scan angle as ellipticity increases rapidly beyond 45 degrees.

TABLE B-2. CHARACTERISTICS OF SEVERAL MULTI-ARRAY CONFIGURATIONS THAT PROVIDE SPHERICAL COVERAGE

Configuration	Number of Arrays, N_A	Maximum Scan Angle, Degrees	Number of Elements Per Array	Total Number of Elements	Element Gain dB	Array Gain, G_A (1 dB loss assumed)
Two pyramidal frustums	10	47.1	N_E	$10N_E = N_T$	4.72	2.96 N_E
Prism	9	48.3	1.052 N_E	0.948 N_T	4.49	2.81 N_E
Prism	8	49.1	1.089 N_E	0.86 N_T	4.34	2.72 N_E
Prism	7	51.0	1.172 N_E	0.82 N_T	4.02	2.53 N_E
Prism	6	54.8	1:35 N_E	0.81 N_T	3.40	2.19 N_E
Prism	5	69.2 side 45.0 end	2.16 N_E side 0.913 N_E side	0.83 N_T	1.37 side 5.10 end	1.37 N_E side 3.24 N_E end

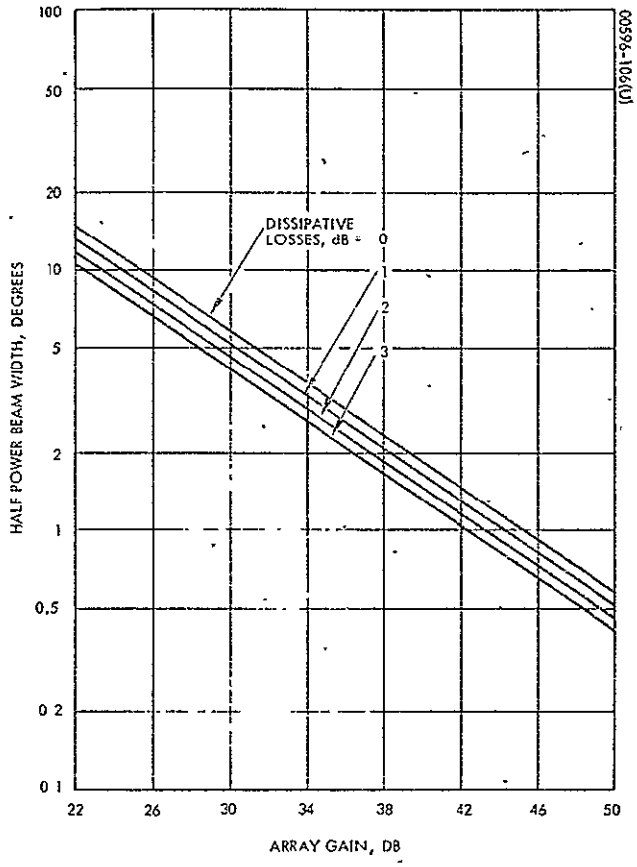

Figure B-2. Halfpower Beamwidth Versus Gain of Uniformly Illuminated Circular Aperture

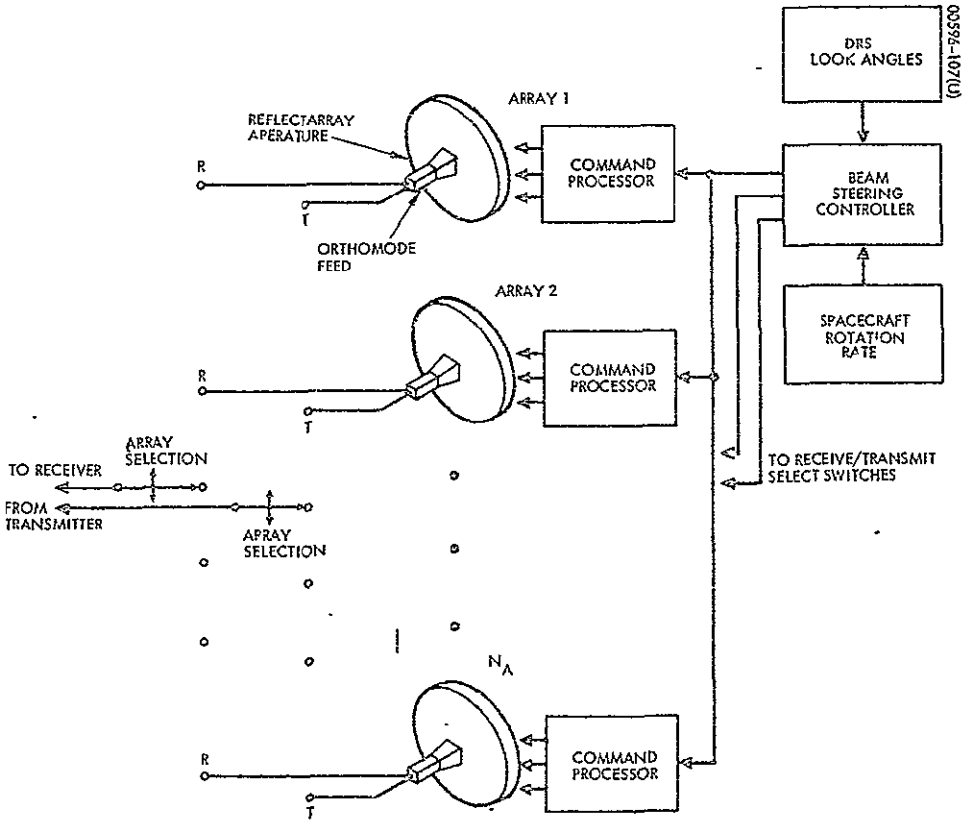

Figure B-3. Electronic Steering Antenna System

REPRESENTATIVE ESA DESIGN

Coverage:	Spherical
Gain:	36.5 dB (minimum)
Frequency:	14 GHz
Polarization:	Dual sense circular transmit and receive.

Steering Technique

The method of electronic steering considered most suitable for the Space Station application is termed command controlled phase scanning. In this technique, the antenna pattern is formed by electronically controlling the relative phase of an incident signal incrementally across the aperture. Other techniques which accomplish the same phase steering by using fixed beam-forming matrices, were considered significantly less attractive because of their attendent weight, bulk and thermo-mechanical distortion problems.

To further reduce weight and volume, in consideration of the large number of elements required, it was decided to use a reflectarray configuration with an orthogonal feed so that a complex corporate feed network would not be required. Figure B-3 is a block diagram of the recommended ESA system.

As shown, each array aperture is fed from an orthomode feed and is electronically configured by instructions from a beam steering controller. The transmit and receive signals are automatically switched from feed to feed as the desired target passes from the visibility of one array to the next. While the target is within the scan angle of a single array, appropriate phase commands are sent to that array's command processor to point its beam accordingly. The beam steering controller requires data on look angles to the desired DRS in Space Station coordinates. (Alternatively, a tracking feed could be used with the reflectarray and tracking signals processed in the normal manner. However, the computer facility required to generate the beam pattern should be able to easily perform look angle calculations.)

System Description

The ESA system that will best meet these requirements consists of one set of electronics that is shared among an array of circular, planar arrays oriented on the faces of a symmetrical prism or two back-to-back frustums of pyramids.* The number of arrays will be between 7 and 10.

* This is the angular relationship required between arrays; their actual mounting locations can be distributed conveniently about the Space Station structure as long as this relationship is maintained.

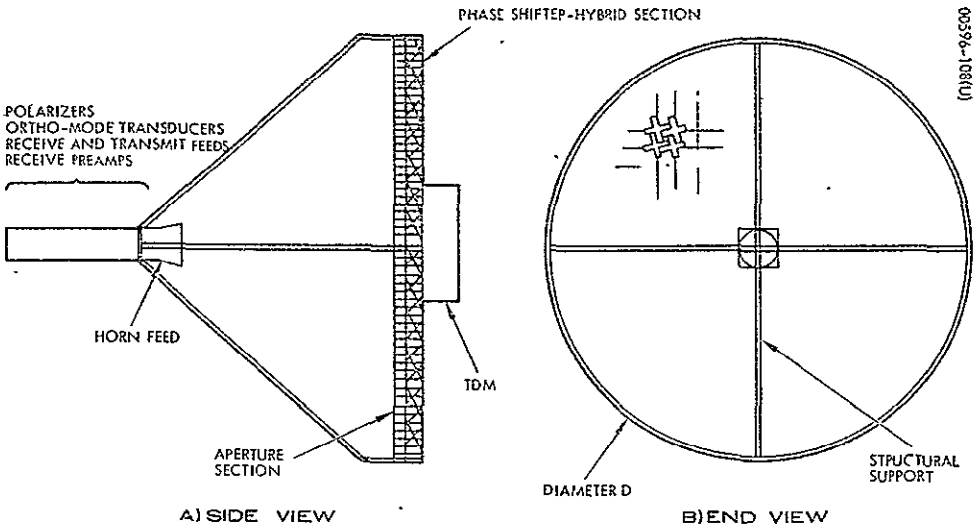

Figure B-4. Reflectarray Design For Command Controlled Phase Scanning Array

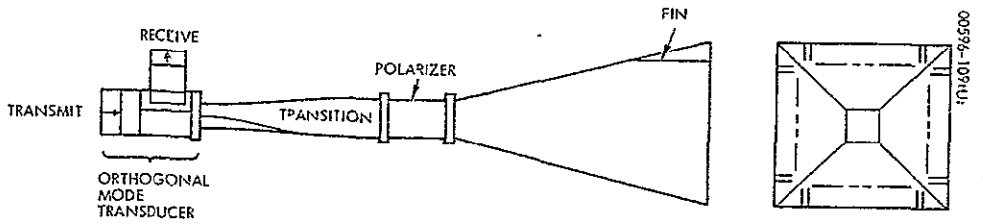

Figure B-5. Circularly Polarized Fin-Loaded Horn

... the configurations were diagrammed in Figure B-1 to show the rel... orientations of the arrays in either the prism or pyramidal frustum ... ement. The arrays are connected to the electronics section, as ... in Figure B-3. Each array is the same and consists of a reflector ... tion containing the array elements and reflective phase shifters and a ... ense CP feed. This design referred to as the reflectarray design is ... n in Figure B-4. Each horn contains a polarizer and orthogonal mode ... ducer. The polarizer converts a linear polarized wave to a circular ...rized wave, and the transducer separates the orthogonal transmit and ...ive signals (see Figure B-5). A typical array element, as shown in ... B-6, includes a crossed waveguide as the radiator, hybrid coupler, ... two phase shifters (one for transmit, and the other for receive). The ... of separate phase shifters solves the beam-pointing error due to the ...ificant frequency separation of the receive and transmit bands. The ...ssed waveguide radiator is uniquely suited for the close packing of ...ient radiators required for wide angle scanning of a circularly-polar... beam. Figure B-7 depicts the best possible packing arrangement for ... waveguide b to a ratio of 0.216.

...ray Size, Radiating Efficiency, and Beamwidth

The gain requirement of 36.5 dB will be met by providing enough ...erture area to compensate for the losses itemized in Table B-3 and for ... 3 dB fall-off in gain when scanning the beam from broadside to the ...gest handover angles.

TABLE B-3. ITEMIZED LOSSES IN 14 GHz REFLECTARRAY

Source of Loss	Loss in dB
Phase shifter, 3-bit PIN diode*†	1.6 minimum
Hybrid coupler†	0.1
Spillover and tapered illumination	1.3 minimum
Feed blockage	0.2
Polarizer†	0.1
Phase quantization*	0.2
Impedance mismatch at aperture due to scanning (≤ 50 degree scan angle)	0.5 maximum
Total loss	4.0 dB

...-bit device is selected as a tradeoff between decreasing loss and in... computer storage capacity as the number of bits increases. A ... device will lead to about 0.9 dB phase quantization loss, a 4-bit ... about 0.1 dB.

... losses

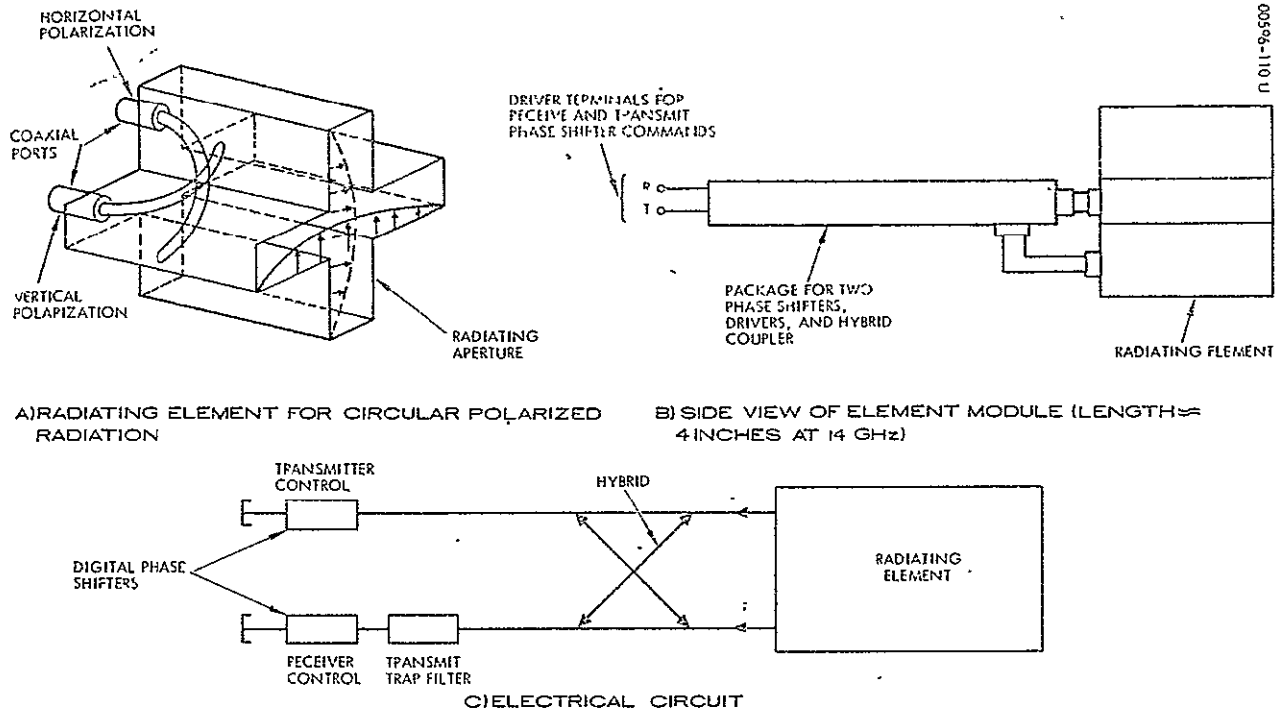

Figure B-6. Array Element Module

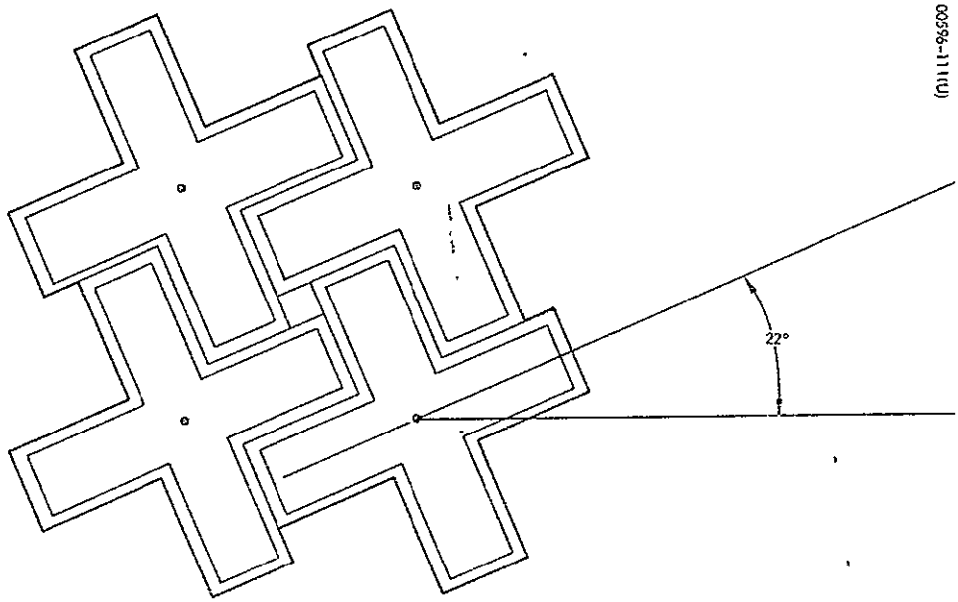

Figure B-7. Closest Packing of Crossed Waveguide Elements (Occurs When Tilted at Angle of Approximately 22 Degrees)

That is, a lossless array with a peak gain of 43.5 dB satisfies the earth-coverage requirement. From Figure B-2, it is seen that the half-power beamwidth will be larger than 1.2 degrees; from Table B-2, the number of elements will be

$$N_E = G_A(1\text{ dB loss})/2.72 = 17,800/2.72 = 6550$$

for an eight-array configuration. Assuming inter-element spacings of 0.56 wavelength (λ) for a square lattice arrangement, the array diameter will be

$$D = 0.56\lambda \left(\frac{4\,N_E}{\pi}\right)^{1/2} = 0.56\,(0.0705)\left(\frac{4\,(6550)}{\pi}\right)^{1/2} = 3.6 \text{ feet}$$

and the surface area

$$A = \frac{\pi D^2}{4} = 10.2 \text{ square feet}$$

Assuming a 2-foot spacing between the primary feed and the array surface, the f/D ratio will be about 1/2. The depth of the array aperture section and phase-shifter hybrid section will be approximately 4 inches (see Figure 6b).

The basic antenna system components and their estimated numbers and weights are listed in Table B-4.

A summary of array performance and mechanical characteristics is given in Table B-5. The choice of a circular shape for the array leads to a 17 dB first sidelobe level if the illumination of the aperture is uniform. Since a tapered illumination is obtained from the basic reflector design, sidelobe levels greater than 20 dB should be achievable.

RECOMMENDATIONS FOR FURTHER DEVELOPMENT

Problem Area	Remarks	Percentage Effort
° Phase shifter	Insertion loss must be reduced from present 2.5 dB to about 1.5 dB. Develop mass production technique.	30

TABLE B-4. PARTS, NUMBERS, AND WEIGHTS OF ESA SYSTEM

Component	Number	Weight, Pounds
Radiating element	52, 400 (eight Arrays)	157
Phase shifter	104, 800	2, 180
Driver		
Hybrid coupler	52, 400	
Frame	8	6
Back plate	8	84
Horn, polarizer, and ortho-mode transducer (four per array)	32	38
Receiver preamplifier, feed supports, and miscellaneous.	8 sets	48
Time division multiplex device	16	
RF waveguide (5 feet)	16	8
Total Antenna System Weight	Eight Arrays	2, 521
Single-pole, 8-throw RF switch	2	
Logic circuits	1	
Beam steering controller	1	
Look angle computer	1	
		42
System Total		2, 563

TABLE B-5. SUMMARY OF REFLECTARRAY CHARACTERISTICS

Realized gain at handover	36.5 dB
Maximum scan angle	49.1 degrees
Radiating efficiency	39.8 percent
Half-power beamwidth at broadside	>1.2 degrees
Sidelobe level	>17.0 dB
Number of elements	6,550
Number of phase shifters	13,100
Diameter	3.6 feet
Surface area	10.2 square feet
Overall depth	~2.5 feet
Weight	~315 pounds

Problem Area	Remarks	Percentage Effort
• Radiating element	Obtain patterns with <1.5 dB ellipticity to 50 degree scan angle. Obtain >25 dB isolation between horizontal and vertical polarized waves. Minimize length. Match within array and determine mutual coupling behavior.	40
• Packaging of two phase shifters, hybrid trap filter, and two driver circuits.	Utilize stripline and microstrip technology. Reduce weight.	30

About 50 percent of the phase shifter research and development work expected to be performed for other ESA applications at X-band and below. The reflectarray design approach proposed in this study is technically feasible because it is an extension of ESAIRA technology and because the radiating element and phase shifter have been built at X-band. However, with 1970-71 state of the art technology, a radiation efficiency of only 20 percent would be realized.